

Aus der Klinik für Unfallchirurgie, Orthopädie und Plastische Chirurgie
(Prof. Dr. med. W. Lehmann)
der Medizinischen Fakultät der Universität Göttingen

Tumor invasion through 3D engineered basement membrane

INAUGURAL-DISSERTATION

zur Erlangung des Doktorgrades
der Medizinischen Fakultät der
Georg-August-Universität zu Göttingen

vorgelegt von

Zhiming Zhao

aus

Xiantao, Hubei, China

Göttingen 2021

Dekan:

Prof. Dr. med. W. Brück

Betreuungsausschuss

Betreuer/in:

Prof. Dr. med. A. Schilling

Ko-Betreuer/in:

Prof. Dr. rer. nat. F. Wouters

Prüfungskommission

Referent/in:

Prof. Dr. med. A. Schilling

Ko-Referent/in:

Drittreferent/in:

Datum der mündlichen Prüfung:

Hiermit erkläre ich, die Dissertation mit dem Titel " Tumor invasion through 3D engineered basement membrane " eigenständig angefertigt und keine anderen als die von mir angegebenen Quellen und Hilfsmittel verwendet zu haben.

Göttingen, den 6.12.2021

Zhiming Zhao
(Unterschrift)

TABLE OF CONTENTS

LIST OF FIGURES	III
LIST OF TABLES	V
ABBREVIATIONS	VI
ABSTRACT	VII
1 INTRODUCTION	1
1.1 BONE METASTASIS.....	1
1.2 BONE METASTATIC LESIONS.....	1
1.3 BONE MICROENVIRONMENT.....	2
1.4 REGULATORY FACTORS OF BONE METASTASIS.....	2
1.5 CURRENT MODELS OF BONE METASTASIS.....	4
1.6 <i>IN VITRO</i> BONE METASTASIS MODELS.....	5
1.7 <i>IN VIVO</i> BONE METASTASIS MODELS.....	8
1.8 AIM OF THESIS.....	10
1.9 HYPOTHESIS.....	10
2 MATERIALS AND METHODS	12
2.1 MATERIALS AND CHEMICALS.....	12
2.2 CELL LINES AND CELL CULTURE.....	18
2.3 STABLE GFP/RFP CELL LINE GENERATION.....	18
2.4 LENTIVIRUS PRODUCTION, CONCENTRATION AND TITRATION.....	18
2.5 3D DESIGN OF THE MOLDS AND THE DEVICES.....	19
2.6 3D PRINTING OF THE MOLDS AND THE DEVICES.....	20
2.7 CASTING OF THE SILICONE COVERS AND BLUE SILICONE RINGS.....	20
2.8 ASSEMBLE THE BIOREACTOR AND LEAKPROOF TEST OF THE 3D BIOREACTOR WITH CONTINUOUS PERFUSION.....	20
2.9 TEST THE POSSIBILITY OF CASTING WITH DIFFERENT CONCENTRATION OF MATRIGEL MATRIX AND PEGDA.....	21
2.10 TEST THE PERMEABILITY OF MATRIGEL MATRIX GEL WITH DIFFERENT CONCENTRATION IN XCELLIGENCE.....	22
2.11 TEST THE PERMEABILITY OF PEGDA GELS WITH DIFFERENT CONCENTRATION IN XCELLIGENCE.....	25
2.12 TEST THE PERMEABILITY OF PEGDA GEL WITH DIFFERENT CONCENTRATION OF MATRIGEL MATRIX IN XCELLIGENCE.....	26
2.13 INHIBITION EXPERIMENT OF SHIKONIN ON MDA-MB-231 AND MCF-7 MIGRATION IN INCUCYTE (SCRATCH WOUND ASSAY).....	27
2.14 INHIBITION OF MDA-MB-231 AND MCF-7 CELLS INVASION THROUGH ENGINEERED BASEMENT MEMBRANE GEL IN XCELLIGENCE.....	28
2.15 TEST THE PERMEABILITY OF ENGINEERED BASEMENT MEMBRANE AFTER IRRADIATION WITH MDA-MB-231 AND MCF-7 IN XCELLIGENCE.....	29
2.16 TEST THE PERMEABILITY OF 2.5WT%PEGDA MEMBRANE AFTER IRRADIATION WITH MDA- MB-231 AND MCF-7 IN XCELLIGENCE.....	30
2.17 IMMUNOFLUORESCENCE OF ENGINEERED BASEMENT MEMBRANE AFTER IRRADIATION.....	30
3 RESULTS	32
3.1 MDA-MB-231 AND MCF-7 GFP/RFP TRANSDUCTION AND SELECTION.....	32
3.2 3D DESIGN OF THE BIOREACTORS.....	33
3.3 3D DESIGN OF THE MOLDS AND THE DEVICES.....	34
3.4 CASTING OF THE SILICONE COVERS AND BLUE SILICONE RINGS.....	35
3.5 3D PRINTING OF THE BIOREACTOR AND SEALING OF THE BIOREACTOR.....	36
3.6 TEST OF THE 3D BIOREACTOR WITH CONTINUOUS PERFUSION.....	37

3.7	GELATION TEST OF DIFFERENT CONCENTRATION OF MATRIGEL MATRIX.....	38
3.8	GELATION TEST OF PEGDA 20,000 GEL SOLUTION.....	39
3.9	TEST THE PERMEABILITY OF MATRIGEL MATRIX GELS WITH DIFFERENT CONCENTRATION IN XCELLIGENCE.....	40
3.10	TEST THE PERMEABILITY OF PEGDA GELS WITH DIFFERENT CONCENTRATION IN XCELLIGENCE.....	42
3.11	TEST THE PERMEABILITY OF ENGINEERED BASEMENT MEMBRANE GELS WITH DIFFERENT CONCENTRATION IN XCELLIGENCE.....	44
3.12	MDA-MB-231 AND MCF-7 CELL MIGRATION INHIBITED BY SHIKONIN IN INCUCYTE (SCRATCH WOUND ASSAY).....	45
3.13	INHIBITION OF MDA-MB-231 AND MCF-7 CELLS INVASION THROUGH ENGINEERED BASEMENT MEMBRANE GELS IN XCELLIGENCE.....	50
3.14	MDA-MB-231 AND MCF-7 CELL INVASION AFTER IRRADIATION OF THE ENGINEERED BASEMENT MEMBRANE IN XCELLIGENCE.....	51
3.15	MDA-MB-231 AND MCF-7 INVASION THROUGH 2.5WT%PEGDA AFTER IRRADIATION.....	53
3.16	IMMUNOFLUORESCENCE LAMININ AND COLLAGEN IV STAINING OF THE ENGINEERED BASEMENT MEMBRANE AFTER IRRADIATION.....	53
4	DISCUSSION.....	55
4.1	ENGINEERED BASEMENT MEMBRANE IN 3D BIOREACTOR.....	55
4.2	CLINICAL DOSE OF IRRADIATION OF THE ENGINEERED BASEMENT MEMBRANE REDUCED THE INVASIVENESS OF MDA-MB-231 CELLS.....	56
4.3	CURRENT <i>IN VITRO</i> 3D TUMOR METASTASIS MODELS.....	57
4.4	LIMITATIONS OF THE THESIS.....	59
4.5	FUTURE DIRECTIONS OF <i>IN VITRO</i> BONE METASTASIS MODELS.....	59
5	CONCLUSIONS.....	61
	APPENDIX.....	62
	PLASMID MAPS.....	62
6	REFERENCES.....	65
	ACKNOWLEDGEMENTS.....	71
	CURRICULUM VITAE.....	72

LIST OF FIGURES

Figure 1: XCELLigence for cell invasion. The RTCA DP instrument consists of the control unit and analyzer.....	22
Figure 2: Cell invasion experiment through Matrigel matrix..	23
Figure 3: Cell invasion experiment through Matrigel matrix..	24
Figure 4: MDA-MB-231 and MCF-7 cells invasion experiment through Matrigel matrix gel..	25
Figure 5: MDA-MB-231 cells invasion experiment through different concentration of PEGDA gel.....	25
Figure 6: MCF-7 cells invasion experiment through different concentration of PEGDA gel.....	26
Figure 7: MDA-MB-231 and MCF-7 cells invasion through engineered membrane.....	27
Figure 8: Scratch wound assay.....	28
Figure 9: MDA-MB-231 and MCF-7 cells invasion through engineered membrane inhibited by shikonin.....	29
Figure 10: Test of the permeability of engineered basement membrane after irradiation.....	29
Figure 11: MDA-MB-231 and MCF-7 cell GFP/RFP transduction and selection.....	32
Figure 12: 3D views of the bioreactor design.....	33
Figure 13: 3D views of the bioreactor with window design.....	34
Figure 14: The molds and devices for the silicone cover and the blue silicone ring in different views.....	35
Figure 15: The views of printed devices and molds for blue silicon ring and silicone cover.....	36
Figure 16: The bioreactor printed with PLA and sealed with glass slides and silicone cover.....	37
Figure 17: The 3D bioreactor with perfusion system.....	38
Figure 18: Possibility of gel casting with different concentration of PEGDA 20,000.....	39
Figure 19: MDA-MB-231 cells invasion through Matrigel matrix gels with different concentration in xCELLigence, 25000 cells per well, (mean±SD, n=3).....	40
Figure 20: MDA-MB-231 cells invasion through Matrigel matrix gels with different concentration in xCELLigence, 40000 cells per well, (mean±SD, n=3).....	41

Figure 21: MCF-7 cells invasion through Matrigel matrix gels with different concentration in xCELLigence, 40000 cells per well, (mean±SD, n=3).	42
Figure 22: MDA-MB-231 cells invasion through PEGDA gels with different concentration (mean±SD, n=3).....	43
Figure 23: MCF-7 cells invasion through PEGDA gels with different concentration (mean±SD, n=3).	44
Figure 24: MDA-MB-231 and MCF-7 cells invasion through engineered basement membrane gels with different concentration, 80,000 cells per well (mean±SD, n=3).....	45
Figure 25: MDA-MB-231 cell migration inhibited by shikonin in Incucyte (mean±SD, n=3)...	46
Figure 26: MDA-MB-231 cell migration inhibited by shikonin in Incucyte.....	48
Figure 27: MCF-7 cell migration inhibited by shikonin in Incucyte.	48
Figure 28: MCF-7 cell migration inhibited by shikonin in Incucyte (mean±SD, n=3).	49
Figure 29: MDA-MB-231 and MCF-7 cell invasion through engineered basement membrane gel inhibited by shikonin in xCELLigence (mean±SD, n=3)..	50
Figure 30: MDA-MB-231 cell invasion after irradiation of the engineered basement membrane..	51
Figure 31: MCF-7 cell invasion after irradiation of the engineered basement membrane.	52
Figure 32: MDA-MB-231 and MCF-7 invasion through 2.5wt%PEGDA after irradiation.....	53
Figure 33: Anti-laminin staining of the engineered basement membrane before and after irradiation..	54
Figure 34: Anti-collagen IV staining of the engineered basement membrane before and after irradiation..	54

LIST OF TABLES

Table 1: Used machines and manufacturer information	12
Table 2: Chemicals and Reagents	14
Table 3: Consumables	15
Table 4: Cell lines	16
Table 5: Plasmids for LV generation and Addgene information	16
Table 6: Software	16
Table 7: Work solutions	17
Table 8: Gel formation of different concentration of Matrigel	38

ABBREVIATIONS

3D	Three dimensions
ATCC	American type culture collection
BMPs	Bone morphogenetic proteins
CI	Cell index
CIM	Cell invasion migration
CXCR4	CXC-chemokine receptor 4
DKK1	Dickkopf-related protein 1
DMEM	Dulbecco's Modified Eagle Medium
DMSO	Dimethylsulfoxid
DP	Dual purpose
DPBS	Dulbecco's phosphate-buffered saline
ECM	Extracellular matrix
EHS	Engelbreth-Holm-Swarm Mouse Sarcoma
FBS	Fetal bovine serum
FGFs	Fibroblast growth factors
GFP	Green fluorescent protein
GY	Gray
kV	Kilovolt
LAP	Lithium phenyl-2,4,6-trimethylbenzo- ylphosphinate
mA	Milliampere
MSCs	Mesenchymal stem cells
P/S	Penicillin/Streptomycin
PBS	Phosphate-buffered saline
PDMS	Polydimethylsiloxane
PEGDA	Polyethylene(glycol)diacrylate
PFA	Paraformaldehyde
PLA	Polylactic acid
PTHrP	Parathyroid hormone related peptide
RANKL	Receptor activator of nuclear factor κ B ligand
RFP	Red fluorescent protein
RTCA-DP	Real time cell analysis
RUNX2	Runt-related transcription factor 2
TGF- β	Transforming growth factor β
UV	Ultraviolet

ABSTRACT

Tumor metastasis is the most important reason of cancer-related death. The progress of tumor metastasis includes intravasation, survival in the circulation, extravasation and colonization. In the process of metastasis intravasation, the basement membrane is the first important barrier. Therefore, engineering a basement membrane in 3D structure might provide a novel 3D model of tumor metastasis, leading to a better understanding of tumor intravasation.

In this thesis, a novel artificial engineered basement membrane (EBM) was fabricated by gelation of Matrigel matrix and PEGDA 20,000 under UV exposure. The function of this EBM was investigated by MDA-MB-231 and MCF-7 cell invasion in xCELLigence.

MDA-MB-231 cells invaded through the membrane successfully but MCF-7 cells failed, showing that the EBM can differentiate between metastatic and non-metastatic tumor cells. The invasion process was significantly influenced by shikonin and irradiation, showing that the EBM allows to study tumor related treatments.

In summary, this thesis established a novel 3D in vitro tumor metastasis model which may serve as a platform for drug screening and study of tumor metastasis.

1 INTRODUCTION

1.1 Bone Metastasis

Tumor metastasis is the most important reason leading to cancer-related deaths (Nannuru and Singh 2010). Bone is one of the most common sites of tumor metastasis (Li et al. 2012). The incidence of bone metastasis in breast cancer and prostate cancer is 65–75% (Coleman 1997) while the incidence in lung cancer, thyroid cancer, kidney cancer and most of the adenocarcinoma primary tumors is much lower (Suva et al. 2011). The median survival in patient with bone metastasis is 2–3 years (Holen et al. 2015). Current therapy for bone metastasis is mostly palliative (Suva et al. 2011). Bone metastasis may result in severe problems like osteolytic bone pain, pathologic fractures, or malignant hypercalcemia (Chow et al. 2008). The first step for bone metastasis is invasion, in which the cancer cells invade through the basement membranes to start metastasis. However, the complexity of the invasion process remains unclear (Akhtar et al. 2019). Better understanding of the invasion process of metastasis may help to prevent or treat bone metastasis.

1.2 Bone Metastatic Lesions

Bone metastatic lesions include osteolytic lesions and osteoblastic lesions. Tumor stimulated osteoclastic bone resorption at the bone marrow plays a very important role in the formation of bone metastasis within the strict environment of mineralized bone and promotes the tumor progression (Martin 2002).

Osteoblastic lesions with increased bone formation are present in many tumoral diseases like prostate carcinoma (Ottewell 2016). It can be diagnosed by radiographs. Osteoblasts form bone through a multistep of proliferation, matrix maturation and mineralization and this can be activated by factors secreted by growing tumor cells.

Another special type is dormant lesion (Gawrzak et al. 2018). Tumor dormancy is a lesion which can stay in silence for a long term and can finally be activated to form a metastatic lesion. The silence term can be months to years. Patients with dormant lesions have a higher risk of tumor recurrence.

1.3 Bone Microenvironment

The bone plays an important role in structural support, movement and maintaining minerals and energy. The bone marrow possesses postnatal hematopoiesis (Frisch 2019). Bone cells are mainly comprised of osteoblasts, osteoclasts, osteocytes and adipocytes (Florencio-Silva et al. 2015). Osteoblasts and osteoclasts maintain balance of bone structure and health through bone-remodeling.

Interestingly, bone metastasis is not the same within different bones (Tanaka et al. 2005). Metastases are found more frequently in red marrow and bones rich in trabeculae such as vertebrae, ribs, pelvis. The mechanism of the more frequent tumor metastasis to red marrow and trabecular rich bones is not clearly understood (Hernandez et al. 2018). One of the hypotheses is that the higher rates of bone turnover, vascularization and more trabecular bone induce tumor cell seeding and colonization (Kakhki et al. 2013).

1.4 Regulatory Factors of Bone Metastasis

Bone matrix is comprised of mineral and organic matrix. The bone matrix not only provides structural support for bone cells but also secretes a variety of factors such as transforming growth factor β (TGF- β), receptor activator of nuclear factor κ B ligand (RANKL), parathyroid hormone related peptide (PTHrP), bone morphogenetic proteins (BMPs), fibroblast growth factors and Wnt pathway molecules, which regulate the bone turnover and tumor cell growth during bone metastasis (Käkönen et al. 2002; Boyce 2013; Johnson et al. 2014; Wu et al. 2016).

TGF- β secreted by both primary tumor and colonization cells in bone, can induce the bone resorption process and release TGF- β from the bone. After the ligand binding to the type II receptor serine kinase (TGF β RII) on target cells, the TGF- β signaling pathway is activated (Shi and Massagué 2003). TGF β RII activation induces phosphorylation of the type I receptor (TGF β RI) and phosphorylation of Smad2 and Smad3. Smad2 and Smad3 binding to Smad4 can induce the translocation to the nucleus and increase target gene transcription (Roberts and Sporn 1993). TGF- β secreted from both bone and tumor cells can suppress T-cell proliferation and activity of natural killer cells. Thus, the immune system is inhibited by TGF- β (Fournier et al. 2006). Also, PTHrP and IL-8 can induce bone resorption through T-cell activation and the T-cell function inhibition through a negative regulation (Fournier et al. 2006). PTHrP, which is secreted by mesenchymal stem cells (MSC) or occasionally secreted by cancer cells, promotes the binding of

RANKL and its receptor RANK, and thereby activates osteoclast formation (Lacey et al. 1998). RANKL is one of the most important mediators of osteoclast formation, function and survival (Roodman and Dougall 2008).

Some osteoblastic factors such as fibroblast growth factors, BMPs and Wnt pathway molecules can stimulate bone formation within bone metastases. Prostate cancer cells express factors including BMPs and Fibroblast growth factors (FGFs) which can activate resident bone and bone marrow cells in bone metastasis (Morrissey et al. 2010). FGFs including acidic and basic FGFs (FGF1 and FGF2) can stimulate the proliferation and differentiation of osteoblasts by upregulating runt-related transcription factor 2 (RUNX2) and BMP2 (Kodama et al. 2009).

Wnts are a large family of glycoproteins related to normal osteoblast development and bone formation (Bennett et al. 2005). Prostate cancer cells produce dickkopf-related protein 1(DKK1), an inhibitor of Wnt signaling at the beginning of the progress of bone metastasis. With the progression of metastasis, DKK1 decreases, thus Wnt signaling increases the activity of osteoblast, causing osteoblastic lesions (Hall et al. 2005).

Apart from soluble factors, also mechanical obstacles like the extracellular matrix of the basement membrane play an important role in tumor metastasis. To start the metastasis, invading through basement membrane is the first important step. The basement membrane is a thin layer of extra cellular matrix which guides normal tissue development (Yurchenco 2011). The basement membranes are self-assembled through binding of laminins, type IV collagens, nidogens, growth factors and proteoglycans (Yurchenco 2011). After invading through basement membrane, the cancer cells can invade into vessels (intravasation) and survive in the circulation. The possible mechanism of invasion has been thought to depend on protease degradation (Glentis et al. 2017). However, in current studies, physical forces generated by cancer cells growing also promotes the invasion through basement membrane (Punovuori and Wickström 2020). Due to the complexity of the metastasis and unclear understanding of the invasion process, it is very important to understand the structure of basement membrane and the mechanism of the invasion through the basement membrane.

Histological confirmation of the surgical margins can ensure complete excision. However, several reports demonstrated that pathological assessment are sometimes not accurate (Holland et al. 1985; Frazier et al. 1989; Silverstein et al. 1994). It was reported that

residual cancer cells were found at 2 cm from the tumor margin in 42% of specimens (Holland et al. 1985). 26% of patients who were confirmed with clear pathological margin had been reported with residual cancer cells (Frazier et al. 1989). A possible way to mitigate this problem is irradiation therapy (Abe et al. 2005). However, the typical clinical dose of irradiation (50–60Gy) does not kill all cancer cells but rather achieves better long-term results with less side-effects (Coles et al. 2005). A part of this effect could be a change of the extracellular matrix of the basement membrane due to the irradiation.

1.5 Current Models of Bone Metastasis

One of the difficulties in studying bone metastasis is the lack of an ideal tumor metastatic model (Thibaudeau et al. 2014a). One of the most important factors is the unclear understanding of the complicated pathophysiological mechanisms in bone metastasis (Thibaudeau et al. 2014b). Stephen Paget proposed the “seed and soil” hypothesis by analyzing autopsy specimens of women who died of breast cancer. The seed only grows if it lands in a proper soil (Akhtar et al. 2019). Since the development of “seed and soil” hypothesis the knowledge of metastatic mechanisms has greatly improved. Nearly 3.2×10^6 cells/g tissue per day escape from the primary tumor (Schilling et al. 2012), and only 0.01% of these cells survive in the circulation and continue metastasis (Butler and Gullino 1975). Proteases which are released by tumor cells play an important role in the escape from the primary tumor. With releasing proteases, the tumor cells can pass through the basement membrane and the endothelium of small blood vessels, enter the circulation, and pass through the blood vessels endothelium into the distant organs. There are several properties which induce high incidence of bone metastasis: high volume of blood flow in bone marrow, mechanical structural support, presence of adhesive cells, angiogenic and bone-resorbing factors. RANKL has been widely known to promote tumor cell bone colonization. Recent research showed that RANKL secreted by osteoblasts improve tumor cell homing and colonization (Campbell et al. 2012).

Models of bone tumor metastasis are mainly divided into two types, *in vivo* models and *in vitro* models. Currently several types of models have been used in the research of bone metastasis. But all have some limitations (Thibaudeau et al. 2014b; Katt et al. 2016).

1.6 *In Vitro* Bone Metastasis Models

Numerous *in vitro* models of bone metastasis have been developed, however reliable, simple, and inexpensive models of the complicated bone environment which can mimic the *in vivo* metastasis are still lacking (Salamanna et al. 2016). *In vitro* bone metastasis models can be classified into several types, transwell-based models, spheroid-based models, hybrid models and tumor-microvessel models (Katt et al. 2016).

Transwell-based models have been widely used to test cancer cell migration and invasion (Kramer et al. 2013). These models with different membranes can be used for drug screening, tumor cell invasion, and extracellular matrix remodeling (Madsen et al. 2015). They are easily implemented, inexpensive, high throughput and can be used to compare metastatic capability of different cell lines. However, the limitation is low physiological relevance.

Spheroid-based models are designed based on cancer cell spheroids grown in suspension or 3D culture (LaBarbera et al. 2012). Tumor spheroids are widely used for drug screening, proliferation and invasion study, immune cell response study, angiogenesis study. There are four methods for fabrication of tumor cell spheroids, suspension culture, microfluidic method, non-adherent surface method and hanging drop method, each differ with advantages and disadvantages (Mehta et al. 2012). Suspension culture aggregates cancer cell spheroids by improving the viscosity of the media. The limitation of this method is uncontrolled size and uniformity.

To overcome this limitation, non-adherent surfaces which prevent cells from attaching to the non-adherent surface had been developed. Spheroid size can be controlled by culturing the cells in microarrays with special round-bottom non adherent 96-well plates (Fennema et al. 2013). Stamped agarose microwells are widely used as non-adherent surface in this method (Gonzalez-Fernandez et al. 2020).

In hanging drop method, cells are suspended from the underside of an adherent tissue culture lid. Cells aggregate to a cluster at the bottom and then the spheroid grows. The size of the spheroid is controllable but with a limitation of low throughput. With the development of microfluidic devices, size and uniformity of spheroid formation became more controllable (Fu et al. 2014).

Hybrid *in vitro* bone metastatic models include embedded *ex vivo* sections, avascular microfluidic models and 3D invasion models. They combine tumor microenvironment and

in vitro model together. Embedded *ex vivo* sections can keep specific heterogeneity of tumor cells, supporting tissue and vascular tissue and have been widely used in study of tumor morphology, growth and chemosensitivity. In this method, collagen type I is usually used to mimic the extracellular matrix, however the gene expression can be regulated by the extracellular matrix (Nguyen-Ngoc et al. 2012). The most widely used applications of the embedded *ex vivo* sections are drug sensitivity test and patient specific treatment test. One limitation of this method is the missing medium perfusion in these models.

3D invasion models mimic invasion by seeding cancer cell spheroids in an extracellular matrix material. In this method, coculture of endothelial cells, fibroblasts and cancer cells using a matrix material has been used to study extracellular matrix material, matrix remodeling, hypoxia on cell adhesion and invasion (Mosadegh et al. 2015). This method is typically used in the study of cancer cell secreted factors, matrix remodeling and cancer cell dormancy (Horie et al. 2015). The limitation of this method is lack of vasculature and lack of tumor complexity.

Avascular microfluidic models are typically designed as tumor cells grown in a 2D microfluidic device. They are widely used in the study of migration. Real-time tracking of cell adhesion to endothelial layers before extravasation can be studied with this model. The limitations are the lack of vasculature and lack of 3D environment in the models (Hsu et al. 2011).

Tumor vasculature is one of the most important components of the tumor microenvironment. Nutrients and oxygen are transported through vasculature to the tumor cells. The factors secreted by the endothelial cells can regulate the tumor growth in several ways (Butler et al. 2010). Tumor-microvessel models are widely used to study interactions between tumor cells and vasculature. They are mainly designed by culturing endothelial cells in extracellular matrix scaffolds or remodeled matrix (Abigail and Sharon 2012).

With a predefined extracellular matrix scaffold method, micro vessels were fabricated by seeding endothelial cells onto a predefined channel in a scaffold (Liu et al. 2008). The most common substances used to fabricate a predefined extracellular matrix are fibrin and collagen I (Liu et al. 2008). After seeding onto the inner surface of the predefined extracellular matrix, the cells form a monolayer. A study reported that vessel permeability responds to vascular factors and cytokines (Chrobak et al. 2006). With a 3D microvessel structure, several types of cells such as smooth muscle cells can be cocultured with tumor cells in this system. It makes it possible to study the tumor cell induced angiogenesis,

intravasation, and extravasation (Wang et al. 2015). Live-cell imaging uncovered one possible mechanism of tumor intravasations: tumor cells can disrupt the endothelial monolayer through cell division (Wong and Searson 2014). The limitation of predefined extracellular matrix scaffold method is the limited vessel diameter and simple linear geometries.

To overcome the limitation of vessel diameter and simple linear geometries of the vessel, microvessel self-assembly method has been developed based on endothelial cells seeding and embedded within a matrix and self-assembling into random vessels smaller than 50 μ m (Sarker et al. 2018). Once microvessel networks have been established, the medium can perfuse through the microvessel network. After perfusion, the tumor cells can move in the network which can mimic the survival of tumor cells in the circulation. It can be used to study tumor cell survival and extravasation. Also, with seeding the tumor cells with the extracellular matrix surrounding the vessel networks, this model can be used to study the interactions of endothelial cells and tumor cell activation and arrestation (Ghajar et al. 2013). However, a limitation of this microvessel self-assembly model is the generation of a random vessel network with unpredictable medium perfusion (Wong and Searson 2014).

Transwell-based metastasis models have the limitation that they mainly evaluate cell motility. Also, the physiological relevance is low compared to *in vivo* models (Katt et al. 2016).

There are several methods to fabricate spheroid-based models. With cell suspension culture method, the limitations are no individual compartments for spheroids and uncontrolled uniformity. With no-adherent surfaces cell culture method and hanging drop technique method, the main limitations are the difficulty of long-term tumor cell culture and low throughput (Mehta et al. 2012).

Hybrid *in vitro* bone metastatic models can be developed in three different ways. With embedded *ex vivo* tumor sections method, the limitation is the lack of medium perfusion through vasculature. With 3D invasion models method, tumor cells are embedded in a gel. The limitations are the lack of vasculature and lack of tumor complexity. With avascular microfluidic method, tumor cells grow in a 2D microfluidic device, mainly used to study migration. The limitations are the lack of vasculature and the lack of 3D environment (Yabushita et al. 2004).

1.7 *In Vivo* Bone Metastasis Models

Before commencing clinical trials in human, treatment must first pass the test *in vivo* animal models (Mak et al. 2014). The first type of *in vivo* animal model is spontaneous bone metastasis model. An *in vivo* model of prostatic cancer metastasize to bone in canines was reported in 2014 (Trost et al. 2014). Such models are usually used to mimic bone metastasis with quick progress, occurring reliably in animals *in vivo*, but it may require months or years of tracking the animals (Langlais et al. 2006).

The second type of *in vivo* bone metastasis model is the intravascular and intraosseous model. Intraosseous model is used to study the progression of cancer cells in the bone microenvironment. This model is fabricated by injecting tumor cells into the bone of the rats directly. The advantage of this method is quick metastasis and thus it can be used for testing strategies for preventing tumor growth (Zheng et al. 2008). But this model only mimics the process after extravasation. It's somehow more similar to the primary tumor (Thibaudeau et al. 2014a). Thus, intravascular models were developed to overcome these limitations and fabricate more suitable metastatic models. Some researchers use intracardiac injection and tail vein injections of cancer cells to mimic bone metastasis (Yi et al. 2002). These models can be used to study the process of hematogenous metastasis, extravasation and colonization. The limitation of these models comes from the use of xenograft. Immune-compromised animals are necessary to secure minimal graft rejection. This property limits the use of this method to study how the immune system affects bone metastasis (Wu et al. 2013).

The third type is a humanized model that uses human cancer cells and bone implants to study metastasis. The advantage is the use of human cancer cells and bone implants for metastasis (Yang et al. 2007; Xia et al. 2012). Humanized models try to mimic the process of tumor progression in mice with various ways of injection of human cells to better represent the process in the human body. Subcutaneous implants of human bone scaffold and direct injection are used in models. Researchers use these models with an intravascular injection to study the ability of the cells to extravasate while direct injection is usually used for evaluating colonization ability of the cells. Recently, Moreau's study evaluated the intravasation, survival in circulation, and extravasation. The main limitation of this model was the limited source of the human tissues (Moreau et al. 2007).

More and more tissue-engineering constructs have been used in creating a controllable microenvironment (Schuster et al. 2006). Tissue-engineered scaffolds provided a reproducible and controllable microenvironment for osteoblast differentiation. However, current models using tissue-engineering scaffolds still need an intravascular injection and immunocompromised animals with the disadvantage of absence of immune response during metastasis (Moreau et al. 2007).

Interaction between the immune system and skeletal system in cellular mechanisms, “osteimmunology” became a new focus (Rho et al. 2004; Walsh et al. 2006). The same molecules which act both in the skeletal system and immune system have been discovered. Cancer cell immunosurveillance happens when the immune system is activated by the signals from tumor cells such as tumor antigens. Normally the CD8⁺ T cells in the immune system eliminate cancer cells, but antitumor immune effects are not always efficient to inhibit cancer cell survival in the circulation (Capietto and Faccio 2014). In order to study the effects of the immune system on possible treatments, immunocompetent models of bone metastasis have been developed (Power et al. 2009). As immunocompetent mice are widely used in these models, they have obvious advantages compared to immunocompromised animal models. However, most of the models still need an intravascular injection of cancer cells (Thibaudeau et al. 2014b). They can be used to study homing and colonization of tumor cells, but cannot be used to study intravasation and niche formation before metastasis because of the lack of primary tumor formation.

Although these types of models have been developed for years, there is still limitation in mimicking the dormancy and homing process during bone metastasis (Linde et al. 2016). Based on the 3D coculture of breast cancer cells and bone marrow cells, a dormant model of bone metastasis was established and implanted subcutaneously into mice. This model can be used for the study of cellular dormancy in bone metastasis (Marlow et al. 2013).

Taken together, there are already several types of *in vivo* and *in vitro* bone metastasis models. However, all of the current models have their limitations.

In spontaneous bone metastasis models, the main limitation is that the spontaneous phenomenon is rare and hard to recreate in most animals (Jinnah et al. 2018). However, in the few larger animal models, the primary tumor can occur and metastasize to bone. The progression of metastasis is very slow and the costs is too high to be widely used in therapeutic testing (Langlais et al. 2006).

In intraosseous models, the main limitation is that the models can only mimic the process after bone colonization, but not homing of tumor cells, extravasation and intravasation (Thibaudeau et al. 2014a). Intravascular injection models which can mimic the survival in circulation, extravasation and colonization have been developed. However, the main limitation is that immune-compromised animals are necessary for the models (Wu et al. 1998). They can't be used to study the role of the immune system in bone metastasis which is also very important in tumor progression.

Immunocompetent bone metastasis models, which have advantages in preclinical models, usually need an intravascular injection of tumor cells. This may affect the mechanisms being studied in the bone (Wright et al. 2016). The limitation is that the models can be used in study of homing and colonization but not intravasation because the lack of a primary tumor (Wright et al. 2016).

Humanized bone metastasis models, use human cancer cells and bone implants to mimic the metastasis (Kuperwasser et al. 2005). The main limitation is the difficulty of availability of human tissues. The complexity of the microenvironment in the animals makes it more difficult to reproduce and control (Xia et al. 2012).

Tissue-engineered bone metastasis models develop a scaffold-based bone microenvironment. The main limitation of this model is the immunocompromised animals used in the method, which leads to a lack of immune system response in the metastatic process (Schuster et al. 2006).

In summary, in order to have better understanding of the first step of bone metastasis, the invasion process, an engineered basement membrane which can mimic the basement membrane *in vivo* is necessary. In this study, the design of an engineered basement membrane for a 3D bone metastasis model to mimic and study bone metastasis was attempted.

1.8 Aim of Thesis

The aim of this thesis was it to create a 3D tissue engineered model of tumor invasion through basement membrane to be able to study this important first metastatic step.

1.9 Hypothesis

The hypothesis was that a 3D tissue engineered model of a basement membrane allows to differentiate between invasive and non-invasive tumor cells, can also show the effect

of chemo-therapy and can be used to study matrix mediated direct effects of irradiation on the metastatic process.

2 MATERIALS AND METHODS

2.1 Materials and Chemicals

Table 1: Used machines and manufacturer information

Machine	Model	Company
Balance	Explorer	Ohaus, USA
Centrifuge	Heraeus Multifuge X1R	ThermoFisher, USA
Freezer(-20°C)		Liebherr, Swiss
Freezer(-80°C)	DF9014	IlShin, Netherlands
Freezer(-150°C)	ULT10140-9-M23	Thermo Scientific, USA
Ice machine	ZBE 70-35	Ice Systems, UK
Cryostat	CM1950	Leica, Germany
Incubator	Cytoperm 2	Thermo Scientific, USA
Incubator	BBD 6220	Thermo Scientific, USA
Microscope	DMi8	Leica, Germany
Vortexer	RS-VA10	Phoenix Instrument, Germany
Water bath	Isotemp GPD 20	Fisher Scientific, USA
Real time cell analyzer	xCELLigence® RTCA DP	ACEA Bioscience, USA
Computer-controlled air pressure pump	Air pressure pump 02	Ibidi GMBH, Germany
Perfusion set	Red (#10962)	Ibidi GMBH, Germany
Fluidic unit	10903	Ibidi GMBH, Germany
Computer	Notebook with pump control software	Ibidi GMBH, Germany
3D printer	Ultimaker 3	Ultimaker, Netherlands
PLA filament	PRO1 Black	BASF, Germany
Live-cell analysis system	Incucyte S3	Essen BioScience, Germany

Safety Cabinet	Hs18	Thermo Heraeus, USA
X strahl Cabinet Irradiators	RS225	Gulmay Medical LTD, USA
Flashlights	Walther Pro UV5	Laserliner, Schweiz
RTCA analyzer	XCELLigence RTCA DP	ACEA Bioscience, USA
Pipette	K28906H	Star Lab, Germany
Neubauer Haemocytometry		Electron Microscopy Sciences, USA

Table 2: Chemicals and Reagents

Compounds	Provider Information
DMSO	Sigma-Aldrich, USA
Trypsin	Pan Biotech, Germany
Ethanol	Carl Roth, Germany
Sucrose	Sigma-Aldrich, USA
SYLGARD 184 Silicone Elastomer Base	Dow Chemical, USA
SYLGARD 184 Silicone Elastomer Curing Agent	Dow Chemical, USA
Mold Star 16 FAST Platinum Silicone Rubber	Smooth-On, USA
LAP	Sigma-Aldrich, USA
PEGDA 20,000	Sigma-Aldrich, USA
Shikonin	Sigma-Aldrich, USA
Matrigel Matrix Standard Formulation 354234	Corning, USA
DMEM	Gibco, USA
Phenol free DMEM	Gibco, USA
DPBS	Pan Biotech, Germany
FBS	Pan Biotech, Germany
Penicillin/Streptomycin	Pan Biotech, Germany
PFA	Th. Geyer, Germany
Tissue-Tek O.T.C	Sakura, USA
Blasticidin (G418 solution)	Sigma-Aldrich, USA
Plasmids	Addgene, USA
Anti-Laminin Ab11575	Abcam, UK

Anti-Collagen IV Ab19808	Abcam, UK
Goat anti-rabbit IgG Ab150080	Abcam, UK
Puromycin	Sigma-Aldrich, USA

Table 3: Consumables

Consumables	Provider Information
PLA filament	BASF, Germany
96-well plate	Thermo Scientific, USA
24-well plate	Greiner bio-one, Germany
Serological pipette 5 ml	Sarstedt, Germany
Serological pipette 10 ml	Sarstedt, Germany
Serological pipette 25 ml	Sarstedt, Germany
Micro tube 1.5 ml SafeSeal	Sarstedt, Germany
Pipette tips 10 μ L	Biozym, USA
Pipette tips 100 μ L	Biozym, USA
Pipette tips 1000 μ L	Biozym, USA
Pipette Reference 10 mL	Eppendorf, Germany
Pipette Reference 100 mL	Eppendorf, Germany
Pipette Reference 1000 mL	Eppendorf, Germany
Culture flask T25	Sarstedt, Germany
Culture flask T75	Sarstedt, Germany
Culture flask T175	Sarstedt, Germany
Mr. Frosty Freezing Container	Thermo Scientific, USA

Needle 20 G	Braun, Germany
Syringe 2 mL	BD, USA
Falcon tube 15 mL	Sarstedt, Germany
Falcon tube 50 mL	Sarstedt, Germany
96-well Imagelock microplate	Essen BioScience, Germany
Coverslip 18*18 mm	Carl Roth, Germany
Coverslip 6*6 mm	Carl Roth, Germany
Vivaspin columns	Sartorius, Germany
CIM plate	ACEA Bioscience, USA

Table 4: Cell lines

Cell line	Description	Distributor information
MDA-MB-231	Human mammary gland	ATCC® HTB-26™
MCF-7	Human mammary gland	ATCC® HTB-22™

Table 5: Plasmids for LV generation and Addgene information

Plasmid	Addgene Number
pLemiR-NS	32809
pLJM1-EGFP	19319
pCMV-VSV-G	8454
psPAX2	12260

Table 6: Software

Software	Manufacturer
Leica Application Suite X 3.4.2.18368	Leica, Germany
Microsoft PowerPoint 2016	Microsoft, USA

Microsoft Word 2016	Microsoft, USA
Microsoft Excel 2016	Microsoft, USA
GraphPad Prism 5	GraphPad Software, USA
Adobe Illustrator 2020	Adobe, USA
Mendeley Desktop 1.19.4	Elsevier, Netherlands
Incucyte S3 2019A	Sartorius, Germany
RTCA Data Analysis Software 1.0	ACEA Bioscience, USA
FreeCAD 0.17	Matra Datavision, France
Ultimaker Cura 3.6.0	Ultimaker, Netherlands

Table 7: Work solutions

Solutions	Recipe
100 μ L Matrigel aliquot	7.6 mg/mL Matrigel solution 100 μ L
Silicone solution	SYLGARD 184 Silicone Elastomer Base 10 mL SYLGARD 184 Silicone Elastomer Curing Agent 1 mL
Blue silicone rubber	Mold Star 16 FAST Platinum Silicone Rubber Part A 5 mL Mold Star 16 FAST Platinum Silicone Rubber Part B 5 mL
200 μ g/mL Matrigel solution	Matrigel aliquot 1.31 μ L DMEM (serum free) 48.69 μ L
400 μ g/mL Matrigel solution	Matrigel aliquot 2.63 μ L DMEM (serum free) 47.38 μ L
800 μ g/mL Matrigel solution	Matrigel aliquot 5.25 μ L DMEM (serum free) 44.75 μ L
1200 μ g/mL Matrigel solution	Matrigel aliquot 7.89 μ L DMEM (serum free) 42.11 μ L
1600 μ g/mL Matrigel solution	Matrigel aliquot 10.50 μ L DMEM (serum free) 39.50 μ L
10 wt% PEGDA gel solution	PEGDA 100 mg Distilled water 900 mg LAP 1 mg
7.5 wt% PEGDA gel solution	10 wt% PEGDA gel solution 750 μ L DMEM (serum free) 250 μ L

5 wt% PEGDA gel solution	10 wt% PEGDA gel solution 500 μ L DMEM (serum free) 500 μ L
2.5 wt% PEGDA gel solution	10 wt% PEGDA gel solution 250 μ L DMEM (serum free) 750 μ L
2.5 wt% PEGDA+400 μ g/mL Matrigel gel solution	10 wt% PEGDA gel solution 250 μ L Matrigel aliquot 52.5 μ L DMEM (serum free) 697.5 μ L

2.2 Cell Lines and Cell Culture

Human breast cancer cell lines MDA-MB-231 and MCF-7 were bought from American Type Culture Collection. The cells were cultivated in DMEM containing 10% FBS, and 1% penicillin and streptomycin at 37°C and 5% CO₂. The medium was changed every 3 days depending on the confluence. The cells were split when the confluence was 70-80%. MCF-7 is a poorly-aggressive and non-invasive cell line and normally being considered to have low metastatic potential. MDA-MB-231 is an aggressive and invasive cell line and has high metastatic potential (Elgundi et al. 2020).

2.3 Stable GFP/RFP Cell Line Generation

MDA-MB-231 and MCF-7 cell lines were maintained in DMEM with 10% FCS and 1% P/S. Fluorescence microscopy pictures were obtained by an inverted microscope (Leica DMi8, Germany) using the filter set BP 525/50 for GFP and filter set BP 605/70 for RFP detection. Exposure time was set to 40 ms for all fluorescence pictures.

MCF-7 and MDA-MB-231 cells were seeded in 24-well plates (50,000 cells/well). After 24 h, cells were infected with lentivirus (500 MOI) carrying VSVG envelope proteins and GFP or RFP as a gene of interest. After 96 h, blasticidin containing media (5 μ g/mL) was added to cells and cells were selected for at least 14 d. After the selection process (100% green/red cells) cells were stored at a -150°C freezer for further experiments.

2.4 Lentivirus Production, Concentration and Titration

VSVG pseudotyped lentiviruses were generated in HEK293FT cells. Cells were seeded in 6-well plates at 1×10^6 cells/mL and directly transfected with pLJM1-EGFP for GFP or pLemir-NS for RFP delivery, psPAX2 for viral capsid proteins and pCMV-VSV-G for

viral envelope proteins (summarized plasmids are listed in Table 5). 16 h after transfection, sodium butyrate containing media (0.01 M) was added for 8 h. Afterwards, media without sodium butyrate was used and collected every 24 h. After 5 da, media was centrifuged for 30 min at 2,000 x g, filtered, and concentrated via Vivaspin columns (10.000 MWCO, Sartorius, Göttingen, Germany). Concentrated virus solutions were stored at -80 °C.

2.5 3D Design of the Molds and the Devices

The molds and the devices were designed using the free and open-source software Freecad 0.17 in this study. A mold was designed to fabricate the transparent silicone cover of the main device. The frame of the mold was a rectangular box with an outer ratio of length, width, and depth 2:2:1. The size was 20 mm x 20 mm x 10 mm. Two rectangular grooves parallel to the boundary of the mold were designed with a rectangular cross section. The width and depth of the cross section of the grooves are 1 mm, 1 mm.

A perfusable cell culture device was designed using Freecad software. In this device, cells can be cultured in 3D hydrogels which contain sustainable perfusion in the middle of the hydrogels. The frame of the device was a rectangular box with an outer ratio of length, width, and depth 20:20:10. The size was 20 mm x 20 mm x 10 mm. Parallel to the boundary of the device, there were two rectangular grooves with a rectangular cross section. The width and depth of the grooves were 1mm. The inner space for cell culture is a rectangular box with a ratio of length, width and depth 8:3:10. The size was 8 mm x 3 mm x 10 mm. The bottom and top surface of the device were hollow and were covered and sealed with silicone cover fabricated in molds or thin glass slides with proper size. In the middle of the device, a 7.2 mm diameter cylindrical channel was design to achieve the sustainable perfusion. Three cylinders with diameters of 3 mm, 5 mm and 7 mm were designed to generate a channel for sustainable perfusion in the hydrogels.

The other molds which were used for fabrication of blue silicone soft rings were designed with Freecad. The molds for blue silicone rings were composed of two parts. Part A was a disc-shaped mold with an upright slim cylinder in the middle of the disc. Part B was a thin-walled hollow cylinder which fits to the part A mold. Two parts were composed together when fabricating the blue silicone rings.

2.6 3D Printing of the Molds and the Devices

After the designing, the FCStd files were created by the software Freecad. Then the FCStd files were exported to STL files. Before printing the molds and devices, the STL files were converted to GCODE files using the free software Ultimaker Cura version 3.6.0. The GCODE files which contained instructions tailored to Ultimaker 3 3D printer were used to print the molds and devices. All the molds and devices were printed with polylactic acid (PLA) filament with a diameter of 2.85 mm on an Ultimaker 3 3D printer. The printing infill density was 100% and the printing speed was 30 mm/s. The molds and devices were printed at extra fine profile with support overhang angle 60°.

2.7 Casting of the Silicone Covers and Blue Silicone Rings

The silicone cover for the main device was fabricated with designed mold. SYLGARD 184 Silicone Elastomer Base and curing agent were mixed completely with volume ratio 10:1. After the silicone solution was poured into the printed mold, the bubbles floated up slowly. Then bubbles were carefully removed by pipetting continuous air flow on top of the silicone solution. The mold with mixture of the silicone solution was incubated in the incubator at 50-55°C for 72 h. The silicone covers were released from the molds after three days incubation.

The blue silicone ring was fabricated with designed molds. Blue silicone rubber material A and B (Mold Star 16 Fast) were mixed completely with volume ratio 1:1. After carefully removed the bubbles in the mixture with pipette, it was poured into the blue silicone mold immediately. The mold with mixture of the silicone materials was incubated in the incubator at 50-55°C for 2 h. The blue silicone rings were released from the molds 2 h later. During the study, the designs of the molds and the devices were modified when problems occur during perfusion testing.

2.8 Assemble the Bioreactor and Leakproof Test of the 3D Bioreactor with Continuous Perfusion

The bioreactor was composed of the main device, the silicone covers and the blue silicone rings. The silicone material mixture was poured into the grooves of the main device and bubbles were carefully removed by pipette. The silicone cover was covered on the device by pressure on the top. The device with silicone cover and liquid silicone material was put into the incubator at 50-55°C for 72 h. After 72 h, the devices with top silicone cover

were moved out of the incubator. The bottom of the device was sealed with silicone cover or glass slide cover in the same way.

The continuous perfusion system was composed of a peristaltic pump, medium supply and bioreactor. The leakproof test of the perfusion system was performed under sterile conditions in a cell culture bench. The bioreactor, the tubes, the cylinders and the medium container were disinfected with 70% ethanol for 30 min before use. The 10% PEGDA and LAP solution was prepared as above. A big cylinder with outer diameter of 7 mm was inserted into the bioreactor. The gel solution was injected by a syringe through the silicone cover and exposed to the UV light for 5 min. After UV exposure, the cylinder was pulled out and solid gel formed in the bioreactor with a medium channel. The pump and medium container were connected to the bioreactor. Proper volume of medium was added to the perfusion set. The software of the perfusion system was set up with pressure 20 millibar. The pump and the bioreactor were put in the incubator at 37°C and 5% CO₂ for 48 h. After running for 48 h, leakproof of the bioreactor was checked.

2.9 Test the Possibility of Casting with Different Concentration of Matrigel Matrix and PEGDA

Matrigel matrix was ordered from Corning. The Matrigel matrix was extracted from the Engelbreth-Holm-Swarm (EHS) mouse sarcoma. The Matrigel Matrix contains mainly laminin, collagen IV, heparan sulfate proteoglycans, entactin/nidogen (Kleinman et al. 1982; Kleinman et al. 1986). Growth factors including TGF-beta, insulin-like growth factor, epidermal growth factor, tissue plasminogen activator, fibroblast growth factor, and other growth factors in natural EHS sarcoma are also found in Matrigel Matrix (Vukicevic et al. 1992). The Matrigel matrix was diluted into 200 µg/mL, 400 µg/mL, 800 µg/mL, 1200 µg/mL, 1600 µg/mL solution each well 50 µL in 96-well plate with DMEM. At the time points 17 h and 24 h, the gels were observed. At 27 h, the gels were diluted with 150 µL distilled water and the gels were observed.

Lithium phenyl-2,4,6-trimethylbenzoylphosphinate (LAP) and PEGDA 20,000 were dissolved in distilled water with final concentration 0.1 wt% and 10 wt%. Then the PEGDA 20,000 and LAP mixture was diluted again into different concentration. The final PEGDA 20,000 concentration of the gel solution is 0.67 wt%, 1 wt%, 2.5 wt%, 5 wt%, 7.5 wt% and 10 wt%. With each concentration, 100 µL gel solution was added into well in 96-well plate. The gel solution was exposed to the UV exposure for 5 min and observed.

2.10 Test the Permeability of Matrigel Matrix Gel with Different Concentration in xCELLigence

Cell invasion assay was performed to test the permeability of Matrigel matrix gels using the xCELLigence RTCA DP instrument. The RTCA DP instrument includes the control unit and the RTCA DP analyzer for measuring impedance-based signals in cell invasion and migration assays. Cells seeded in the upper chamber invaded through the membrane and porous into the lower chamber with chemoattractant. The change of impedance was measured in real time by the analyzer. With xCELLigence, the real time cell index was measured during the invasion and migration.

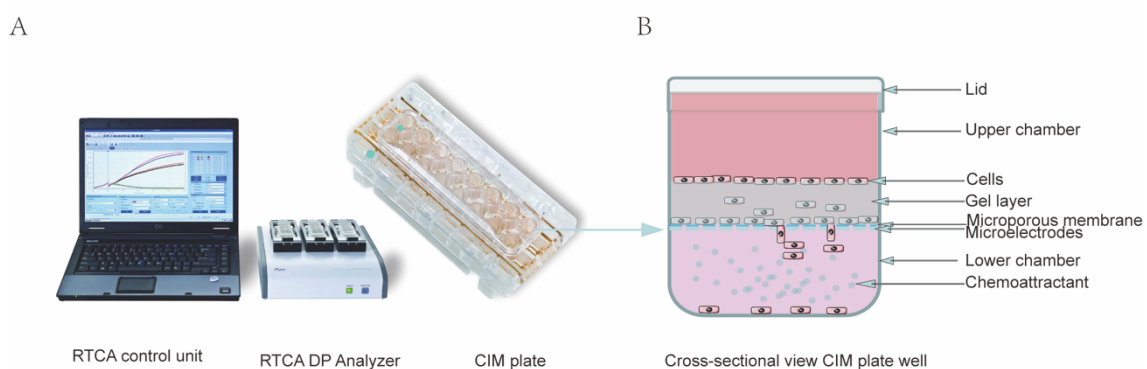


Figure 1: XCELLigence for cell invasion. The RTCA DP instrument includes the control unit and analyzer. The CIM plate was used for cell invasion and migration (A). The cells which were seeded in the upper chamber invaded through the membrane and porous into the lower chamber with chemoattractant (B).

FBS was used as the chemoattractant. The Matrigel matrix was from Corning company with concentration 7.6 mg/mL. MDA-MB-231 invasion with different cell number was tested in different concentration of Matrigel. The cell number for the first testing experiment was 25000/well in CIM-plate.

The day before the experiment, pipette tips, Eppendorf tubes, a tube of aliquoted Matrigel and the CIM-Plate were stored at 4°C overnight. The cells were deprived from FBS 24 h before experiment. The Matrigel was diluted with pre-cooled serum free medium on ice in pre-cooled Eppendorf tubes. Matrigel matrix was diluted to 300 µg/mL, 800 µg/mL, 1200 µg/mL, 1600 µg/mL as described below (Figure 2).

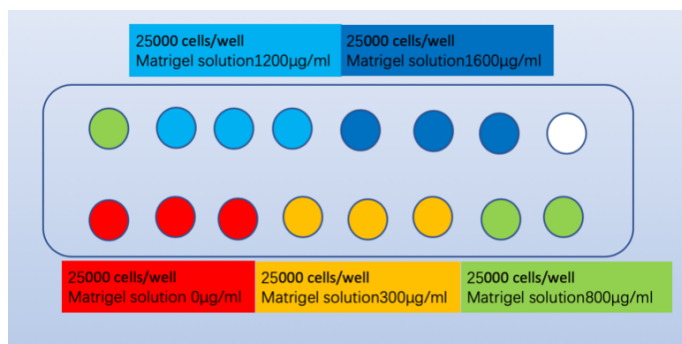


Figure 2: Cell invasion experiment through Matrigel matrix. The concentration of the Matrigel Matrix was 0 µg/mL in red wells, 300 µg/mL in gold wells, 800 µg/mL in green wells, 1200 µg/mL in cerulean wells, 1600 µg/mL in blue wells. The number of cells in each well was 25000.

50 µL of Matrigel solution was added into each well of upper chamber. Serum free medium was used as control group. The plate was gently tapped to ensure the Matrigel evenly covers the entire surface of each well. 30 µL of Matrigel solution was carefully removed from each well. Then the upper chamber coated with Matrigel was placed in 37°C incubators for 4 h.

After the Matrigel had polymerized, the upper chamber was brought to the tissue culture hood. The CIM plate assembly tool was placed inside the hood with the blue markings facing away the operator and kept the plate sitting flat. Each well was filled with 160 µL of media containing 10% fetal bovine serum. A meniscus was formed at the top of each well to prevent air bubbles. The upper and lower chambers were locked together. 30 µL serum free medium was added to each well of the upper chamber to cover the membrane surface. The CIM-Plate 16 was placed into the xCELLigence RTCA DP instrument inside the 37°C incubators for 1 h to allow the CIM membrane to reach equilibrium with the media.

During the incubation, cells were prepared. The media was removed from the T75 flask and cell monolayer was gently rinsed with PBS. The cells were trypsinized and trypsinization was stopped by adding media containing 10% fetal bovine serum. The media containing cells was centrifugated for 5 min at 500 x g. After centrifugation, the supernatant was removed and serum free media was added to resuspend the cells. Centrifugation was running again to get cell pellet without FBS. Serum free medium was added again to resuspend the cell pellet. Determined cell concentration under a microscope using a Neubauer haemocytometry. The concentration of the cell suspension was adjusted to 250000 cells/mL using serum free medium. For each experimental condition being examined triplicates or quadruplicates were used.

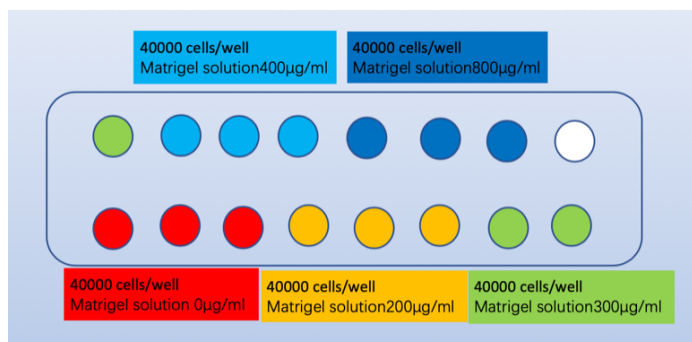


Figure 3: Cell invasion experiment through Matrigel matrix. The concentration of the Matrigel Matrix was 0 µg/mL in red wells, 200 µg/mL in gold wells, 300 µg/mL in green wells, 400 µg/mL in cerulean wells, 800 µg/mL in blue wells. The number of cells in each well was 40000.

100 µL of cell suspension was added to each well of the upper chamber and the final number of cells per well was 25000 for the first test. The CIM-plate was placed in the hood at room temperature for 30 min to allow the cells to settle evenly onto the bottom surface of the upper chamber. The CIM-plate was placed into the RTCA DP instrument inside the incubator. RTCA software was programmed a run of 72 h with recording every 15 min. The cell index was studied and analyzed with GraphPad Prism 5. One-way ANOVA was used to compare means of cell index among the groups at 6 h, 12 h, 20 h, 24 h time points. A P value less than 0.05 was considered as statistically significant.

As the result showed that the cell index is too low. We changed cell number of MDA-MB-231 cells to 40,000/well. Matrigel matrix was diluted to 200 µg/mL, 300 µg/mL, 400 µg/mL, 800 µg/mL in the further experiments. For the invasion of MCF-7 cells the condition of the test was the same as the second experiment (Figure 3).

According to the results of the experiment of MDA-MB-231 and MCF-7 cells, we tested the invasion of the two cell lines under the same condition (Figure 4).

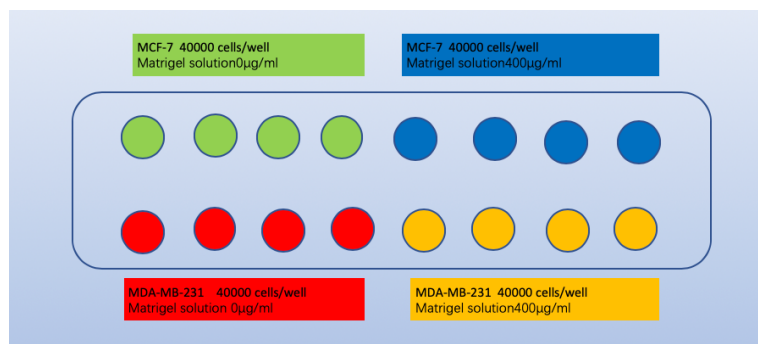


Figure 4: MDA-MB-231 and MCF-7 cells invasion experiment through Matrigel matrix gel. The concentration of the Matrigel Matrix was 0 $\mu\text{g/mL}$ in red wells, 400 $\mu\text{g/mL}$ in gold wells, 0 $\mu\text{g/mL}$ in green wells, 400 $\mu\text{g/mL}$ in blue wells. The number of cells in each well was 40000.

2.11 Test the Permeability of PEGDA Gels with Different Concentration in xCELLigence

For testing the permeability of PEGDA gels, the PEGDA gel solution was diluted into 2.5 wt%, 5 wt%, and 10 wt%. The number of the MDA-MB-231 cells for the testing experiment is 40000/well and 80000/well in CIM-plate 16. Experimental condition being examined were described as plate map below.

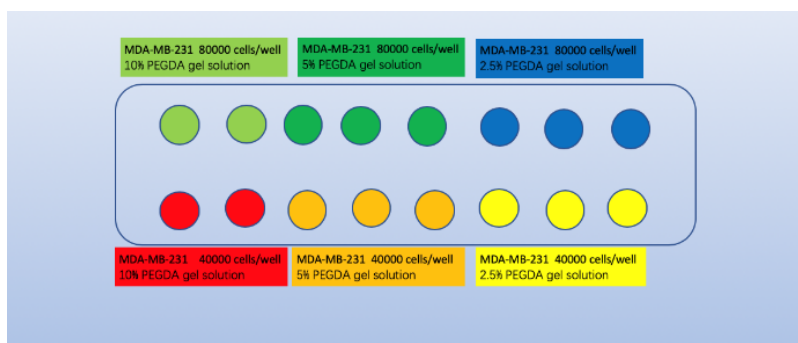


Figure 5: MDA-MB-231 cells invasion experiment through different concentration of PEGDA gel. The concentration of the PEGDA was 10 wt% in red wells, 5 wt% in gold wells, 2.5 wt% in yellow wells. The number of cells in each well was 40000. The concentration of the PEGDA was 10 wt% in green wells, 5 wt% in emerald wells, 2.5 wt% in blue wells. The number of cells in each well was 80000.

Two experiments with MDA-MB-231 and MCF-7 were performed in the test of PEGDA gels. The first experiment was different number of MDA-MB-231 cells invasion through different concentration of PEGDA gels. The plate map was described above (Figure 5). 50 μL of PEGDA gel solution was added into each well of upper chamber. 30 μL of PEGDA gel solution was carefully removed from each well. All wells were exposed to the UV light for 5 min for gelation. The CIM plate was incubated at 37°C and 5% CO_2 incubator for 4 h. The cells were prepared and added in to the CIM plate according to the

protocol for xCELLigence which described above. The cell index was studied and analyzed with GraphPad Prism 5. One-way ANOVA was used to compare means of cell index among the groups at 6 h, 12 h, 20 h, 24 h time points. A P value less than 0.05 was considered as statistically significant.

The second experiment was different number of MCF-7 cells invasion through different concentration of PEGDA gels. The plate map was described as below (Figure 6). The protocol was as the same as the MDA-MB-231 cells invasion through different concentration of PEGDA gels. The result showed that 80,000 per well was suitable for the invasion experiment through PEGDA. MCF-7 cells were not able to invade through PEGDA gels in the concentration in this experiment.

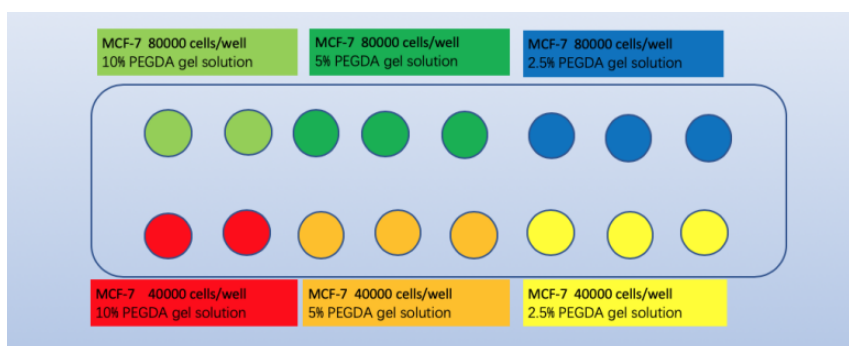


Figure 6: MCF-7 cells invasion experiment through different concentration of PEGDA gel. The concentration of the PEGDA was 10 wt% in red wells, 5 wt% in gold wells, 2.5 wt% in yellow wells. The number of cells in each well was 40000. The concentration of the PEGDA was 10 wt% in green wells, 5 wt% in emerald wells, 2.5 wt% in blue wells. The number of cells in each well was 80000.

2.12 Test the Permeability of PEGDA Gel with Different Concentration of Matrigel Matrix in xCELLigence

Based on the results of the permeability of the Matrigel membrane and the PEGDA gel membrane, two cell lines were tested in one CIM plate to study the permeability of the PEGDA membrane with or without Matrigel. The cells were designed into 6 groups as described below (Figure 7). The cell number was 80000 per well. For testing the permeability, the PEGDA gel solution was diluted into 2.5 wt% with or without 400 $\mu\text{g}/\text{mL}$ Matrigel. The protocol was the same as described above. The result showed the MDA-MB-231 cells invaded through 2.5 wt% PEGDA gels and 2.5 wt% PEGDA with 400 $\mu\text{g}/\text{mL}$ or 200 $\mu\text{g}/\text{mL}$ Matrigel. But the MCF-7 cells didn't invade through 2.5 wt% PEGDA gels and 2.5 wt% PEGDA with 400 $\mu\text{g}/\text{mL}$ or 200 $\mu\text{g}/\text{mL}$ Matrigel. The cell index was studied and analyzed with GraphPad Prism 5. One-way ANOVA was used to

compare means of cell index among the groups at 6 h, 12 h, 20 h, 24 h time points. A P value less than 0.05 was considered as statistically significant.

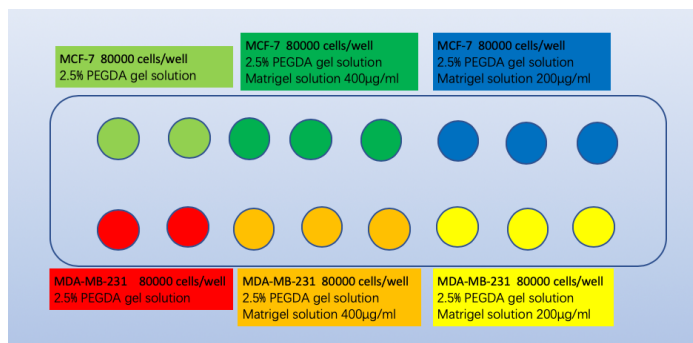


Figure 7: MDA-MB-231 and MCF-7 cells invasion through engineered membrane. The red wells and green were coated with 2.5 wt% PEGDA. The gold wells and emerald wells were coated with 2.5 wt% PEGDA+400 µg/mL Matrigel Matrix. The yellow wells and blue wells were coated with 2.5 wt% PEGDA+200 µg/mL Matrigel Matrix. MDA-MB-231 and MCF-7 cells were seeded into wells as described in the figure.

2.13 Inhibition Experiment of Shikonin on MDA-MB-231 and MCF-7 Migration in Incucyte (Scratch Wound Assay)

According to the results of the permeability of the engineered basement membrane (PEGDA+ Matrigel Matrix gel), wound healing assay was used to test the effect of shikonin on the cell migration in 24-well plate and Incucyte. Different number of cells, 80,000/well, 160,000/well, 240,000/well, 320,000/well, were seeded in 24-well plate. Pictures were taken after 24 hours. The result showed that 320,000 cells/well was the proper number for 24-well plate. To determine the concentration of the shikonin for the inhibition experiment, a test experiment was performed in 24-well plate. 320,000 cells were seeded in 1mL DMEM containing 10% FBS. The plate was incubated at 37°C and 5% CO₂. The cell monolayer was scratched with a sterile pipette tip. The cells were washed with 1mL DMEM containing different concentration of shikonin. The concentration of shikonin was set at 0 µM, 2 µM, 5 µM, 10 µM. The cells were cultured with DMEM containing different concentration of shikonin at 37°C and 5% CO₂. The pictures of the wounds were captured at time point 12 h, 24 h, 36 h and 48 h. The wound healing area was measured. The results showed that the cells couldn't survive in DMED containing 10 µM shikonin.

The concentration of shikonin was set at 0 µM, 2 µM, 3 µM, 4 µM, 5 µM and the experiment was repeated again in 24-well plate with cell number 320,000/well. The pictures were captured at time points 0 h, 12 h, 24 h and 36 h.

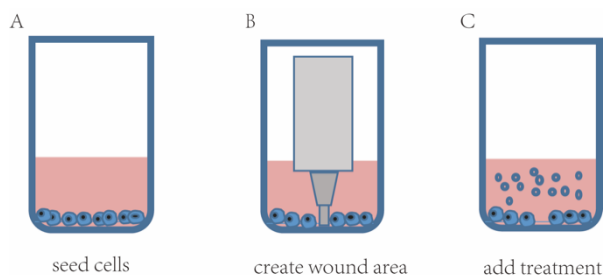


Figure 8: Scratch wound assay. Cells were seeded at the bottom of the wells at the confluence of 60-70% and were cultured to confluence 95-100% (A). Wound area was created by the WoundMaker (B). Treatment was added to the well and the wound healing process was captured by camera every 30 minutes (C).

Scratch wound assay was performed in Incucyte system (Figure 8). The proper cell number for 96-well plate was 40,000/well according to the area of the wells. The concentration of shikonin in DMEM was 0 μM , 1 μM , 2 μM , 3 μM , 4 μM and 5 μM . 40,000 cells were seeded in 96-well plate and incubated at 37°C and 5% CO₂ overnight. The ImageLock plate was removed from the incubator carefully, and wounds were created with the WoundMaker. After wounding, the media from each well was removed immediately and the wells were carefully washed with DMEM containing different concentration of shikonin twice. Cells were cultured with 100 μL DMEM containing different concentration of shikonin. The cell plate was placed into the Incucyte live-cell analysis system and allowed to warm at 37°C for 30 min prior to scanning. The wound healing pictures were captured every 30 min. The WoundMaker was washed and stored according to the wash protocol. The data was analyzed by the Incucyte S3 2019A. The relative wound density was studied and analyzed with GraphPad Prism 5. One-way ANOVA was used to compare means of cell index among the groups at 6 h, 12 h, 20 h, 24 h time points. A P value less than 0.05 was considered as statistically significant.

2.14 Inhibition of MDA-MB-231 and MCF-7 cells Invasion through Engineered Basement Membrane Gel in xCELLigence

The MDA-MB-231 and MCF-7 invasion experiment through engineered basement membrane showed that MDA-MB-231 invaded through but MCF-7 didn't. Shikonin in different concentrations was used to test the inhibition effect on the invasion process through the engineered basement membrane. The experiment was performed in xCELLigence RTCA DP. The plate map was showed as below (Figure 9). The cells well were designed into 6 groups. Cell number per well was 80,000. Serum free medium was used as control in the experiment. The protocol was as same as described before. The cell index was

studied and analyzed with GraphPad Prism 5. One-way ANOVA was used to compare means of cell index among the groups at 6 h, 12 h, 20 h, 24 h time points. A P value less than 0.05 was considered as statistically significant.

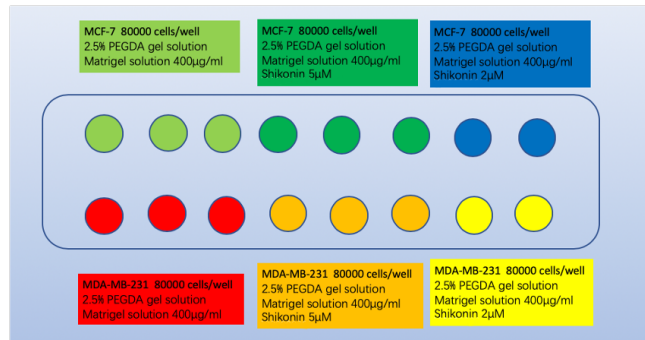


Figure 9: MDA-MB-231 and MCF-7 cells invasion through engineered membrane inhibited by shikonin. Each well was coated with 2.5 wt% PEGDA+400 µg/mL Matrigel Matrix. MDA-MB-231 and MCF-7 cells (80000 per well) were seeded into wells with different concentration of shikonin as described above.

2.15 Test the Permeability of Engineered Basement Membrane after Irradiation with MDA-MB-231 and MCF-7 in xCELLigence

The effect of irradiation on the engineered basement membrane was studied in xCELLigence RTCA DP. The experiment was designed into 5 groups. The cell number was 80,000 per well. The plate map was described as below (Figure 10). The dose of irradiation in groups were 0 Gy, 12.5 Gy, 25 Gy, 37.5 Gy and 50 Gy. The engineered basement membrane was composed of Matrigel matrix and PEGDA gel solution. The final concentration of PEGDA was 2.5 wt% and Matrigel matrix was 400 µg/mL. The day before the experiment, pipette tips, Eppendorf tubes, a tube of aliquoted Matrigel and the CIM Plate were stored at 4°C overnight. The cells were deprived from FBS 24 h before experiment.

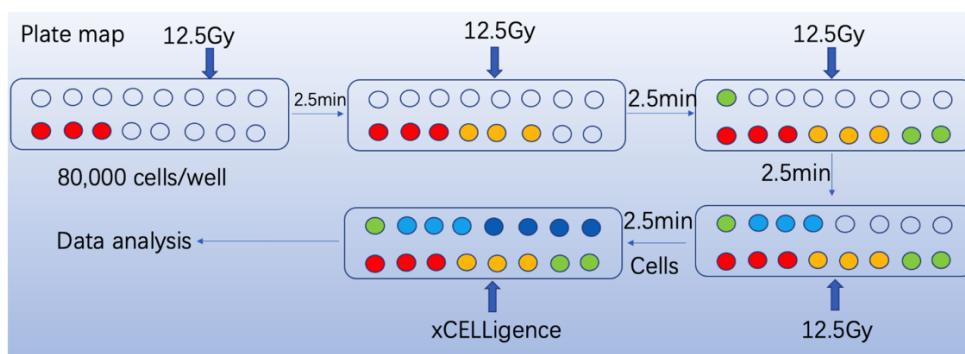


Figure 10: Test of the permeability of engineered basement membrane after irradiation. The wells in different colors were coated with engineered basement membrane. First, the red wells were coated and treated with irradiation (12.5 Gy). Then, the gold wells were coated with engineered basement membrane and the plate was treated with irradiation (12.5 Gy). The other wells were treated in the same way and does

of irradiation. The MDA-MD-231 and MCF-7 cells invasion experiment were performed in the plate as described before.

50 μ L of gel solution was added into the 50 Gy wells of upper chamber. 30 μ L of gel solution was carefully removed and the wells were exposed to the UV for 5 min for gel crosslink. Then the plate was placed into the X strahl cabinet for 2.5 min with a dose of 12.5 Gy. The plate was moved out and gel solution was added and removed as above. The irradiation was given at 5 Gy per minute with 200 KV and 15 MA. The 0 Gy wells were only exposed to the UV not exposed to the X ray. After irradiation the CIM plate coated with gels was incubated for 4 h at 37°C and 5% CO₂. Cells were added as same as the protocol described above. The MDA-MB-231 and MCF-7 cells invasion experiments with irradiation were repeated for 3 times. The cell index was studied and analyzed with GraphPad Prism 5. One-way ANOVA was used to compare means of cell index among the groups at 6 h, 12 h, 20 h, 24 h time points. A P value less than 0.05 was considered as statistically significant.

2.16 Test the Permeability of 2.5wt%PEGDA Membrane after Irradiation with MDA-MB-231 and MCF-7 in xCELLigence

MDA-MB-231 and MCF-7 cells invasion through 2.5 wt% PEGDA membrane was used to study whether irradiation effected the permeability of the engineered basement membrane by changing the permeability of 2.5 wt% PEGDA membrane. The 2.5 wt% PEGDA membrane was treated with 50 Gy irradiation and 0 Gy as control. MDA-MB-231 and MCF-7 cells were added 80,000/per well and protocol as same as above. Each experiment was performed at least in biological triplicates with four technical repeats in each CIM plate.

2.17 Immunofluorescence of Engineered Basement Membrane after Irradiation

Immunofluorescence staining was used to study the mechanism of how irradiation changed permeability of the engineered basement membrane. The engineered basement membrane was treated with 50 Gy irradiation and 0 Gy as control and the volume of the membrane was 100 μ L per well in 96-well plate. Gels were fixed with 4% PFA at 4°C overnight and transferred to 50% glucose at 4°C overnight. The gels were transferred to Tissue-Tek optimum cutting temperature at 4°C overnight and then stored at -80°C. The

gels were cut at 20 μm thick cryostat sections and stored at -80°C . The slides were washed carefully 2*5min in TBS plus 0.025% Triton X-100. The slides were blocked in 10% normal serum with 1% BSA in TBS for 2 h at room temperature. Primary antibody (Laminin ab11575 1:200; Collagen IV ab19808 1:400) was diluted in TBS with 1% BSA and applied to the slides at 4°C overnight. The slides were rinsed 2*5 min with TBS+0.025% Triton. Fluorophore-conjugated secondary antibody (ab150080 1:200) was diluted in TBS with 1% BSA and applied to the slides for 1 h at room temperature. Then slides were rinsed 3*5 min with TBS and mounted using fluoroshield medium and covered with coverslip. The slides were checked under fluorescence microscope. The excitation spectra of red fluorescence were 540-580 nm, DC 585 nm and emission spectra 592-668 nm. The excitation spectra of green fluorescence were 460-500 nm, DC 505 nm and emission spectra 512-542 nm.

3 RESULTS

3.1 MDA-MB-231 and MCF-7 GFP/RFP Transduction and Selection

MDA-MB-231 and MCF-7 cell wild type were transduced with GFP and RFP to show the live image of the cell migration and invasion with engineered basement membrane in 3D bioreactor. Wild type of MDA-MB-231 and MCF-7 were used as control. The green and red fluorescence of the wild type showed negative signal. In MDA-MB-231 GFP group, the GFP protein signal was positive while the red fluorescence was negative. In MDA-MB-231 RFP and MCF-7 RFP group, the RFP protein signal was positive while the green fluorescence was negative (Figure 11).

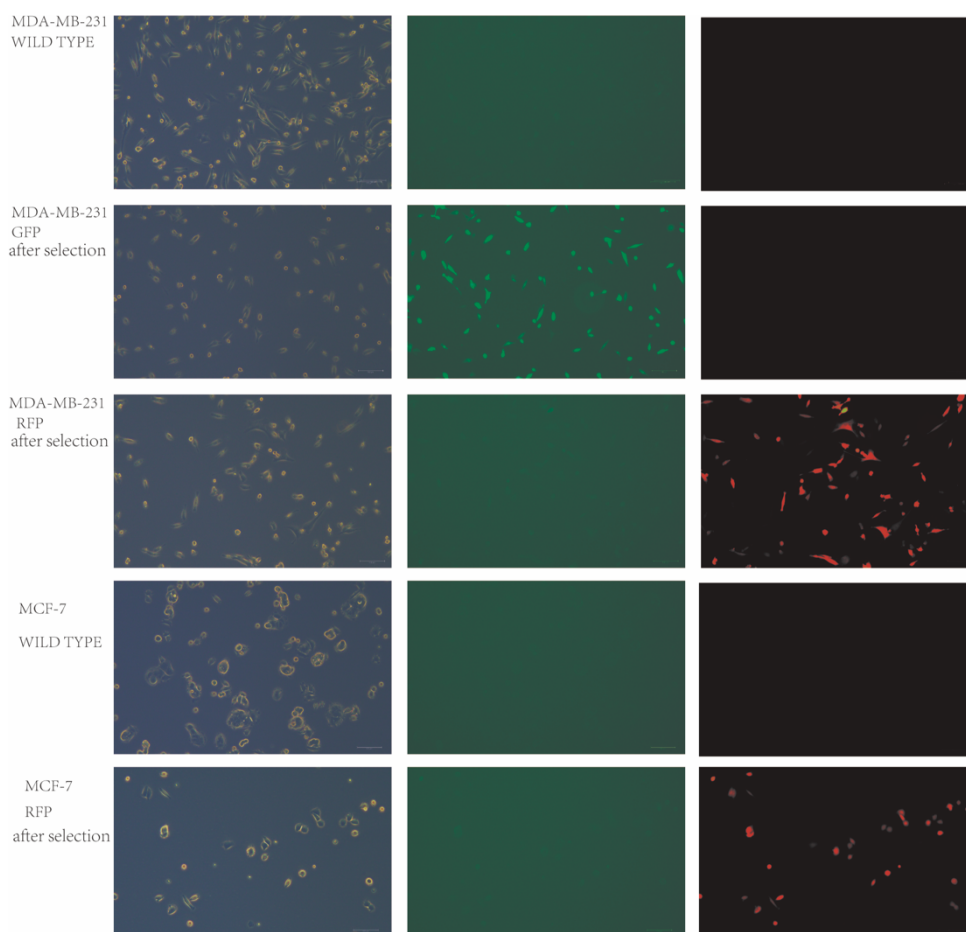


Figure 11: MDA-MB-231 and MCF-7 cell GFP/RFP transduction and selection. MDA-MB-231 and MCF-7 cell were selected and images were captured via fluorescence microscope using the filter set BP 525/50 for GFP and filter set BP 605/70 for RFP detection. Exposure time was 40 ms for all fluorescence images. Scale bar = 100 μ m.

3.2 3D Design of the Bioreactors

A series of 3D bioreactors were designed with Freecad software. All the details of the molds and devices was printed precisely. The main bioreactor was a rectangular box with 20 mm in length, 20 mm in width and 10 mm in height. The inner space was a rectangular box with 8 mm in length, 8 mm in width and 10 mm in height. At the top and bottom side of the bioreactor, two rectangular grooves with 1 mm in depth and 1 mm in width were printed precisely. The grooves were covered with a silicone cover at the top and a glass slide at the bottom of the bioreactor which were sealed with liquid silicone and incubated for 3 d. There's a cylindrical channel in the middle of the bioreactor which can connect with the perfusion set and ibidi pump system (Figure 12).

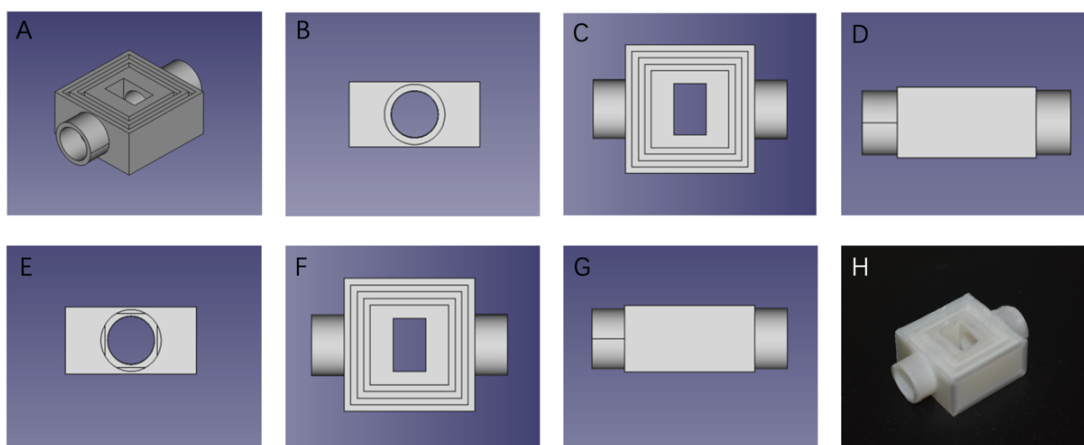


Figure 12: 3D views of the bioreactor design. Axonometric view, the main bioreactor was 20 mm in length, 20 mm in width and 10 mm in height (A). Front view, the inner diameter of the channel was 7.2 mm and the outer diameter of the channel was 9.2 mm (B). Top view, the inner space was 8 mm in length, 8 mm in width and 10 mm in height (C). Right view, the size of the right surface was 20 mm*10 mm (D). Rear view, the inner diameter of the channel was 7.2 mm and the outer diameter of the channel was 9.2 mm (E). Bottom view, the inner space was 8 mm in length, 8 mm in width and 10 mm in height (F). Left view, the size of the left surface was 20 mm*10 mm (G). The bioreactor was printed by desktop 3D printer (H).

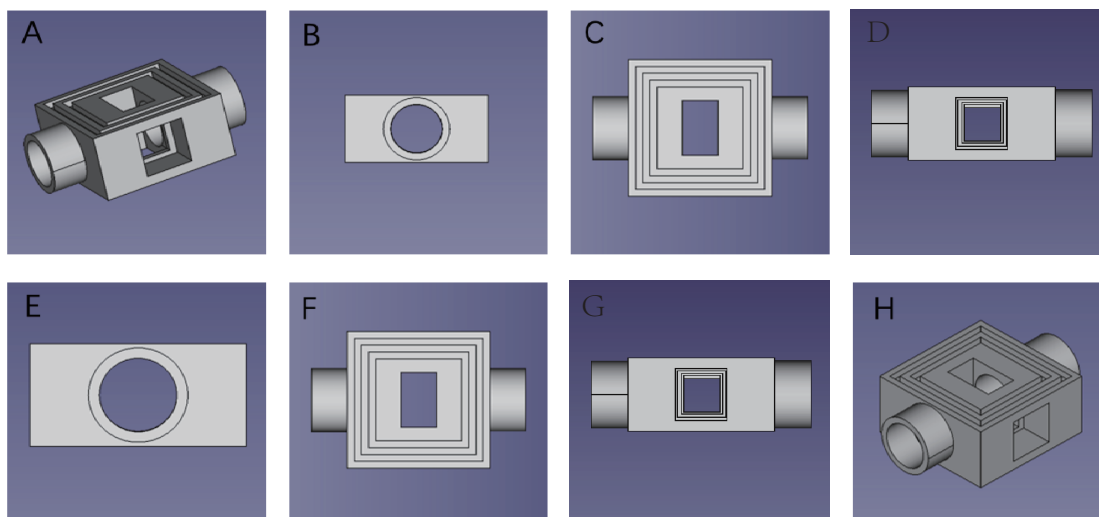


Figure 13: 3D views of the bioreactor with window design. Axonometric view, the main bioreactor was 20 mm in length, 20 mm in width and 10 mm in height. The size of the window on the left was 7 mm*7 mm and the size of the bottom surface was 5 mm*5 mm (A). Front view, the inner diameter of the channel was 7.2 mm and the outer diameter of the channel was 9.2 mm (B). Top view, the inner space was 8 mm in length, 8 mm in width and 10 mm in height (C). Right view, the size of the right surface was 20 mm*10 mm (D). Rear view, the inner diameter of the channel was 7.2 mm and the outer diameter of the channel was 9.2 mm (E). Bottom view, the inner space was 8 mm in length, 8 mm in width and 10 mm in height (F). Left view, the size of the window on the left was 7 mm*7 mm and the size of the bottom surface was 5 mm*5 mm (G). Axonometric view of the bioreactor (H).

A series of bioreactors with windows at the side were designed with Freecad based on the main bioreactors. The main body was as same as the main bioreactor. On the left side of the bioreactor, a window with 7 mm in width and 7 mm in length was designed and were covered with glass slide with proper size. The glass window was sealed with liquid silicone and solidified in incubator for 3 d. The bioreactor can be used to observe the living status of the 3D culturing cells with a light sheet microscope (Figure 13). The size of the bioreactors can be changed according to the size of the gel and perfusion channel.

3.3 3D Design of the Molds and the Devices

Molds and devices were designed for fabrication of the silicone cover and blue silicone ring. The mold for silicone cover was a square model with 22 mm in length and 22 mm in width. There are two grooves in the model with cross section 1 mm in width and 1 mm in depth. The liquid silicone was added into the square model and after 3 d incubation the silicone cover was fabricated successfully. The devices for the blue silicone ring were composed with upper part and lower part. The upper part was a hollow cylinder which was 7 mm in inner diameter and 8 mm in outer diameter. The lower part of the device

with a cylinder in the middle was designed to fabricate the blue silicone ring which can be used to connect the perfusion set (Figure 14).

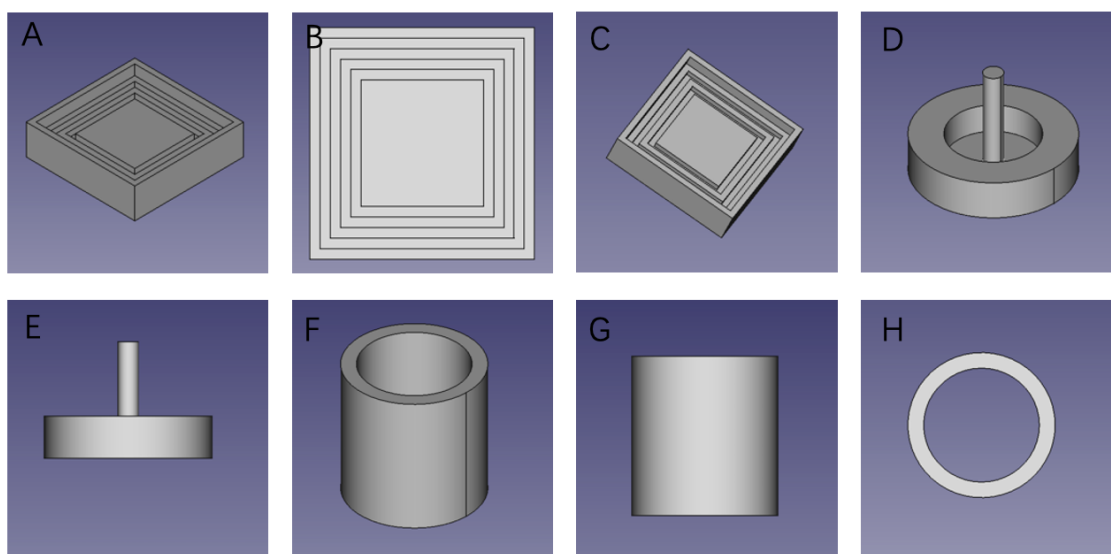


Figure 14: The molds and devices for the silicone cover and the blue silicone ring in different views. Axonometric view, the mold for the silicone cover was 22 mm in length, 22 mm in width and 6 mm in height (A). Top view, the inner diameter of the mold was 20 mm*20 mm. Two positive rectangle circles were designed with 1 mm in length and 1 mm in height to generate two grooves in the silicone cover (B). Axonometric view, the mold for the silicone cover was 22 mm in length, 22 mm in width and 6 mm in height (C). Axonometric view, the bottom device for the blue silicone ring was 16 mm in outer diameter and 9 mm in inner diameter (D). Front view, the diameter of the center cylinder was 2 mm (E). Axonometric view, size of the cylinder was 7 mm in inner diameter and 8 mm in outer diameter (F). Front view of the device for blue silicone ring (G). Top view of the device for blue silicone ring (H).

3.4 Casting of the Silicone Covers and Blue Silicone Rings

The molds and devices for the silicone cover and the blue silicone ring were precisely printed as design with PLA by desktop 3D printer. The upper part and lower part were combined together. Equal amounts of liquid parts A and B were mixed thoroughly and poured into the molds. After 2 h incubation, the blue silicone ring was fabricated successfully. For fabrication of the silicone cover, the SYLGARDTM 184 silicone elastomer base and curing agent was mixed 10:1 in volume thoroughly. The mixture was added into the mold and incubated at 55°C for 3 d. The silicone cover for the bioreactor was successfully fabricated (Figure 15). The blue silicone ring was soft rubber and elastic and used to avoid leaking of the connections. The transparent silicone cover was mild hard and transparent which can be used for injection of the gel solution.

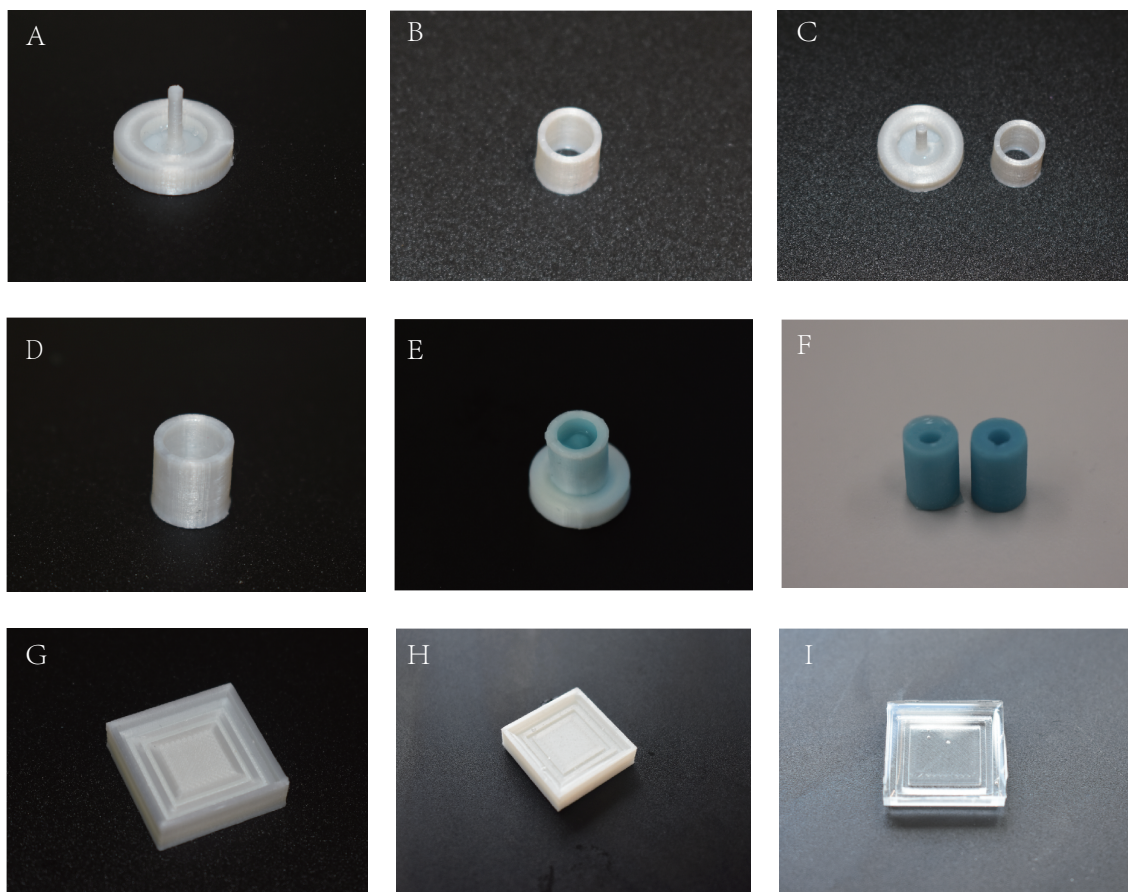


Figure 15: The views of printed devices and molds for blue silicon ring and silicone cover. Axonometric view of the bottom device for blue silicone ring, the device was 16 mm in outer diameter and 9 mm in inner diameter. The center cylinder was 2 mm in diameter (A). Axonometric view of the upper device for blue silicone ring, the device was 7 mm in inner diameter and 8 mm in outer diameter (B). Axonometric view of the upper and bottom devices (C). Front view of the upper part of the device (D). Blue silicone in the combined devices, the blue silicone was added into the devices for 30 min and the blue silicone ring was fabricated (E). Axonometric view of the blue silicone rings; the blue silicone rings were soft and used for connection of the perfusion system (F). Axonometric view of the mold for silicone cover (G). Axonometric view of the mold for silicone cover with silicone in the mold, the silicone in the mold was incubated in incubator for 3 d to get the silicone cover (H). Axonometric view of the silicone cover generated in the mold after incubation which was used to cover the top of the bioreactor and sealed with silicone (I).

3.5 3D Printing of the Bioreactor and Sealing of the Bioreactor

The bioreactor with widow was printed precisely with PLA by desktop 3D printer. The top of the bioreactor was covered with glass slide and the bottom of the bioreactor was covered with transparent silicone cover. The windows at the left and right side were also covered with glass slides with 6 mm*6 mm in size. The sealing procedure was proceeded in three steps. Firstly, the window was sealed with glass slide using liquid silicone and incubated at 55°C for 3 d. Then the transparent silicone cover was used to seal the bottom using liquid silicone. The incubation time was 3 d at 55°C. Finally, the glass slide for the top was sealed with liquid silicone and incubated at 55°C for 3 d. The bioreactor was used

in 3 layers coculture and living observing of the migration and invasion of the cells with a light sheet microscope.

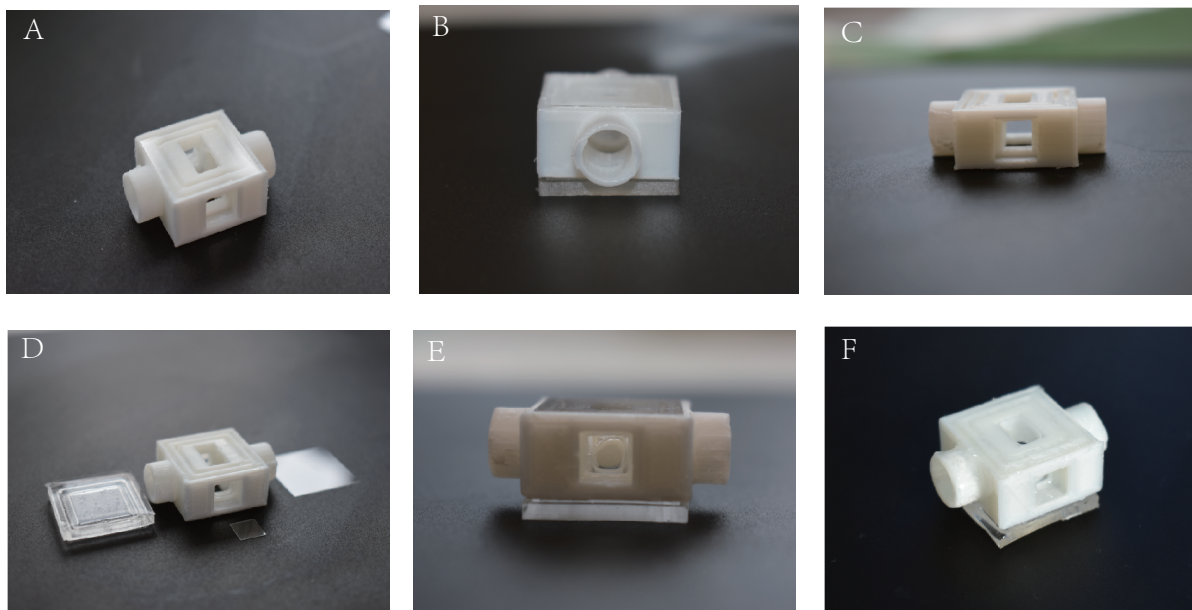


Figure 16: The bioreactor printed with PLA and sealed with glass slides and silicone cover. Axonometric view of the bioreactor, the bioreactor was printed with PLA by desktop 3D printer (A). Front view of the bioreactor, the bioreactor was covered with glass slide on the top and side window while the bottom was covered with silicone cover (B). Axonometric view of the bioreactor, the side windows were designed to get living image under light sheet microscope during perfusion (C). Axonometric view of the bioreactor and the covers, the glass slides were used to cover the top and side windows while the silicone cover was used for the bottom (D). Side view of the bioreactor with windows for overserving with a light sheet microscope (E). Axonometric view of the assembled bioreactor, the bottom cover was sealed with liquid silicone in incubator for 3 days and then the top and side window were sealed in the same way (F).

3.6 Test of the 3D Bioreactor with Continuous Perfusion

The multilayer gel approach in 3D bioreactor system was established successfully with continuous perfusion. MCF-7 RFP cells were cultured in the bioreactor with controllable perfusion for 48 h. No leaking was found during the test (Figure 17). The MCF-7 RFP cells were found in the outer layer and no cells were found in the inner layer.

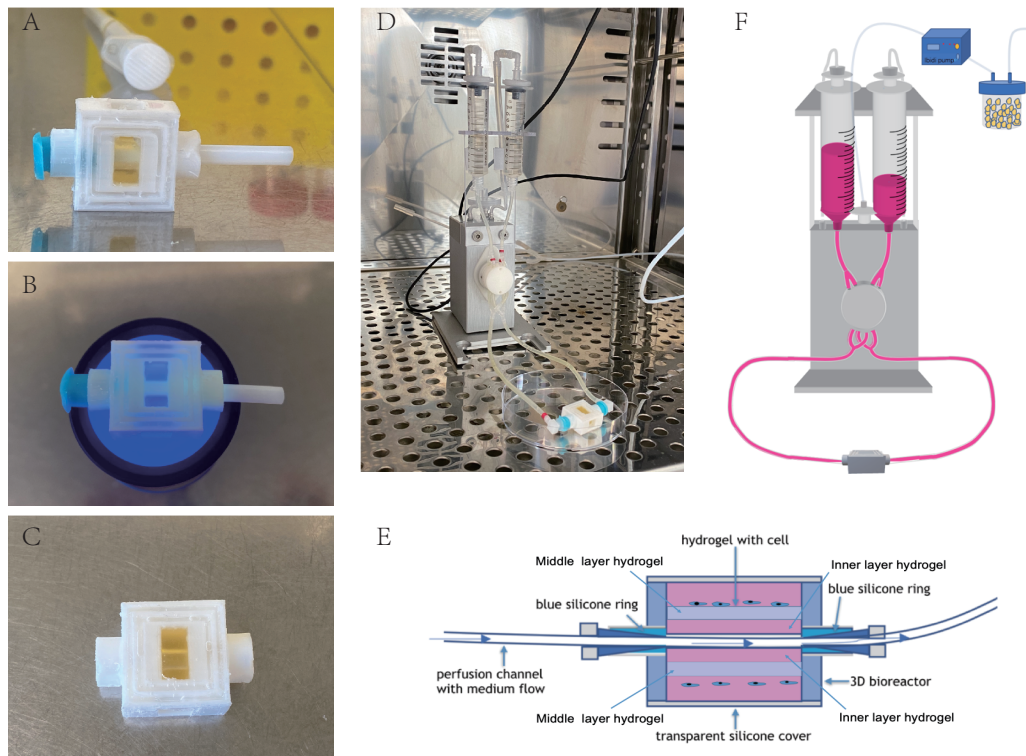


Figure 17: The 3D bioreactor with perfusion system. 3D bioreactor with cell embedded gel, the gel solution with cells was injected into the bioreactor around the cylinder (A). UV exposure of the gel in the bioreactor (B). Cell embedded gel with central channel in 3D bioreactor (C). The bioreactor connected with the perfusion set and the fluidic unit; the fluidic unit connected with pump was used to generated proper pressure for medium flow in the system (D). Cells were embedded outer layer gel and the middle layer gel was the engineered basement membrane (E). 3D bioreactor with continuous perfusion (F).

3.7 Gelation Test of Different Concentration of Matrigel Matrix

The gelation test of different concentration of Matrigel matrix was performed in 96-well plate. Matrigel matrix was diluted into Different concentration (200 $\mu\text{g/mL}$, 400 $\mu\text{g/mL}$, 800 $\mu\text{g/mL}$, 1200 $\mu\text{g/mL}$, 1600 $\mu\text{g/mL}$) with serum free medium. The gel suspended in the diluted solution was found in all wells except control well. The results showed that the Matrigel matrix concentration higher than 200 $\mu\text{g/mL}$ can form gel after 4 h incubation at 37°C and 5% CO_2 .

Table 8: Gel formation of different concentration of Matrigel

Concentration of Matrigel	Gel formation
200 $\mu\text{g/mL}$	Yes
400 $\mu\text{g/mL}$	Yes

800 $\mu\text{g/mL}$	Yes
1200 $\mu\text{g/mL}$	Yes
1600 $\mu\text{g/mL}$	Yes

3.8 Gelation Test of PEGDA 20,000 Gel Solution

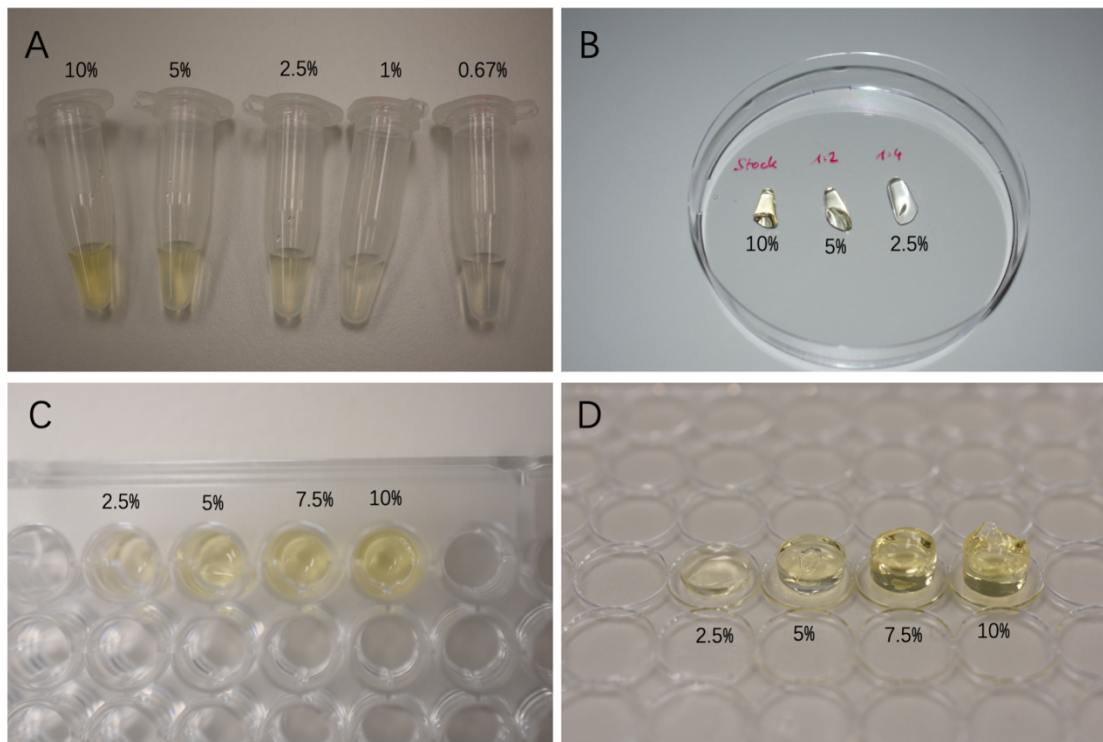


Figure 18: Possibility of gel casting with different concentration of PEGDA 20,000. PEGDA 20,000 solution + LAP of different concentrations was in Eppendorf tubes. The concentrations were 10 wt%, 5 wt%, 2.5 wt%, 1 wt%, 0.67 wt% (A). Gels of PEGDA 20,000 in different concentrations, the 2.5 wt%, 5 wt%, 10 wt% solution formed gels successfully after 5 min UV exposure while 1 wt% and 0.67 wt% solutions didn't form gel (B). PEGDA 20,000 solution + LAP of different concentrations in 96-well plate, the concentrations were 2.5 wt%, 5 wt%, 7.5 wt% and 10 wt% (C). Gels of PEGDA 20,000 in different concentrations, the 2.5 wt%, 5 wt%, 7.5 wt%, 10 wt% solution formed gels in 96-well plate after 5 min UV exposure (D).

To overcome the limitation of the long-time gelation of the Matrigel matrix membrane, a new component PEGDA was added to the gel. PEGDA 20,000 was taken in this work due to its proper size of the gel porous and quick gelation. The gelation test of different concentration of PEGDA 20,000 solution was performed in Eppendorf tubes and 96-well plate. PEGDA 20,000 was mixed with LAP and diluted with serum free medium. The gel solution was exposed to UV light for 5 min. The results showed that the 2.5 wt%, 5 wt%,

7.5 wt%, 10 wt% solution formed gels in 96-well plate after 5 min UV exposure. The 0.67 wt% and 1 wt% gel solution failed in gelation after 5 min UV exposure. Taken together, PEGDA 20,000 solution with concentration higher than 2.5 wt% formed gel successfully after UV exposure.

3.9 Test the Permeability of Matrigel Matrix Gels with Different Concentration in xCELLigence

Experiments were performed to test the proper concentration of Matrigel matrix gels for tumor cell invasion in xCELLigence. The first experiment was designed to find out the proper number of cells for the invasion experiments. The result showed that the cell index at 24 h was up to only 0.4. At 6 h time point, the difference of cell index between 0 $\mu\text{g}/\text{mL}$ group and 300 $\mu\text{g}/\text{mL}$ group was non-significant. The differences of other groups compared to the control group at 6 h, 12 h, 20 h, 24 h were significant. It indicated that the cell index was too low and cell number per well was not enough. There were not enough cells invaded through the Matrigel matrix membrane.

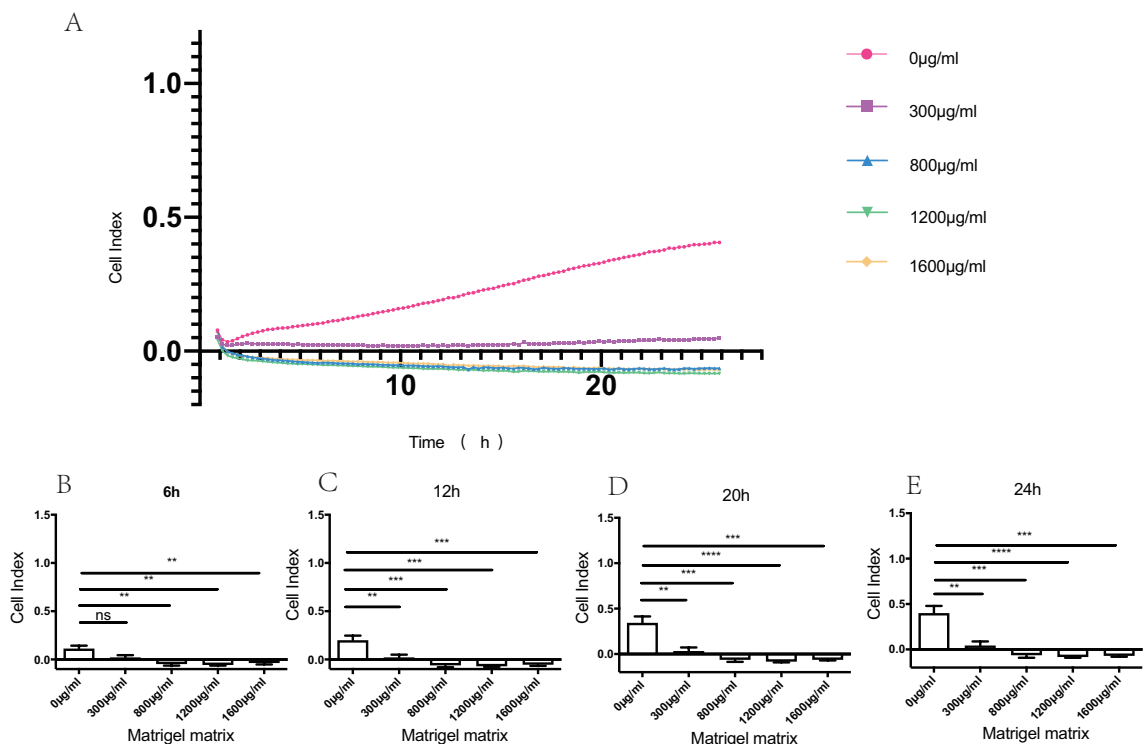


Figure 19: MDA-MB-231 cells invasion through Matrigel matrix gels with different concentration in xCELLigence, 25000 cells per well, (mean \pm SD, n=3). MDA-MB-231 cells invasion through Matrigel matrix gel with concentration 0 $\mu\text{g}/\text{mL}$, 300 $\mu\text{g}/\text{mL}$, 800 $\mu\text{g}/\text{mL}$, 1200 $\mu\text{g}/\text{mL}$, 1600 $\mu\text{g}/\text{mL}$, 25000 cells per well (A). 6 h after starting, there were significant difference between 0 $\mu\text{g}/\text{mL}$ group and 800 $\mu\text{g}/\text{mL}$, 1200 $\mu\text{g}/\text{mL}$ and 1600 $\mu\text{g}/\text{mL}$ groups (B). 12 h after starting, there were significant difference between 0 $\mu\text{g}/\text{mL}$

group and 300 $\mu\text{g}/\text{mL}$, 800 $\mu\text{g}/\text{mL}$, 1200 $\mu\text{g}/\text{mL}$ and 1600 $\mu\text{g}/\text{mL}$ groups (C). 20 h after starting, there were significant difference between 0 $\mu\text{g}/\text{mL}$ group and 300 $\mu\text{g}/\text{mL}$, 800 $\mu\text{g}/\text{mL}$, 1200 $\mu\text{g}/\text{mL}$ and 1600 $\mu\text{g}/\text{mL}$ groups (D). 24 h after starting, there were significant difference between 0 $\mu\text{g}/\text{mL}$ group and 300 $\mu\text{g}/\text{mL}$, 800 $\mu\text{g}/\text{mL}$, 1200 $\mu\text{g}/\text{mL}$ and 1600 $\mu\text{g}/\text{mL}$ groups (E).

According to the cell index in last experiment was lower than 0.5, the possible reason was the cell number per well was not enough. The MDA-MB-231 cell number was set at 40,000 per well in the next experiment. The result showed that the cell index of the control group was around 1.0. At time points 6 h, 12 h, 20 h and 24 h, the difference of the cell index between control group and the other groups were compared. There was no significant difference between the control group and the groups (300 $\mu\text{g}/\text{mL}$ and 400 $\mu\text{g}/\text{mL}$) at all time points, but the difference between 0 $\mu\text{g}/\text{mL}$ group and 800 $\mu\text{g}/\text{mL}$ group was significant. It indicated that the MDA-MB-231 cells invaded through the Matrigel matrix membrane as the same as the control group when the concentration was set at 300 $\mu\text{g}/\text{mL}$ and 400 $\mu\text{g}/\text{mL}$.

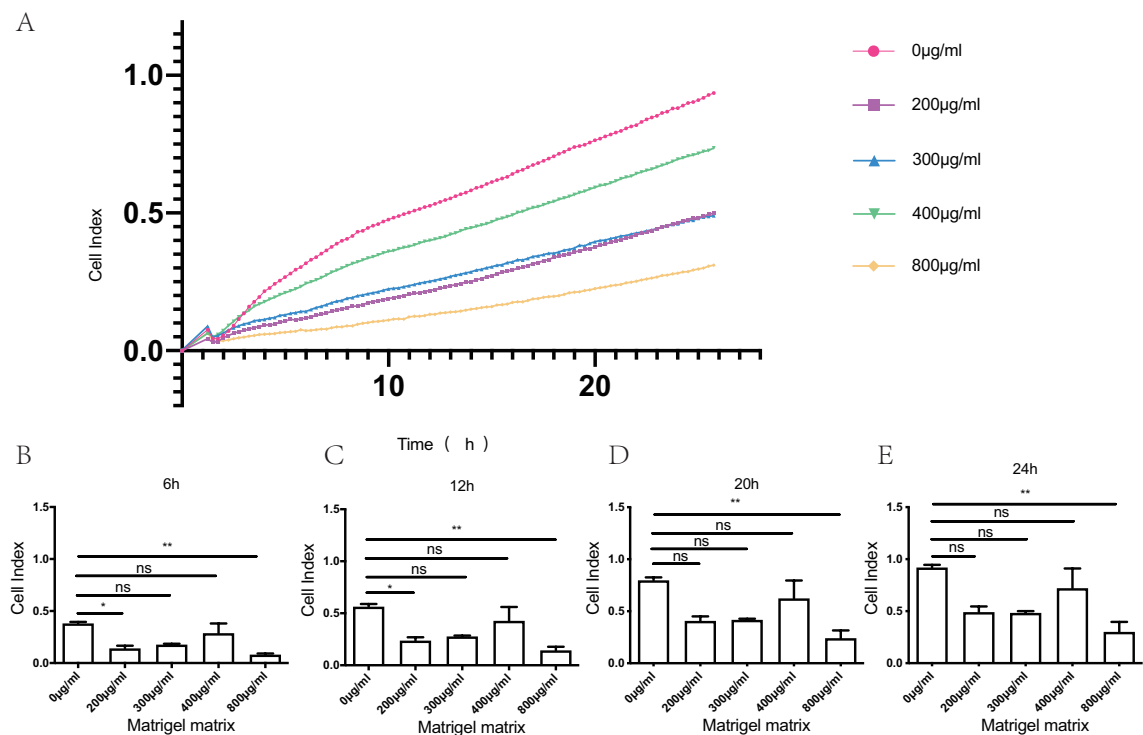


Figure 20: MDA-MB-231 cells invasion through Matrigel matrix gels with different concentration in xCELLigence, 40000 cells per well, (mean \pm SD, n=3). MDA-MB-231 cells invasion through Matrigel matrix gel with concentration 0 $\mu\text{g}/\text{mL}$, 200 $\mu\text{g}/\text{mL}$, 300 $\mu\text{g}/\text{mL}$, 400 $\mu\text{g}/\text{mL}$, 800 $\mu\text{g}/\text{mL}$, 40000 cells per well (A). 6 h after starting, there were significant difference between 0 $\mu\text{g}/\text{mL}$ group and 200 $\mu\text{g}/\text{mL}$, 800 $\mu\text{g}/\text{mL}$ groups. There was no significant difference between 0 $\mu\text{g}/\text{mL}$ group and 300 $\mu\text{g}/\text{mL}$, 400 $\mu\text{g}/\text{mL}$ groups (B). 12 h after starting, there were significant difference between 0 $\mu\text{g}/\text{mL}$ group and 200 $\mu\text{g}/\text{mL}$, 800 $\mu\text{g}/\text{mL}$ groups. There was no significant difference between 0 $\mu\text{g}/\text{mL}$ group and 300 $\mu\text{g}/\text{mL}$, 400 $\mu\text{g}/\text{mL}$ groups (C). 20 h after starting, there was significant difference between 0 $\mu\text{g}/\text{mL}$ group and 800 $\mu\text{g}/\text{mL}$ groups. There was no significant difference between 0 $\mu\text{g}/\text{mL}$ group and 200 $\mu\text{g}/\text{mL}$, 300 $\mu\text{g}/\text{mL}$, 400 $\mu\text{g}/\text{mL}$ groups (D). 24 h after starting, there was significant difference between 0 $\mu\text{g}/\text{mL}$ group and 800

$\mu\text{g/mL}$ group. There was no significant difference between 0 $\mu\text{g/mL}$ group and 200 $\mu\text{g/mL}$, 300 $\mu\text{g/mL}$, 400 $\mu\text{g/mL}$ groups (E).

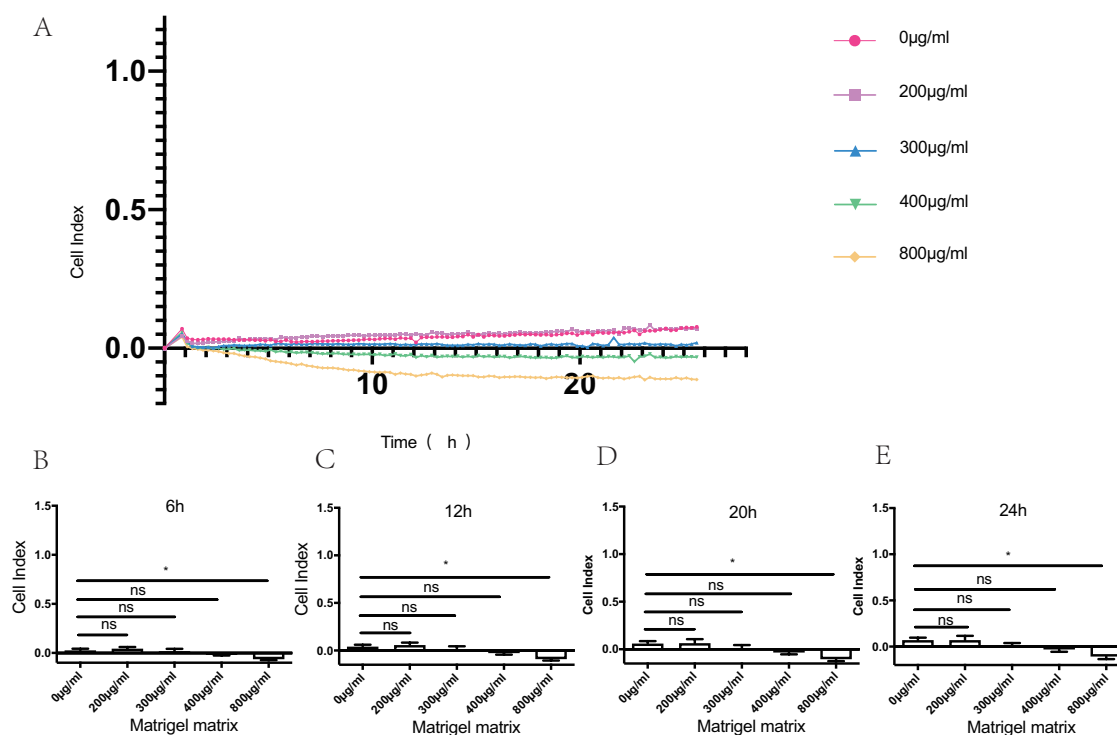


Figure 21: MCF-7 cells invasion through Matrigel matrix gels with different concentration in xCELLigence, 40000 cells per well, (mean \pm SD, n=3). MCF-7 cells invasion through Matrigel matrix gel with concentration 0 $\mu\text{g/mL}$, 200 $\mu\text{g/mL}$, 300 $\mu\text{g/mL}$, 400 $\mu\text{g/mL}$, 800 $\mu\text{g/mL}$, 40000 cells per well (A). 6 h, 12 h, 20 h, 24 h after starting, there was significant difference between 0 $\mu\text{g/mL}$ group and 800 $\mu\text{g/mL}$ group. There was no significant difference between 0 $\mu\text{g/mL}$ group and 200 $\mu\text{g/mL}$, 300 $\mu\text{g/mL}$, 400 $\mu\text{g/mL}$ groups (B, C, D, E).

Non-invasive cancerous cell line MCF-7 cell was used to test the permeability of the Matrigel matrix membrane as negative control. The cell number was 40,000 per well and the concentration was set at 200 $\mu\text{g/mL}$, 300 $\mu\text{g/mL}$, 400 $\mu\text{g/mL}$ and 800 $\mu\text{g/mL}$. The result showed that the cell index was lower than 0.1. At time points 6 h, 12 h, 20 h and 24 h, the difference of the cell index between control group and the other groups were compared. There was no significant difference of permeability between the control group and the groups (200 $\mu\text{g/mL}$, 300 $\mu\text{g/mL}$ and 400 $\mu\text{g/mL}$) at all time points, but the difference between 0 $\mu\text{g/mL}$ group and 800 $\mu\text{g/mL}$ group was significant.

3.10 Test the Permeability of PEGDA Gels with Different Concentration in xCELLigence

PEGDA gel due to its fast gelation, was supposed to be a possible component of the engineered basement membrane. Two experiments were performed to test the permeability

of PEGDA gels with different concentration in xCELLigence. One was designed to find out the proper number of cells for the PEGDA gel invasion. The result showed that 6 h, 12 h, 20 h, 24 h after starting, there was no significant difference between the groups with same concentration of PEGDA gels which differ in cell number. However, the group with 80,000 cells per well in 2.5 wt% PEGDA gels had a higher value of cell index.

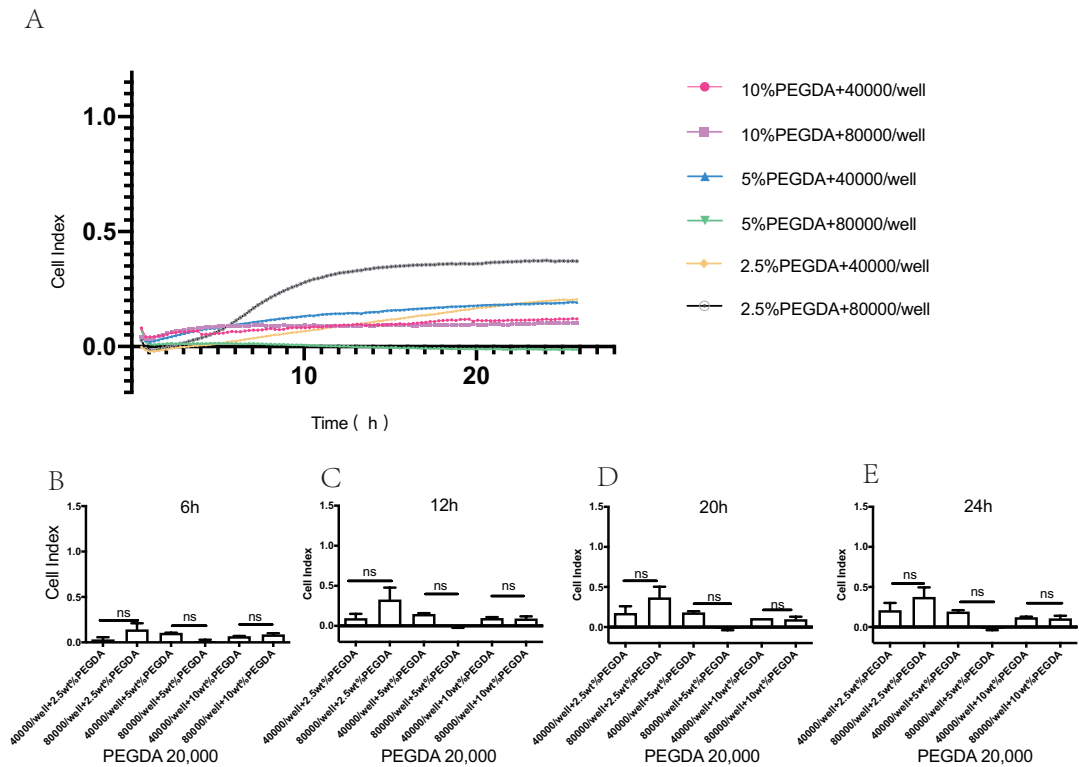


Figure 22: MDA-MB-231 cells invasion through PEGDA gels with different concentration (mean \pm SD, n=3). 40,000 per well and 80,000 per well MDA-MB-231 cells invasion through PEGDA gels with concentration 2.5 wt%, 5 wt%, 10 wt%(A). 6 h, 12 h, 20 h, 24 h after starting, there was no significant difference between the groups which had same concentration of PEGDA gels but differ in MDA-MB-231 cell number. However, the group with 80,000 cells per well in 2.5 wt% PEGDA gels had a higher value of cell index (B, C, D, E).

The MCF-7 invasion experiment through PEGDA gels was performed in xCELLigence and designed as the same condition as the MDA-MB-231 cells. The result showed that 6 h, 12 h, 20 h, 24 h after starting, there was no significant difference between the groups which had similar PEGDA concentrations but different amounts of MCF-7 cells.

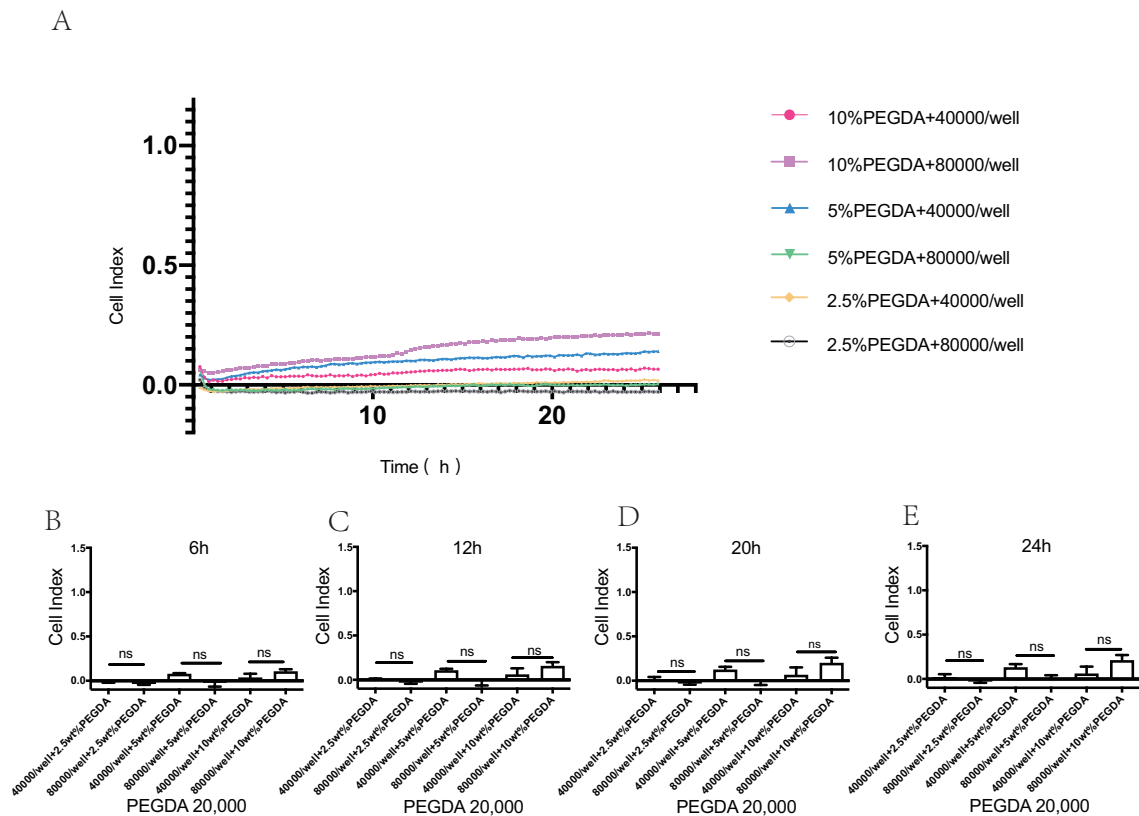


Figure 23: MCF-7 cells invasion through PEGDA gels with different concentration (mean \pm SD, n=3). 40,000 per well and 80,000 per well MCF-7 cells invasion through PEGDA gels with concentration 2.5 wt%, 5 wt%, 10 wt%(A). 6 h, 12 h, 20 h, 24 h after starting, there was no significant difference between the groups which had same concentration of PEGDA gels but differ in MCF-7 cell number (B, C, D, E).

3.11 Test the Permeability of Engineered Basement Membrane Gels with Different Concentration in xCELLigence

Accordingly, 2.5 wt% PEGDA PEGDA and 200 μ g/mL, 400 μ g/mL Matrigel matrix was suitable for the invasion of MDA-MB-231 and MCF-7 cells. Based on the results above, the concentration was set at 2.5 wt% PEGDA+200 μ g/mL Matrigel matrix and 2.5 wt% PEGDA+400 μ g/mL Matrigel matrix. With both 2.5 wt% PEGDA+200 μ g/mL Matrigel matrix and 2.5 wt% PEGDA+400 μ g/mL Matrigel matrix groups, there was significant difference between MDA-MB-231 and MCF-7 cells at 12 h, 20 h, 24 h after starting. It indicated that the MDA-MB-231 cells invaded through the membrane while the MCF-7 didn't invade through. In the further experiments, 2.5 wt% PEGDA+400 μ g/mL Matrigel matrix was used as the engineered basement membrane because of a higher concentration of Matrigel matrix provide more laminin and collagen IV for the membrane (Figure 24).

A

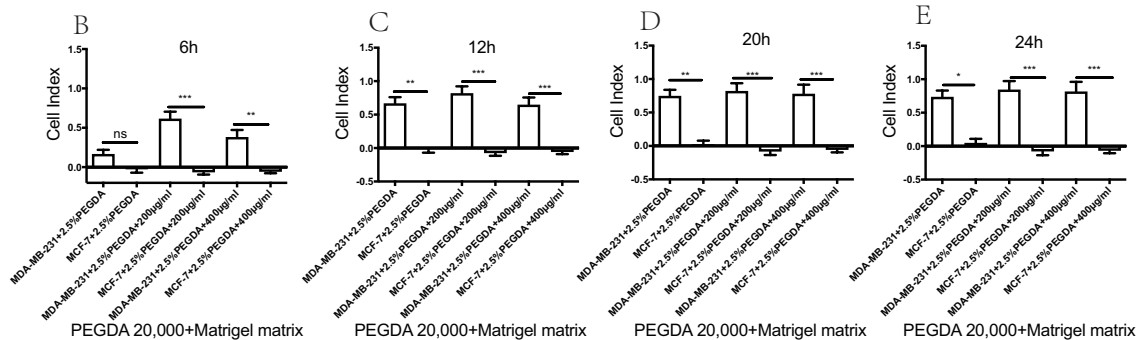
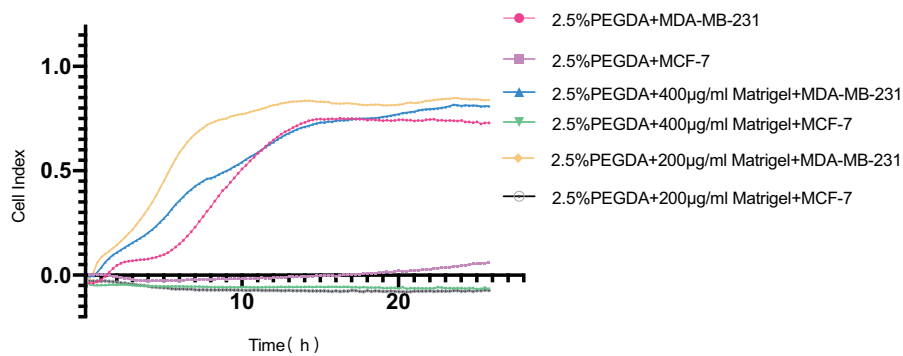


Figure 24: MDA-MB-231 and MCF-7 cells invasion through engineered basement membrane gels with different concentration, 80,000 cells per well (mean \pm SD, n=3). MDA-MB-231 and MCF-7 cells invasion through engineered basement membrane (A). 6 h after starting, in 2.5 wt% PEGDA+200 μ g/mL Matrigel matrix groups, there was significant difference between MDA-MB-231 and MCF-7 cells in cell index (B). 12 h, 20 h, 24 h after starting, there was significant difference between MDA-MB-231 and MCF-7 cells in all compared groups (2.5 wt% PEGDA, 2.5 wt% PEGDA+200 μ g/mL Matrigel matrix, 2.5 wt% PEGDA+400 μ g/mL Matrigel matrix) (C, D, E).

3.12 MDA-MB-231 and MCF-7 Cell Migration Inhibited by Shikonin in Incucyte (Scratch Wound Assay)

Shikonin, which isolated from a traditional chinese medicinal herb zicao, has been reported as an inhibitor of MDA-MB-231 and MCF-7 cell migration and invasion (Jang et al. 2014). In this study, shikonin was used to test the inhibition of the migration and invasion through the engineered basement membrane.

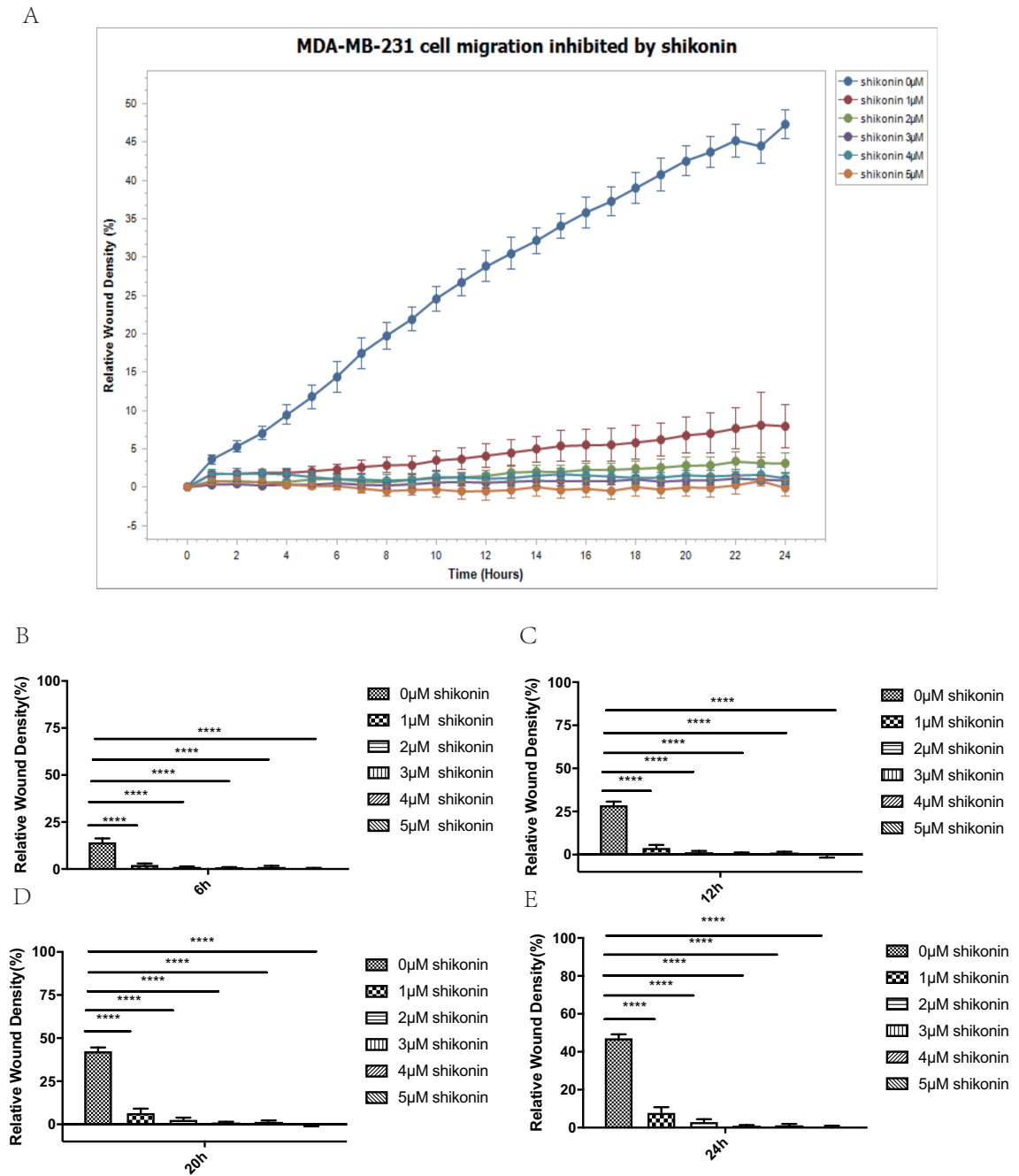


Figure 25: MDA-MB-231 cell migration inhibited by shikonin in Incucyte (mean±SD, n=3). MDA-MB-231 cell migration in Incucyte; $\%RWD(t) = 100 \cdot \frac{(w(t)-w(0))}{(c(t)-w(0))}$, $w(t)$ =Density of wound region at time, (t) $c(t)$ =Density of cell region at time, (t) (A). 6h, 12h, 20h, 24h after starting, there was significant difference between 0 µM group and the other groups. The migration of MDA-MB-231 cell migration was significantly inhibited (B, C, D, E).

Wound healing assay was used to test the effect of shikonin on the MDA-MB-231 and MCF-7 cell migration. The result showed that 6 h, 12 h, 20 h, 24 h after starting, the migration of MDA-MB-231 cells in 1 µM, 2 µM, 3 µM, 4 µM, 5 µM groups was significantly inhibited compared to 0 µM group. Pictures at the wound area in each group was captured every hour. Wound area pictures at 0 h, 24 h after scratch were captured. The

wound area at 24 h were significantly larger in shikonin groups than in the control group (Figure 25, Figure 26).

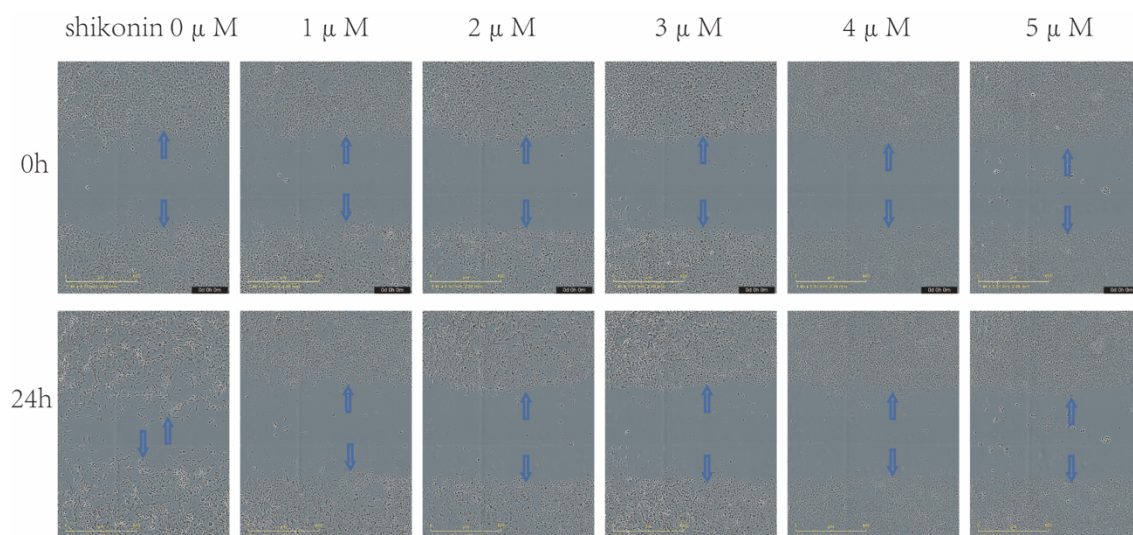


Figure 26: MDA-MB-231 cell migration inhibited by shikonin in Incucyte. Wound area at 24 h in shikonin groups were larger than in the control group (0 h, 24 h). The blue arrows indicated the border of the wound area.

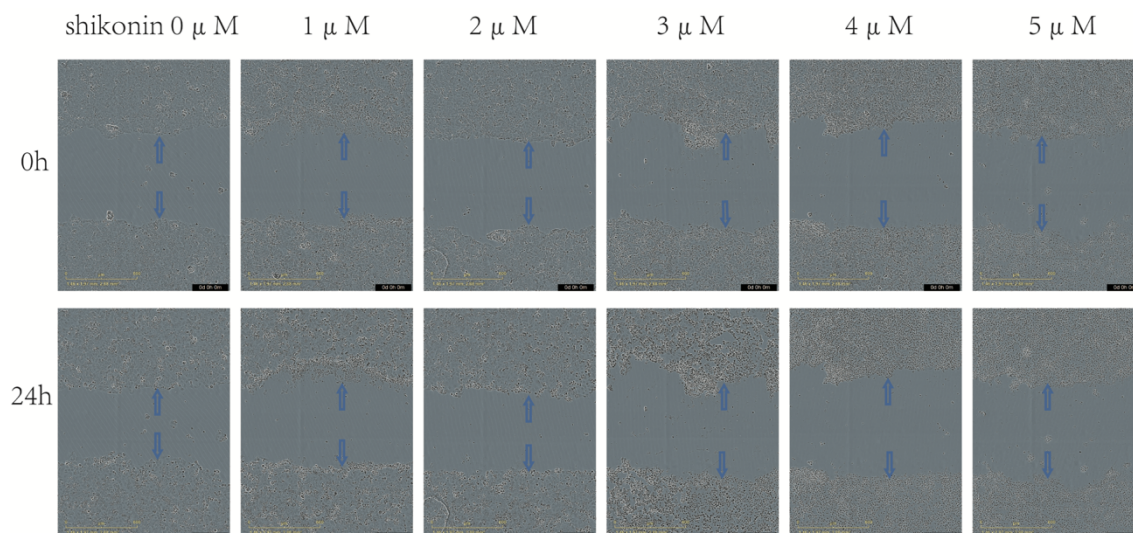
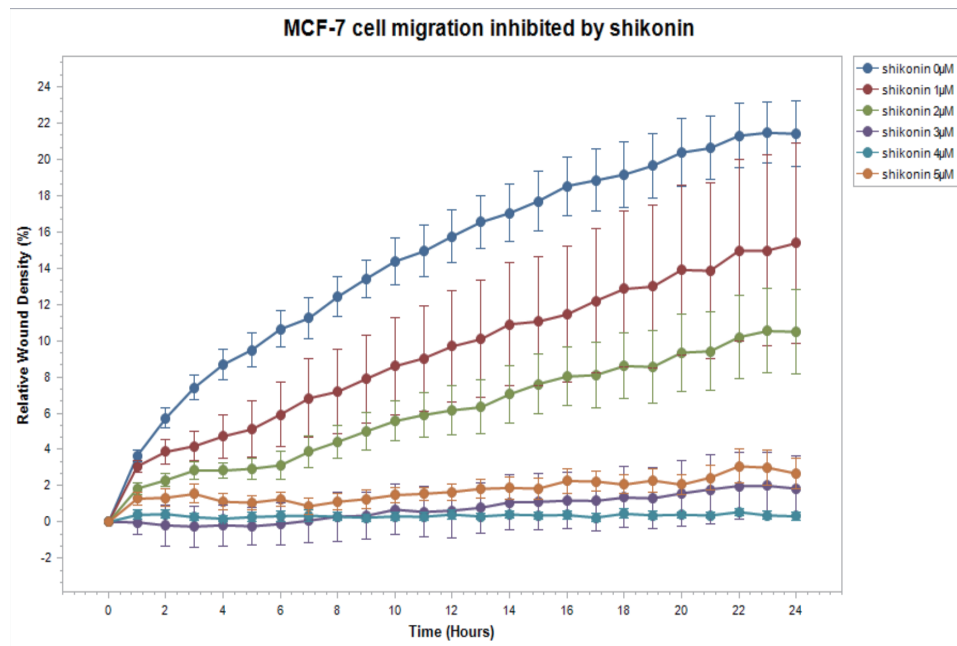
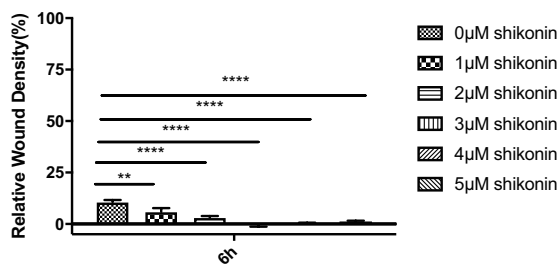


Figure 27: MCF-7 cell migration inhibited by shikonin in Incucyte. Wound area at 24 h in shikonin groups were larger than in the control group (0 h, 24 h). The blue arrows indicated the border of the wound area.

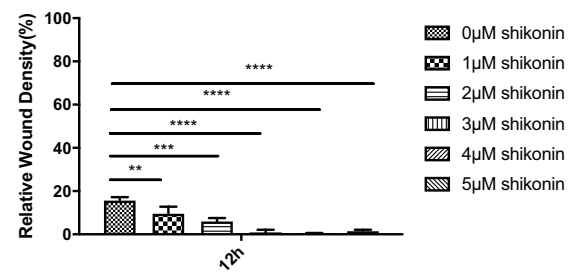
A



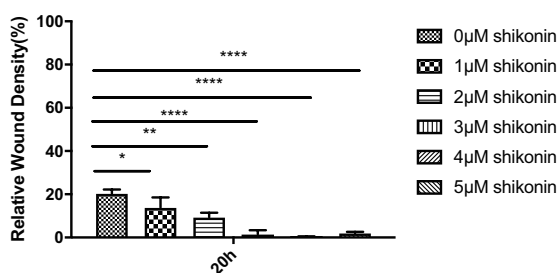
B



C



D



E

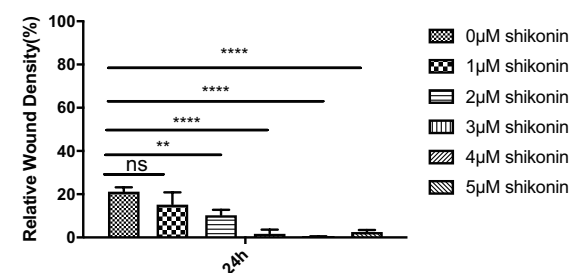


Figure 28: MCF-7 cell migration inhibited by shikonin in Incucyte (mean±SD, n=3). MCF-7 cell migration inhibited by different concentration of shikonin (A). 6 h, 12 h, 20 h after scratch, there was no significant difference between the relative wound density value in control group and the shikonin groups. 24 h after scratch, there was no difference between control group and 1µM group while the relative wound density in 2µM, 3µM, 4µM, 5µM groups were significantly lower than the control group (B, C, D, E).

MCF-7 migration experiment was performed to evaluate the effect of shikonin. The relative wound density in the shikonin groups compared with the control group had no significant difference at 6 h, 12 h and 20 h. At 24 h, there was no significant difference between the control group and 1µM group while the difference between the control group and 2µM, 3µM, 4µM, 5µM groups was significant. The wound area pictures captured at 24 h also showed that the wound areas were larger than the control group. The results

indicated that 1 μM shikonin was too low in concentration for inhibition of the migration. The migration of MDA-MB-231 and MCF-7 cells were inhibited by shikonin at 6 h, 12 h, 20 h, 24 h time points (Figure 27, Figure 28).

3.13 Inhibition of MDA-MB-231 and MCF-7 Cells Invasion through Engineered Basement Membrane Gels in xCELLigence

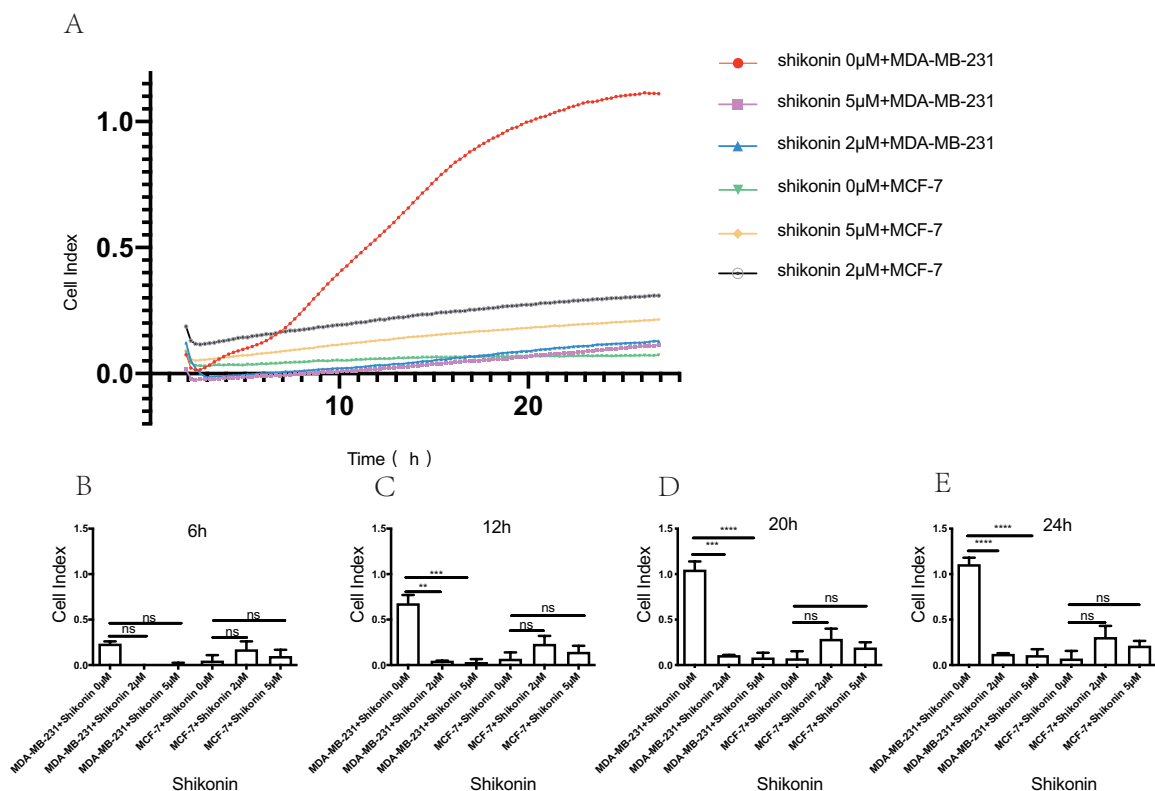


Figure 29: MDA-MB-231 and MCF-7 cell invasion through engineered basement membrane gel inhibited by shikonin in xCELLigence (mean \pm SD, n=3). MDA-MB-231 and MCF-7 cells invasion through engineered basement membrane inhibited by shikonin (A). 6 h after starting, there was no significant difference between the MDA-MB-231 and MCF-7 groups (B). 2h after starting, there was significant difference between 0 μM and 2 μM , 5 μM group in MDA-MB-231 while there was no significant difference in MCF-7 groups (C). 20h after starting, there was significant difference between 0 μM and 2 μM , 5 μM group in MDA-MB-231 while there was no significant difference between 0 μM and 2 μM , 5 μM group in MCF-7 cells (D). 24h after starting, there was significant difference between 0 μM and 2 μM , 5 μM group in MDA-MB-231 while there was no significant difference between 0 μM and 2 μM , 5 μM group in MCF-7 cells (E).

Experiment was performed to study whether the invasion through engineered basement membrane could be inhibited by shikonin. The cell number was 80,000 per well and engineered basement membrane was composed of 2.5 wt% PEGDA and 400 $\mu\text{g}/\text{mL}$ Matrigel matrix. The result showed that 12 h, 20 h and 24 h after starting the cell index of MDA-MB-231 cells in 2 μM shikonin and 5 μM shikonin group was significantly lower than the control group while the cell index of MCF-7 cells has no significant difference with the shikonin group. It indicated that the MDA-MB-231 cells invasion through the

engineered basement membrane was significantly inhibited by shikonin. The MCF-7 invasion cell index remained low and no MCF-7 cells invaded through the membrane (Figure 29).

3.14 MDA-MB-231 and MCF-7 Cell Invasion after Irradiation of the Engineered Basement Membrane in xCELLigence

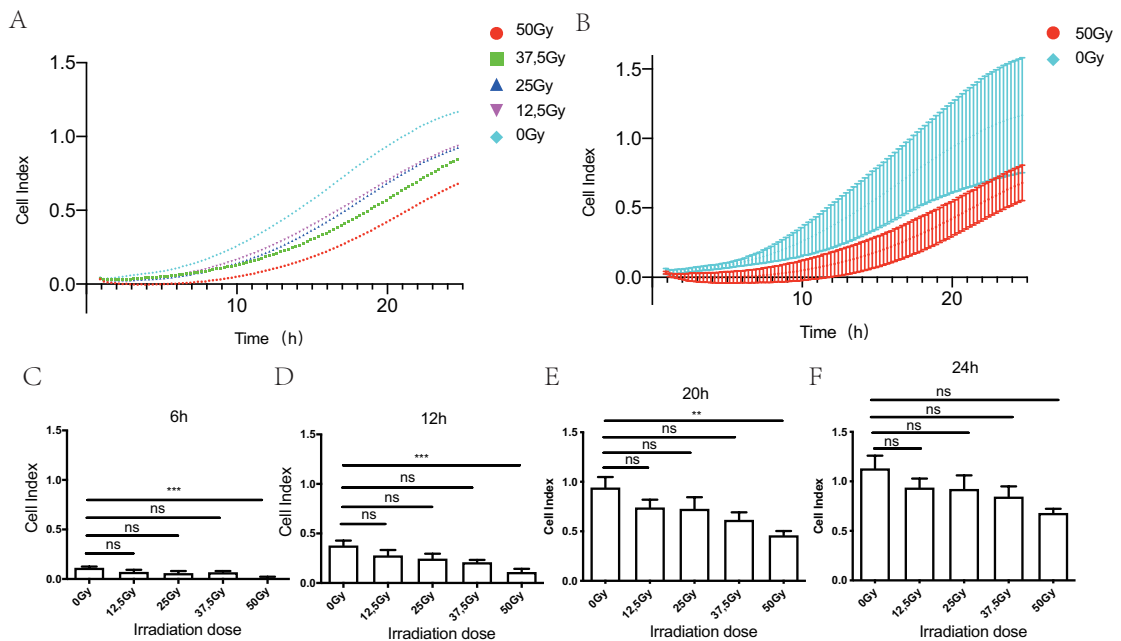


Figure 30: MDA-MB-231 cell invasion after irradiation of the engineered basement membrane. MDA-MB-231 cell invasion cell index (mean) after irradiation of the engineered basement membrane, cell number 80,000 per well, n=9 (A). MDA-MB-231 cell invasion cell index (mean±SD) (B). 6 h, 12 h, 20 h after starting, cell index of 50Gy group was significant different with the control group (C, D, E). 24 h after starting, there was no significant difference between control group and irradiation groups (F).

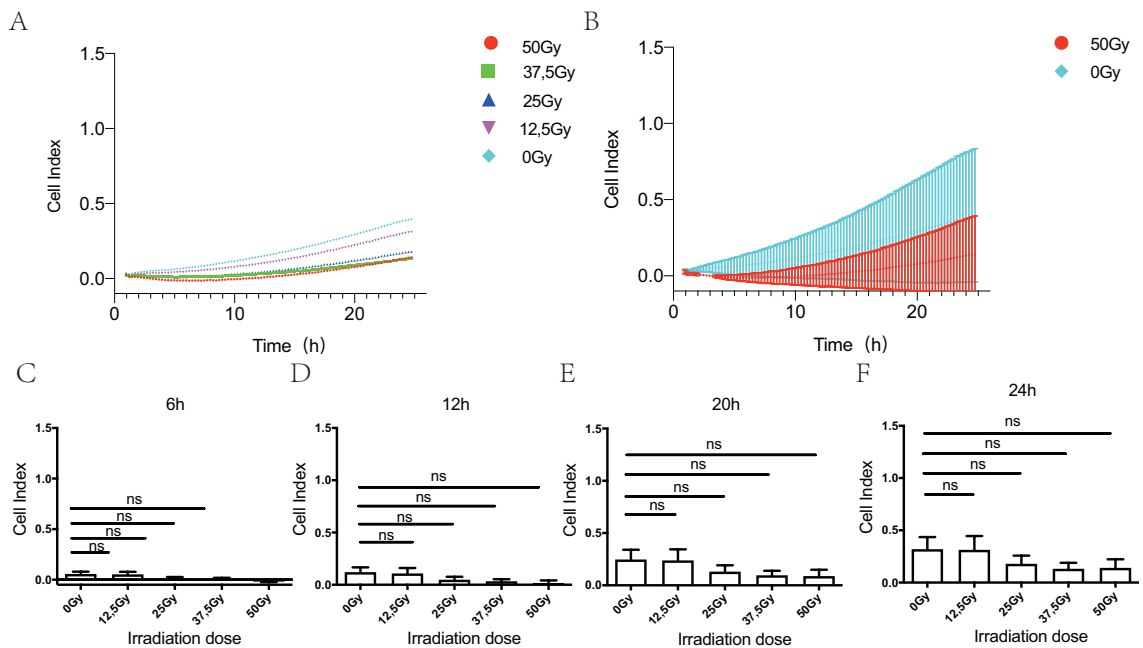


Figure 31: MCF-7 cell invasion after irradiation of the engineered basement membrane. MCF-7 cell invasion cell index (mean) after irradiation of the engineered basement membrane, cell number 80,000 per well, n=9 (A). MCF-7 cell invasion cell index (mean±SD) (B). 6 h, 12 h, 20 h, 24 h after starting, there was no significant difference between control group and irradiation groups (C, D, E, F).

Invasion experiment was performed to study the invasiveness of the MDA-MB-231 and MCF-7 after different dose of irradiation on the membrane. The cell index of MDA-MB-231 invasion in 50Gy group was significantly lower than the control group at 6 h, 12 h, 20 h after starting. There was no significant difference of cell index of MDA-MB-231 cells between 12.5 Gy, 25 Gy, 37.5 Gy groups and the 0 Gy group. The cell index of MDA-MB-231 cells was significantly lower than 0 Gy group after 50 Gy irradiation of the engineered basement membrane (Figure 30).

The cell index of MCF-7 cells in all irradiation groups were lower than the control group. But there was no significant difference with the control group at 6 h, 12 h, 20 h and 24 h after starting.

After 50 Gy irradiation, the cell index of MDA-MB-231 cells was reduced significantly and the cell index of MCF-7 cells was also reduced but without significant difference (Figure 31).

3.15 MDA-MB-231 and MCF-7 Invasion through 2.5wt%PEGDA after Irradiation

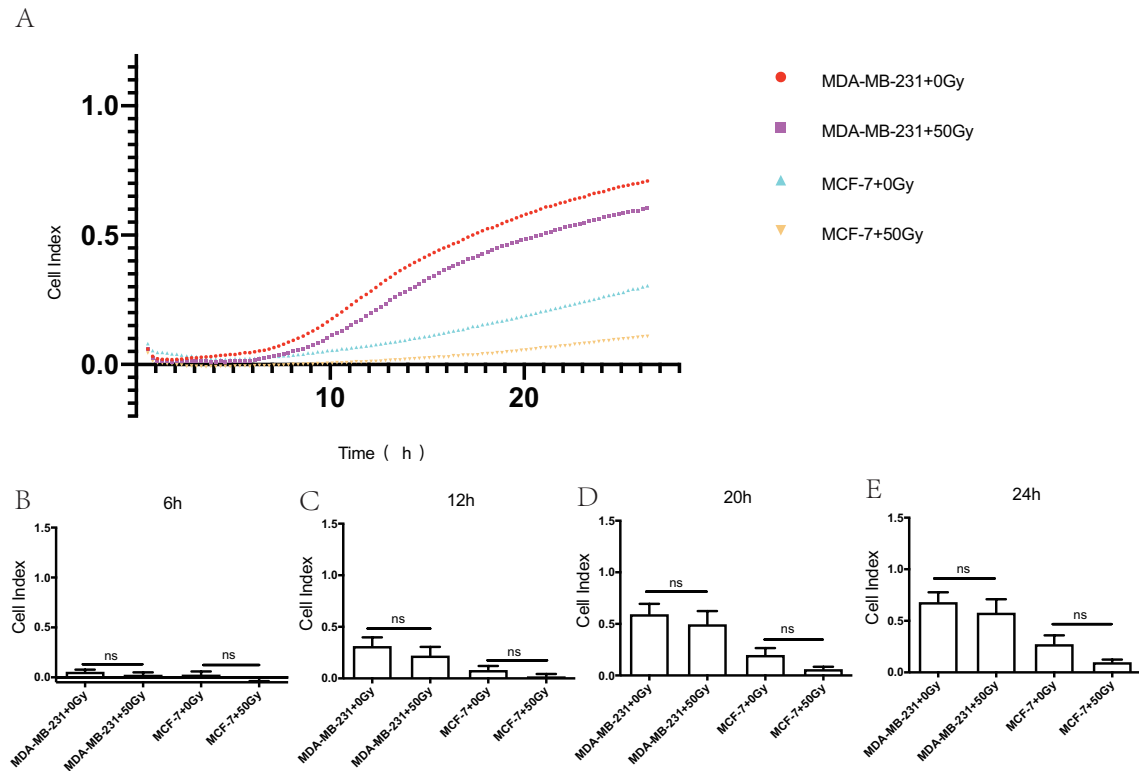


Figure 32: MDA-MB-231 and MCF-7 invasion through 2.5wt%PEGDA after irradiation. MDA-MB-231 and MCF-7 cell invasion cell index (mean±SD) after irradiation of the 2.5 wt% PEGDA membrane, cell number 80,000 per well, n=12 (A). 6h, 12h, 20h, 24h after starting, there was no significant difference between control group and irradiation groups (B, C, D, E, F).

To evaluate whether the change of invasiveness was related to PEGDA gel, experiment was performed with irradiation on the 2.5 wt% PEGDA gel. At 6 h, 12 h, 20 h, 24 h time points, there was no significant difference of cell index of MDA-MB-231 and MCF-7 cells between 50 Gy irradiation group and control group. This result indicated that there was no significant change of permeability after irradiation on 2.5 wt% PEGDA gel. The inhibition of invasiveness of MDA-MB-231 cells after 50 Gy irradiation of engineered basement membrane may related to the change of Matrigel matrix rather than 2.5 wt% PEGDA gel (Figure 32).

3.16 Immunofluorescence Laminin and Collagen IV Staining of the Engineered Basement Membrane after Irradiation

Based on the result of cell invasion through 2.5 wt% PEGDA after irradiation, immunofluorescence laminin and collagen staining experiments were performed to study the mechanism of the irradiation inhibited the engineered basement membrane. Anti-laminin

staining showed the laminin distribution on the membrane clearly. However, the red immunofluorescence images didn't show obvious difference in 50 Gy and 0 Gy group (Figure 33).

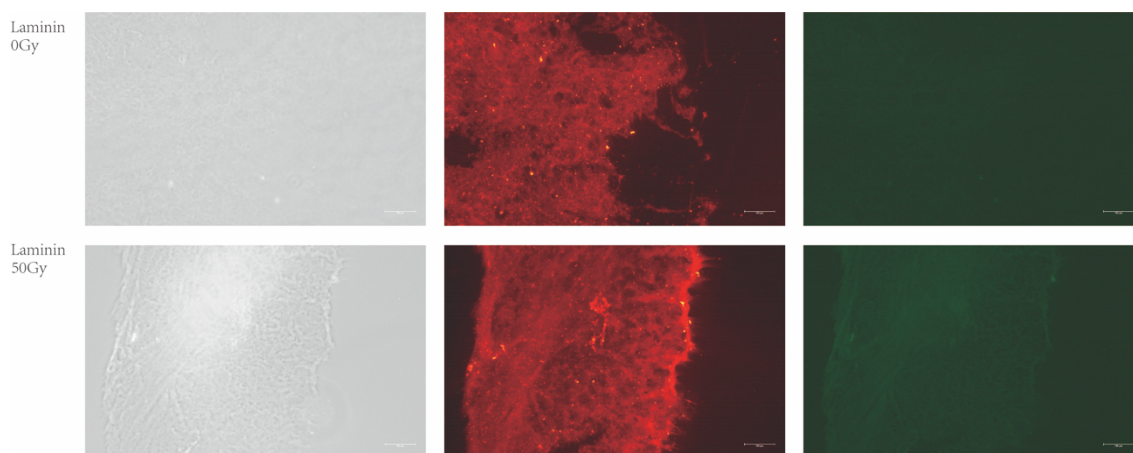


Figure 33: Anti-laminin staining of the engineered basement membrane before and after irradiation. Immunofluorescence image of anti-laminin staining of the engineered basement membrane 0 Gy and after 50 Gy irradiation (Red fluorescence and green fluorescence). Scale bar = 100 μm .

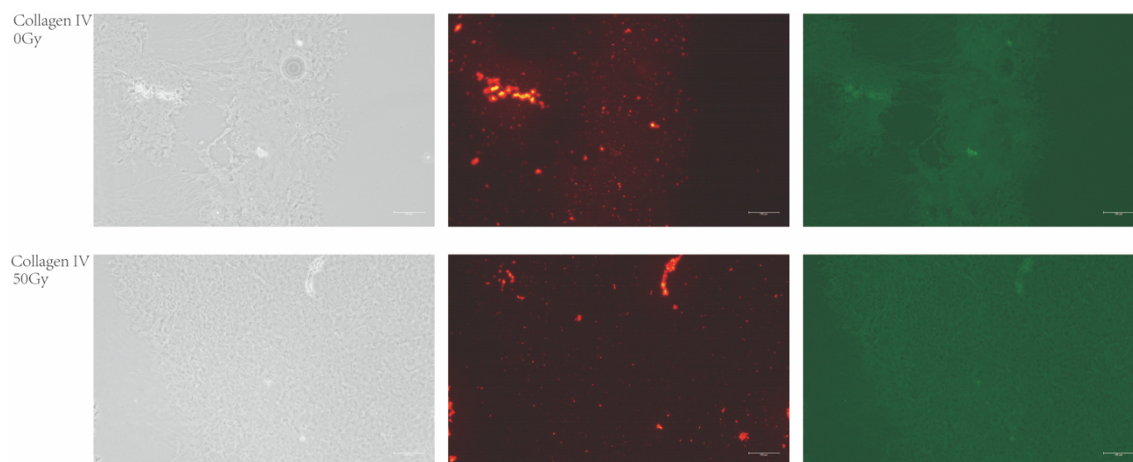


Figure 34: Anti-collagen IV staining of the engineered basement membrane before and after irradiation. Immunofluorescence image of anti-collagen IV staining of the engineered basement membrane 0 Gy and after 50 Gy irradiation (Red fluorescence and green fluorescence). Scale bar = 100 μm .

Anti-collagen IV staining of the engineered basement membrane didn't show clear collagen IV distribution due to the weak fluorescence. Also, there was no obvious difference between 50 Gy and 0 Gy groups (Figure 34).

4 DISCUSSION

Tumor metastasis is the majority cause of death in tumor patients. It is reported that 66.7% of cancer deaths were related with metastasis in solid tumor group in Norway 2015 (Dillekås et al. 2019). Tumor invasion through the basement membrane is the first and important step of tumor metastasis. Therefore, in order to stop or prevent tumor metastasis, it is very important to study the mechanism of tumor invasion through basement membrane.

4.1 Engineered Basement Membrane in 3D Bioreactor

Basement membrane is the first and important barrier of tumor invasion (Chang and Chaudhuri 2019). Tumor invasion through basement membrane is one of the key steps in tumor metastasis. A series of events including adhesion of tumor cells to the receptors within the basement membrane, degradation of the basement membrane by enzymes, migration of tumor cells into tissues with chemotactic stimulation were proceeded in tumor invasion. There were several methods to mimic the invasion through basement membrane *in vitro* using extracts from chick chorioallantoic (Armstrong et al. 1982), amnion (Liotta et al. 1980), lens capsule (Starkey et al. 1984) and bladder wall (Fidler and George 1980). However, the experiments using these extracts were intricate due to the complexity of tissue preparing (Vukicevic et al. 1992). In current studies, more extracellular matrices were used to study tumor invasion. Matrigel which was purified from the Engelbreth-Holm-Swarm mouse sarcoma was used widely in experiments of *in vitro* tumor invasion (Paquette et al. 2007; Comşa et al. 2012; Ibrahim et al. 2018). Although, it is closer to the substrate of basement membrane *in vivo*, Matrigel needs several hours for crosslinking. Also, it's hard to form a special 3D shape which is more similar to the environment *in vivo*.

To overcome these limitations of Matrigel, it is important to engineer new permeable basement membrane which can crosslinking fast and form special 3D shape. In this thesis, we engineered basement membrane based on Matrigel and PEGDA 20000. Matrigel provided components of basement membrane while PEGDA 20000 provided fast crosslinking and the possibility of forming special 3D shape. According to our results, the membrane which composed of 2.5% PEGDA and 400 µg/mL Matrigel formed gel in less than 5 min UV exposure and formed 3D membrane in 3D bioreactor which provided the possibility to study distal metastasis.

In this study, the MDA-MB-231 cells invaded through the engineered basement membrane but the MCF-7 cells didn't. The pore size of PEGDA 20000 gel is 38–42 μm while the size of MCF-7 and MDA-MB-231 cell is smaller than 20–25 μm (Lin et al. 2011). The size of cells smaller than the pore size of PEGDA 20000 gel provided the possibility of cell invasion and migration. We tested the system with inhibitor shikonin and found that the invasion process was inhibited significantly. These experiments showed that the permeability of the engineered basement membrane might be able to be used in the study of tumor invasion. The property of form 3D shape can be used in 3D bioreactors. This membrane in our 3D bioreactor mimics the process of tumor invasion through the basement membrane, which might be available to drug screening. However, only two cell lines were tested in this study, so further work with other cell lines should be performed in the future.

4.2 Clinical Dose of Irradiation of the Engineered Basement Membrane Reduced the Invasiveness of MDA-MB-231 Cells

Irradiation therapy was proved to be an effective therapy to treat breast cancer. However, the irradiation dose in the clinic (50-60 Gy) was not designed to kill all the cancer cells escaped from the primary breast cancer but to improve the long-term results with less complications (Miller et al. 2018). Although, excision margins was confirmed by histologic assessment, it was shown that residual cancer cells were found in 26% of patients with pathological clear margins (Frazier et al. 1989). It means that some cancer cells were not removed after surgery and irradiation therapy maybe an effective way to stop these residual cancer cells from metastasis.

How the clinical dose of irradiation influenced the invasion of MDA-MB-231 and MCF-7 cells was evaluated in this study. The results showed that the invasiveness of MDA-MB-231 cells were significantly reduced after 50 Gy irradiation on the engineered basement membrane while the invasiveness of MDA-MB-231 and MCF-7 cells was not reduced significantly after 50 Gy irradiation on the 2.5 wt% PEGDA gels. The result indicated that 2.5 wt% PEGDA 20,000 in the engineered basement membrane was not responsible for the inhibition of MDA-MB-231 invasiveness.

Meanwhile, the engineered basement membrane after 50 Gy irradiation was assessed using laminin and collagen IV staining of the membrane. There was no significant change of architecture and distribution of laminin and collagen IV. Similar to our result, it was

reported that clinical dose of irradiation reduced the matrix stiffness without significantly altering the architecture. The adhesion and migration of the cancer cells were reduced in the irradiated matrix (Miller et al. 2018). The basement membrane showed a different molecular structure after irradiation. However, one study reported that *in vitro* irradiation of basement membrane increases the invasiveness of MDA-MB-231 cells by improving the release of pro-invasive factors MMP-2 stored in Matrigel (Paquette et al. 2007).

Integrin in basement membrane is very important for matrix degradation and stiffness which promotes tumor invasion (Miller et al. 2018). It's also reported that laminin-421 promotes migration of tumor cells derived from melanomas, gliomas and carcinomas through integrin (Ishikawa et al. 2014). MDA-MB-231 cells have been shown to express $\beta 1$ integrin (Hou et al. 2016). The hypothesis for the decrease of invasiveness of MDA-MB-231 cells in this study may related to integrin. Tumor cells cannot attach and migrate through matrix because of lacking integrin binding sites.

4.3 Current *In Vitro* 3D Tumor Metastasis Models

Many *In vitro* and *in vivo* models were developed for tumor metastasis study in the past decades. However, 3D bioreactors which mimic the invasion through the basement membrane were rarely reported (Fu et al. 2014; Liu et al. 2016; Salamanna et al. 2017).

In this study, 3D designing with open-source software Freecad, 3D printing, molding and casting approach were used to design and fabricate 3D bioreactors. A series of 3D bioreactors with central perfusion channel were designed and fabricated, in which a multilayer basement membrane mimicking the invasion process was generated. The designing, fabricating and assembling of the bioreactors was economic, customized and easily to be achieved. This design owned the originality with transparent side windows, which provides the possibility to get living 3D image of the tumor invasion with a light sheet microscope.

With a desktop 3D printer Ultimaker 3 and Freecad, it is feasible to design individualized bioreactors with controlled medium perfusion and allows the other researchers to create their own multilayer basement membranes to study the complexity of tumor invasion in the laboratories.

In the past years, a series of bioreactors were designed to mimic the process of tumor invasion including transwell-based models, spheroid-based models, hybrid platforms and

tumor-microvessel models (Arrigoni et al. 2016; Katt et al. 2016; Ni et al. 2019). Ni et al developed a plug-and-play *in vitro* metastasis system based on insert transwell, allowing the culture of human cancer cells and quantitative analysis to evaluate different stage of tumor metastasis (Ni et al. 2019). Puls et al engineered a spheroid-based tumor invasion model for high-throughput drug screening using 3D printed platform which was low-cost and supported tumor spheroid within the surrounding gel of matrix (Puls et al. 2018). However, the disadvantage of these two models is lack of vasculature and typically 3D environment. Ko et al reported a tumor spheroid model that can be used in studying tumor angiogenesis and drug screening. The 3D printed platform contained a rail guide for cell patterning and medium perfusion both sides (Ko et al. 2019). The limitation of this model was low throughput and long-term culture was difficult. Horie et al developed a 3D co-culture model in which A549 cancer cells were co-cultured on the collagen gel which was embedded with lung fibroblasts. After 5 d floating culture, the cancer cells with collagen gel were cultured in air-liquid interface medium. This model was used to evaluate the effects of lung cancer-associated fibroblasts on lung cancer invasion, proliferation (Horie et al. 2015). Lack of typical vasculature and 3D environment was the main limitation of this model. Wong and Searson engineered a live-cell imaging of invasion and intravasation model using predefined microvessel channels in ECM scaffold. This platform can be applied to analyze the interplay between metastatic cancer cells and microvessels (Wong and Searson 2014). The main disadvantage of this model was simple vessel structure with limited diameter. Several models were developed in tumor invasion. 3D designing and printing creates possibility to fabricate engineered models with individual structures in the models.

However, each existing model for tumor invasion has different limitations such as lack of controlled perfusion, no live-cell image or no multilayer structure which can mimic the escape and intravasation process. For example, transwell-based models were low physiological relevance and used only for monolayer cell structure which may leading to different results as spheroid cancer cell invasion (Horie et al. 2015). Spheroid-based models had difficulties on long-term culture, collecting cells for analysis and no live-cell image (Puls et al. 2018). Hybrid platforms lacked perfusion through vascular structures. Tumor-microvessel models were limited by linear structure and diameter (Buchanan et al. 2014). In this study, 3D bioreactors were engineered with simple structure which can be precisely printed with desktop 3D printer. Compared to other models, the central channel

can be connected with controlled perfusion by ibidi pump system. The glass window design on both sides provided the possibility for live-cell image with a light sheet microscope system. The main device was assembled with a glass cover and silicone cover without much manual work. The multilayer approach provided the possibility to mimic a tumor microenvironment, tumor invasion through basement membrane and intravasation. The gelation finished in only a few minutes by using PEGDA gel in our work. The gelation process was much easier than in other models. By using the engineered basement membrane, we created a 3D basement membrane in this model, which is more likely the environment *in vivo*. In further study, it is possible to build a tumor distal metastasis model by connecting two or more bioreactors together. The tumor cells can invade through the basement membrane into the circulation and metastasize to the distal bioreactor.

4.4 Limitations of the Thesis

In this thesis, a basement membrane was engineered successfully and the function of the basement membrane on preventing tumor cell invasion was tested in a 3D tumor metastasis model in a 3D-printed bioreactor. It showed quick gelation and biocompatibility. 3D metastasis model for tumor invasion with basement membrane was established successfully. However, there were some limitations. Firstly, the perfusion channel in this model had a simple structure. Complicated vessel like structures need to be created and studied in the further research. Additionally, the mechanism of invasiveness change of MDA-MB-231 cells after irradiation on the engineered basement membrane was still not clear. More work needs to be done to investigate the underlying mechanism.

4.5 Future Directions of *In Vitro* Bone Metastasis Models

The development of the *in vitro* models of bone metastasis makes it possible to reproduce the complexity of the tumor microenvironment with specific cells, extracellular matrixes and other factors. By controlling specific components in the *in vitro* models, it can be useful to study the interactions of the specific factors such as TGF- β , PTHrP, RANKL, FGFs, BMPs and Wnt pathway, the tumor cells and tumor microenvironment while it is too complicated in the *in vivo* models due to the complexity of the *in vivo* environment. Tumor-microvessel models are widely used to study tumor angiogenesis, intravasation, extravasation and tumor vessel interactions due to the sustained perfusion and vessel

structure in the models. The future direction of this type may be to coculture the relevant cell types within the extracellular matrix and modify the properties of the vessels such as shear stress and networks. Designing an engineered basement membrane which can mimic the basement membrane of tumor nodule *in vivo* and combining it in the models maybe interesting. Coculturing the other cell types within the extracellular matrix for studying the invasion through the basement membrane and the interactions of tumor cells and matrix may be more relevant to the *in vivo* process.

The further direction of this study is studying the mechanism of how the irradiation effected the basement membrane and the invasiveness of the tumor cells. Another direction is fabricating more complicated structure of perfusion channels and co-culture cell lines in 3D bioreactor such as chondrocytes to mimic bone environment. Connecting two bioreactors together maybe also a good choice to observe real-time images of tumor distal metastasis using light sheet microscope.

5 CONCLUSIONS

Studying the structure of basement membrane and the mechanism of the invasion through the basement membrane may help to understand the invasion process and the complexity of tumor metastasis.

In this study, a novel permeable and fast gelation basement membrane with 3D structure was engineered successfully by mixing Matrigel Matrix and PEGDA 20,000 gel. It was also demonstrated that clinical dose of irradiation reduced the invasiveness of tumor cells. Using open-source software and desktop 3D printer, 3D bioreactors were established. Our methods provide a cost-effective way to fabricate customized 3D bioreactors with engineered basement membrane. A novel 3D tumor metastasis model which showed great functionality and potential for the study of tumor distal metastasis, was established successfully with this engineered basement membrane.

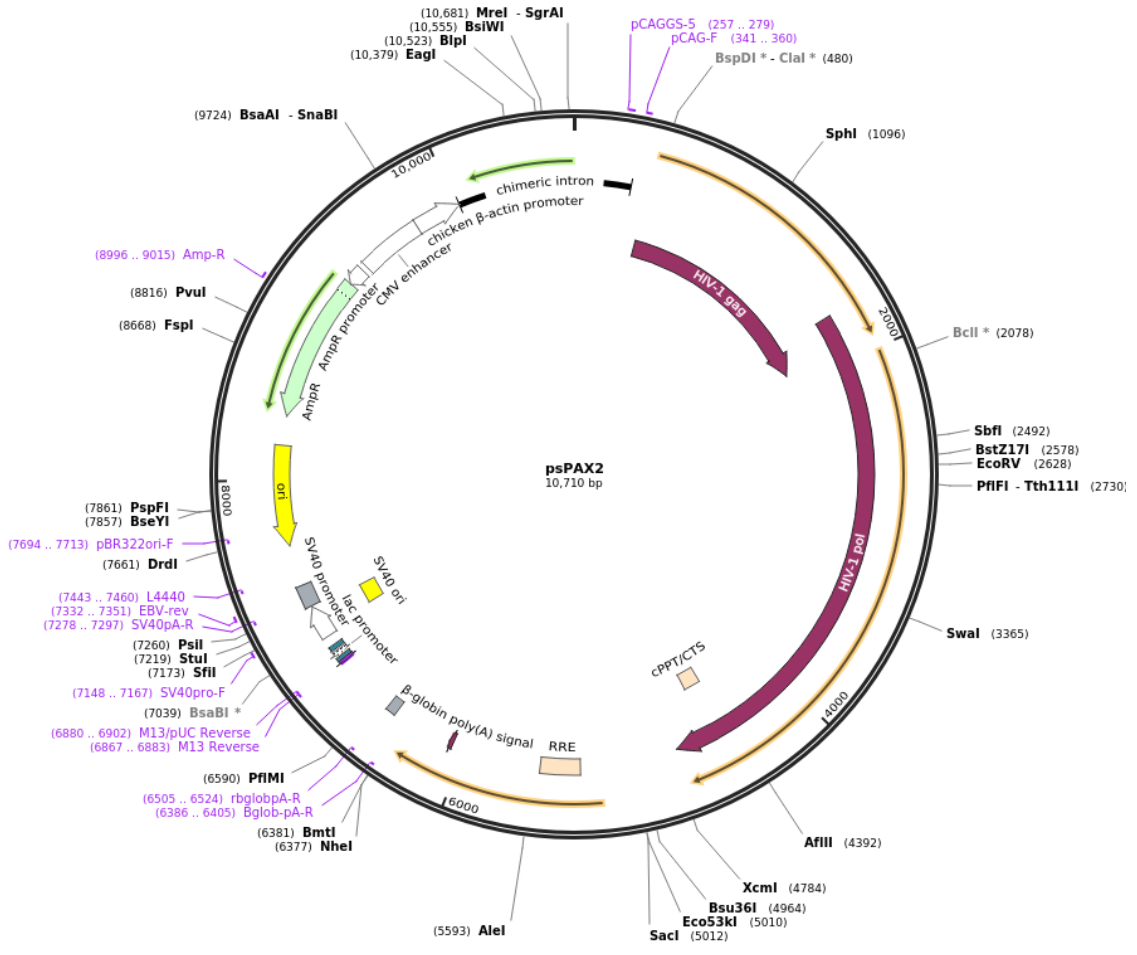
Generally, a permeable basement membrane which might be useful for tumor invasion study was engineered successfully. Our methods and membrane provide an economical way to design and fabricate customized 3D bioreactors and metastasis models.

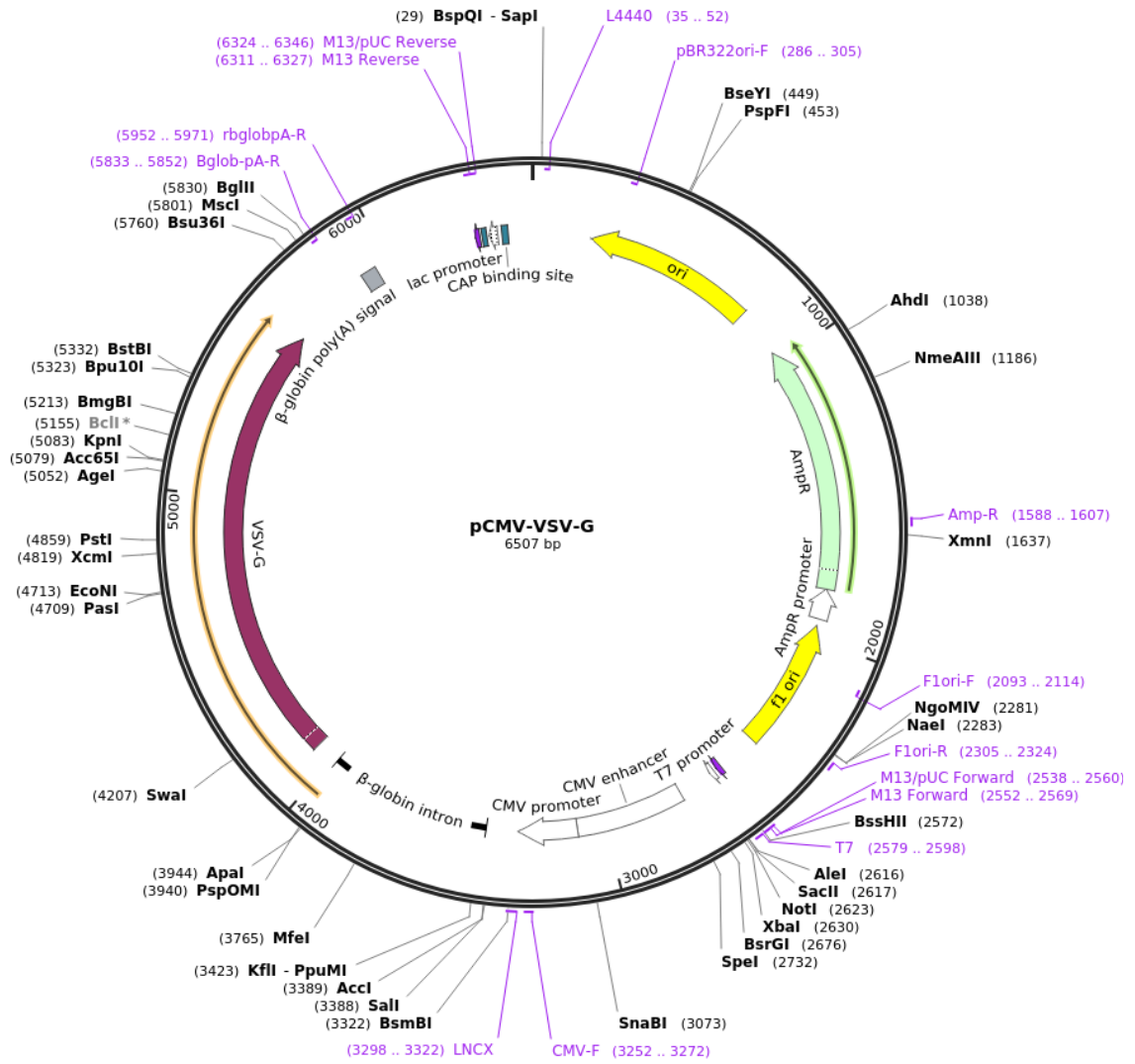
Further study will be 3D bioreactor with multilayer gel approach and engineered basement membrane in distal tumor metastasis study. Furthermore, side windows in this bioreactor provide the possibility to get real-time images of tumor invasion under light sheet microscope. Further study about the mechanism of the invasiveness change of MDA-MB-231 cells after irradiation on the membrane should be done in the next step.

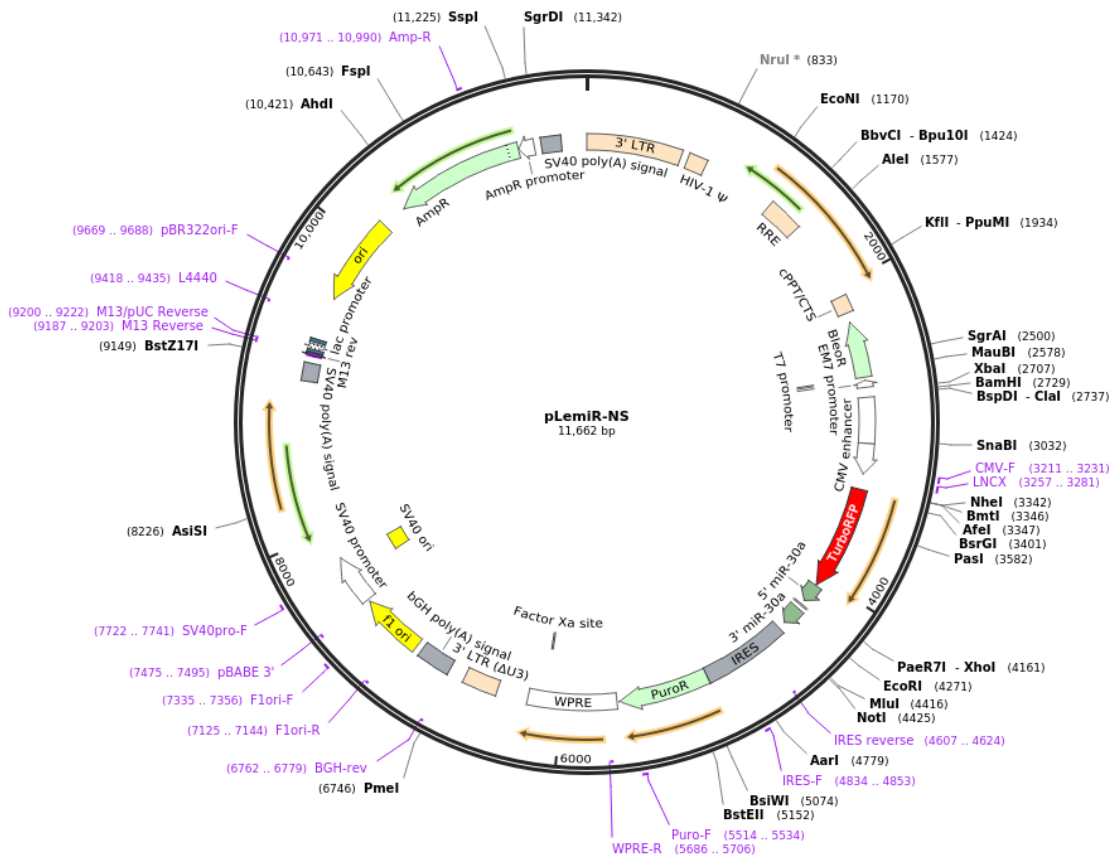
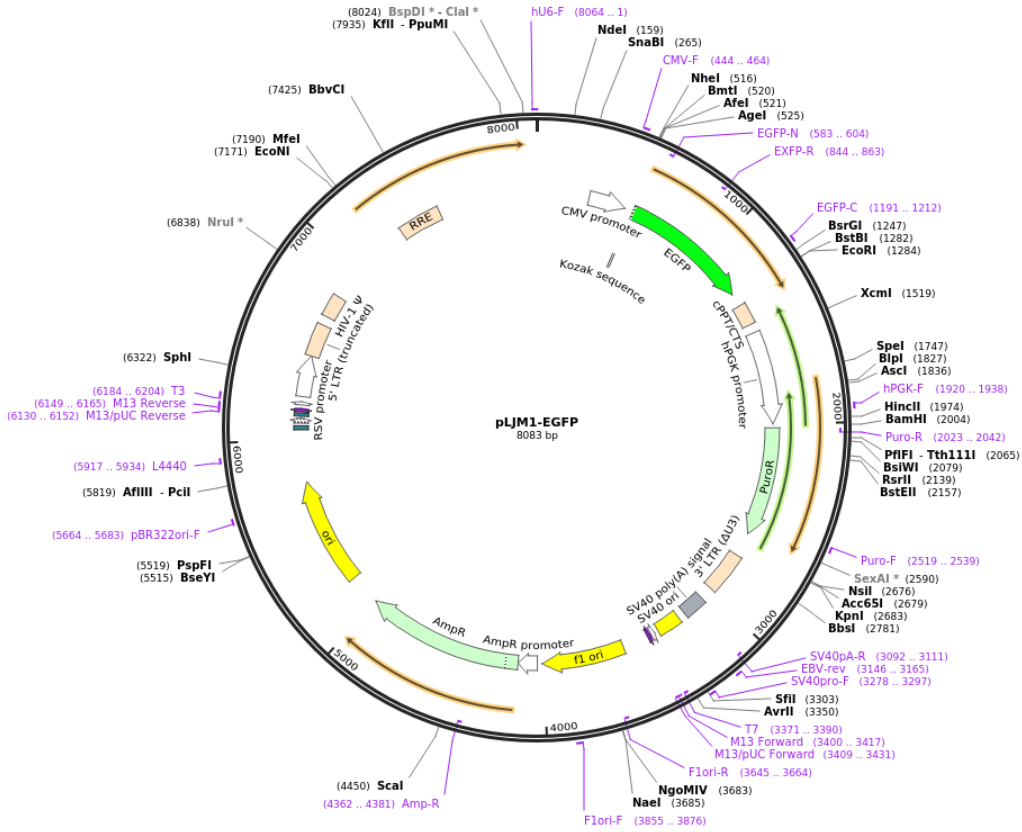
The engineered basement membrane could be used to study 3D tumor metastasis and drug screening. It may serve as a novel platform for tumor distal metastasis. It may be useful for real-time observing of tumor metastasis.

APPENDIX

Plasmid maps







6 REFERENCES

- Abe O, Abe R, Enomoto K, Kikuchi K, Koyama H, Masuda H, Nomura Y, Sakai K, Sugimachi K, Tominaga T, et al. (2005): Effects of radiotherapy and of differences in the extent of surgery for early breast cancer on local recurrence and 15-year survival: An overview of the randomised trials. *Lancet* **366**, 2087–2106
- Abigail H, Sharon G (2012): Engineering approaches for investigating tumor angiogenesis exploiting the role of the extracellular matrix. *Cancer Res* **72**, 6089–6096
- Akhtar M, Haider A, Rashid S, Al-Nabet ADMH (2019): Paget’s „seed and Soil“ Theory of Cancer Metastasis: An Idea Whose Time has Come. *Adv Anat Pathol* **26**, 69–74
- Armstrong PB, Quigley JP, Sidebottom E (1982): Transepithelial Invasion and Intramesenchymal Infiltration of the Chick Embryo Chorioallantois by Tumor Cell Lines. *Cancer Res* **42**, 1826–1837
- Arrigoni C, Bersini S, Gilardi M, Moretti M (2016): In vitro co-culture models of breast cancer metastatic progression towards bone. *Int J Mol Sci* **17**, 1405
- Bennett CN, Longo KA, Wright WS, Suva LJ, Lane TF, Hankenson KD, MacDougald OA (2005): Regulation of osteoblastogenesis and bone mass by Wnt10b. *Proc Natl Acad Sci U S A* **102**, 3324–3329
- Boyce BF (2013): Advances in the regulation of osteoclasts and osteoclast functions. *J Dent Res* **92**, 860–867
- Buchanan CF, Verbridge SS, Vlachos PP, Rylander MN (2014): Flow shear stress regulates endothelial barrier function and expression of angiogenic factors in a 3D microfluidic tumor vascular model. *Cell Adhes Migr* **8**, 517–524
- Butler JM, Kobayashi H, Rafii S (2010): Instructive role of the vascular niche in promoting tumour growth and tissue repair by angiocrine factors. *Nat Rev Cancer* **10**, 138–146
- Butler TP, Gullino PM (1975): Quantitation of Cell Shedding Into Efferent Blood of Mammary Adenocarcinoma. *Cancer Res* **35**, 512–516
- Campbell JP, Karolak MR, Ma Y, Perrien DS, Masood-Campbell SK, Penner NL, Munoz SA, Zijlstra A, Yang X, Sterling JA, Elefteriou F (2012): Stimulation of host bone marrow stromal cells by sympathetic nerves promotes breast cancer bone metastasis in mice. *PLoS Biol* **10**, e1001363
- Capietto A-H, Faccio R (2014): Immune regulation of bone metastasis. *Bonekey Rep* **3**, 600
- Chang J, Chaudhuri O (2019): Beyond proteases: Basement membrane mechanics and cancer invasion. *J Cell Biol* **218**, 2456–2469
- Chow E, Tharmalingam, Harris, Hird, Sinclair (2008): Quality of life measurement in bone metastases: A literature review. *J Pain Res* **1**, 49–58
- Chrobak KM, Potter DR, Tien J (2006): Formation of perfused, functional microvascular tubes in vitro. *Microvasc Res* **71**, 185–196
- Coleman RE (1997): Skeletal complications of malignancy. *Cancer* **80**, 1588–1594
- Coles CE, Moody AM, Wilson CB, Burnet NG (2005): Reduction of radiotherapy-induced late complications in early breast cancer: The role of intensity-modulated radiation therapy and partial breast irradiation. Part II - Radiotherapy strategies to reduce radiation-induced late effects. *Clin Oncol* **17**, 98–110
- Comşa Ş, Ciuculescu F, Raica M (2012): Mesenchymal stem cell-tumor cell cooperation in breast cancer vasculogenesis. *Mol Med Rep* **5**, 1175–1180
- Dillekås H, Rogers MS, Straume O (2019): Are 90% of deaths from cancer caused by metastases? *Cancer Med* **8**, 5574–5576

- Elgundi Z, Papanicolaou M, Major G, Cox TR, Melrose J, Whitelock JM, Farrugia BL (2020): Cancer Metastasis: The Role of the Extracellular Matrix and the Heparan Sulfate Proteoglycan Perlecan. *Front Oncol* 9, 1482
- Fennema E, Rivron N, Rouwkema J, van Blitterswijk C, De Boer J (2013): Spheroid culture as a tool for creating 3D complex tissues. *Trends Biotechnol* 31, 108–115
- Fidler IJ, George P (1980): The pathogenesis of cancer metastasis. *Nature* 283, 139–146
- Florencio-Silva R, Sasso GRDS, Sasso-Cerri E, Simões MJ, Cerri PS (2015): Biology of Bone Tissue: Structure, Function, and Factors That Influence Bone Cells. *Biomed Res Int* 2015, 421746
- Fournier PGJ, Chirgwin JM, Guise TA (2006): New insights into the role of T cells in the vicious cycle of bone metastases. *Curr Opin Rheumatol* 18, 396–404
- Frazier TG, Wong RWY, Rose D (1989): Implications of Accurate Pathologic Margins in the Treatment of Primary Breast Cancer. *Arch Surg* 124, 37–38
- Frisch BJ (2019): The hematopoietic stem cell niche: What's so special about bone? *Bone* 119, 8–12
- Fu CY, Tseng SY, Yang SM, Hsu L, Liu CH, Chang HY (2014): A microfluidic chip with a U-shaped microstructure array for multicellular spheroid formation, culturing and analysis. *Biofabrication* 6, 015009
- Gawrzak S, Rinaldi L, Gregorio S, Arenas EJ, Salvador F, Urosevic J, Figueras-Puig C, Rojo F, Del Barco Barrantes I, Cejalvo JM, et al. (2018): MSK1 regulates luminal cell differentiation and metastatic dormancy in ER + breast cancer. *Nat Cell Biol* 20, 211–221
- Ghajar CM, Peinado H, Mori H, Matei IR, Evason KJ, Brazier H, Almeida D, Koller A, Hajar KA, Stainier DYR, et al. (2013): The perivascular niche regulates breast tumour dormancy. *Nat Cell Biol* 15, 807–817
- Glentis A, Oertle P, Mariani P, Chikina A, El Marjou F, Attieh Y, Zaccarini F, Lae M, Loew D, Dingli F, et al. (2017): Cancer-associated fibroblasts induce metalloprotease-independent cancer cell invasion of the basement membrane. *Nat Commun* 8, 924
- Gonzalez-Fernandez T, Tenorio AJ, Kent Leach J, Kent Leach J (2020): Three-Dimensional Printed Stamps for the Fabrication of Patterned Microwells and High-Throughput Production of Homogeneous Cell Spheroids. *3D Print Addit Manuf* 7, 139–147
- Hall CL, Bafico A, Dai J, Aaronson SA, Keller ET (2005): Prostate cancer cells promote osteoblastic bone metastases through Wnts. *Cancer Res* 65, 7554–7560
- Hernandez RK, Wade SW, Reich A, Pirolli M, Liede A, Lyman GH (2018): Incidence of bone metastases in patients with solid tumors: Analysis of oncology electronic medical records in the United States. *BMC Cancer* 18, 44
- Holen I, Nutter F, Wilkinson JM, Evans CA, Avgoustou P, Ottewell PD (2015): Human breast cancer bone metastasis in vitro and in vivo : a novel 3D model system for studies of tumour cell-bone cell interactions. *Clin Exp Metastasis* 32, 689–702
- Holland R, Veling SHJ, avunac M, Hendriks JHCL (1985): Histologic multifocality of tis, T1–2 breast carcinomas implications for clinical trials of breast-conserving surgery. *Cancer* 56, 979–990
- Horie M, Saito A, Yamaguchi Y, Ohshima M, Nagase T (2015): Three-dimensional co-culture model for tumor-stromal interaction. *J Vis Exp* 96, e52469
- Hou S, Isaji T, Hang Q, Im S, Fukuda T, Gu J (2016): Distinct effects of β 1 integrin on cell proliferation and cellular signaling in MDA-MB-231 breast cancer cells. *Sci Rep* 6, 18430

- Hsu JW, Yasmin-Karim S, King MR, Wojciechowski JC, Mickelsen D, Blair ML, Ting HJ, Wen-Lung M, Lee YF (2011): Suppression of prostate cancer cell rolling and adhesion to endothelium by $1\alpha,25$ -dihydroxyvitamin D₃. *Am J Pathol* 178, 872–880
- Ibrahim AM, Sabet S, El-Ghor AA, Kamel N, Anis SE, Morris JS, Stein T (2018): Fibulin-2 is required for basement membrane integrity of mammary epithelium. *Sci Rep* 8, 14139
- Ishikawa T, Wondimu Z, Oikawa Y, Gentilcore G, Kiessling R, Egyhazi Brage S, Hansson J, Patarroyo M (2014): Laminins 411 and 421 differentially promote tumor cell migration via $\alpha6\beta1$ integrin and MCAM (CD146). *Matrix Biol* 38, 69–83
- Jang SY, Lee JAEK, Jang EUNH, Jeong SEOY, Kim J (2014): Shikonin blocks migration and invasion of human breast cancer cells through inhibition of matrix metalloproteinase-9 activation. *Oncol Rep* 31, 2827–2833
- Jinnah AH, Zacks BC, Gwam CU, Kerr BA (2018): Emerging and established models of bone metastasis. *Cancers (Basel)* 10, 176
- Johnson RW, Merkel AR, Page JM, Ruppender NS, Guelcher SA, Sterling JA (2014): Wnt signaling induces gene expression of factors associated with bone destruction in lung and breast cancer. *Clin Exp Metastasis* 31, 945–959
- Kakhki VRD, Anvari K, Sadeghi R, Mahmoudian AS, Torabian-Kakhki M (2013): Pattern and distribution of bone metastases in common malignant tumors. *Nucl Med Rev* 16, 66–69
- Käkönen SM, Selander KS, Chirgwin JM, Yin JJ, Burns S, Rankin WA, Grubbs BG, Dallas M, Cui Y, Guise TA (2002): Transforming growth factor- β stimulates parathyroid hormone-related protein and osteolytic metastases via Smad and mitogen-activated protein kinase signaling pathways. *J Biol Chem* 277, 24571–24578
- Katt ME, Placone AL, Wong AD, Xu ZS, Searson PC (2016): In vitro tumor models: Advantages, disadvantages, variables, and selecting the right platform. *Front Bioeng Biotechnol* 4, 12
- Kleinman HK, McGarvey ML, Liotta LA, Robey PG, Tryggvason K, Martin GR (1982): Isolation and Characterization of Type IV Procollagen, Laminin, and Heparan Sulfate Proteoglycan from the EHS Sarcoma. *Biochemistry* 21, 6188–6193
- Kleinman HK, McGarvey ML, Hassell JR, Star VL, Cannon FB, Laurie GW, Martin GR (1986): Basement Membrane Complexes with Biological Activity. *Biochemistry* 25, 312–318
- Ko J, Ahn J, Kim S, Lee Y, Lee J, Park D, Jeon NL (2019): Tumor spheroid-on-a-chip: A standardized microfluidic culture platform for investigating tumor angiogenesis. *Lab Chip* 19, 2822–2833
- Kodama N, Nagata M, Tabata Y, Ozeki M, Ninomiya T, Takagi R (2009): A local bone anabolic effect of rhFGF2-impregnated gelatin hydrogel by promoting cell proliferation and coordinating osteoblastic differentiation. *Bone* 44, 699–707
- Kramer N, Walzl A, Unger C, Rosner M, Krupitza G, Hengstschläger M, Dolznig H (2013): In vitro cell migration and invasion assays. *Mutat Res* 752, 10–24
- Kuperwasser C, Dessain S, Bierbaum B, Garnet D (2005): A mouse model of breast cancer metastasis to the choroid of the eye. *Cancer Res* 65, 6130–6138
- LaBarbera D V., Reid BG, Yoo BH (2012): The multicellular tumor spheroid model for high-throughput cancer drug discovery. *Expert Opin Drug Discov* 7, 819–830
- Lacey DL, Timms E, Tan HL, Kelley MJ, Dunstan CR, Burgess T, Elliott R, Colombero A, Elliott G, Scully S, et al. (1998): Osteoprotegerin ligand is a cytokine that regulates osteoclast differentiation and activation. *Cell* 93, 165–176
- Langlais LM, Gibson J, Taylor JA, Caswell JL (2006): Pulmonary adenocarcinoma with metastasis to skeletal muscle in a cat. *Can Vet J* 47, 1122–1123

- Li S, Peng Y, Weinhandl ED, Blaes AH, Cetin K, Chia VM, Stryker S, Pinzone JJ, Acquavella JF, Arneson TJ (2012): Estimated number of prevalent cases of metastatic bone disease in the US adult population. *Clin Epidemiol* 4, 87–93
- Lin S, Sangaj N, Razafiarison T, Zhang C, Varghese S (2011): Influence of physical properties of biomaterials on cellular behavior. *Pharm Res* 28, 1422–1430
- Linde N, Fluegen G, Aguirre-Ghiso JA (2016): The Relationship Between Dormant Cancer Cells and Their Microenvironment. *Adv Cancer Res* 132, 45–71
- Liotta LA, Lee CW, Morakis DJ (1980): New method for preparing large surfaces of intact human basement membrane for tumor invasion studies. *Cancer Lett* 11, 141–152
- Liu CZ, Xia ZD, Han ZW, Hulley PA, Triffitt JT, Czernuszka JT (2008): Novel 3D collagen scaffolds fabricated by indirect printing technique for tissue engineering. *J Biomed Mater Res - Part B Appl Biomater* 85, 519–528
- Liu J, Zheng H, Krempf F, Su L, Machens HG, Schilling AF (2016): Open source 3D-printing approach for economic and fast engineering of perfusable vessel-like channels within cell-laden hydrogels. *3D Print Addit Manuf* 3, 23–31
- Madsen CD, Hooper S, Tozluoglu M, Bruckbauer A, Fletcher G, Erler JT, Bates PA, Thompson B, Sahai E (2015): STRIPAK components determine mode of cancer cell migration and metastasis. *Nat Cell Biol* 17, 68–80
- Mak IWY, Evaniew N, Ghert M (2014): Lost in translation: Animal models and clinical trials in cancer treatment. *Am J Transl Res* 6, 114–118
- Marlow R, Honeth G, Lombardi S, Cariati M, Hesse S, Pipili A, Mariotti V, Buchupalli B, Foster K, Bonnet D, et al. (2013): A novel model of dormancy for bone metastatic breast cancer cells. *Cancer Res* 73, 6886–6899
- Martin TJ (2002): Manipulating the environment of cancer cells in bone: A novel therapeutic approach. *J Clin Invest* 110, 1399–1401
- Mehta G, Hsiao AY, Ingram M, Luker GD, Takayama S (2012): Opportunities and challenges for use of tumor spheroids as models to test drug delivery and efficacy. *J Control Release* 164, 192–204
- Miller JP, Borde BH, Bordeleau F, Zanotelli MR, LaValley DJ, Dylan J. Parker 1, Lawrence J. Bonassar, 1, 3 Susan C. Pannullo, 1 4 and, Reinhart-Kingl CA, Parker DJ, Bonassar LJ, et al. (2018): Clinical doses of radiation reduce collagen matrix stiffness. *APL Bioeng* 2, 031901
- Moreau JE, Anderson K, Mauney JR, Nguyen T, Kaplan DL, Rosenblatt M (2007): Tissue-engineered bone serves as a target for metastasis of human breast cancer in a mouse model. *Cancer Res* 67, 10304–10308
- Morrissey C, Brown LG, Pitts TEM, Vessella RL, Corey E (2010): Bone morphogenetic protein 7 is expressed in prostate cancer metastases and its effects on prostate tumor cells depend on cell phenotype and the tumor microenvironment. *Neoplasia* 12, 192–205
- Mosadegh B, Lockett MR, Minn KT, Simon KA, Gilbert K, Hillier S, Newsome D, Li H, Hall AB, Boucher DM, et al. (2015): A paper-based invasion assay: Assessing chemotaxis of cancer cells in gradients of oxygen. *Biomaterials* 52, 262–271
- Nannuru KC, Singh RK (2010): Tumor-stromal interactions in bone metastasis. *Curr Osteoporos Rep* 8, 105–113
- Nguyen-Ngoc KV, Cheung KJ, Brenot A, Shamir ER, Gray RS, Hines WC, Yaswen P, Werb Z, Ewald AJ (2012): ECM microenvironment regulates collective migration and local dissemination in normal and malignant mammary epithelium. *Proc Natl Acad Sci U S A* 109, e2595–e2604
- Ni BS, Tzao C, Huang JH (2019): Plug-and-Play In Vitro Metastasis System toward Recapitulating the Metastatic Cascade. *Sci Rep* 9, 18110

- Ottewell PD (2016): The role of osteoblasts in bone metastasis. *J Bone Oncol* 5, 124–127
- Paquette B, Baptiste C, Therriault H, Arguin G, Plouffe B, Lemay R (2007): In vitro irradiation of basement membrane enhances the invasiveness of breast cancer cells. *Br J Cancer* 97, 1505–1512
- Power CA, Pwint H, Chan J, Cho J, Yu Y, Walsh W, Russell PJ (2009): A novel model of bone-metastatic prostate cancer in immunocompetent mice. *Prostate* 69, 1613–1623
- Puls TJ, Tan X, Husain M, Whittington CF, Fishel ML, Voytik-Harbin SL (2018): Development of a Novel 3D Tumor-tissue Invasion Model for High-throughput, High-content Phenotypic Drug Screening. *Sci Rep* 8, 13039
- Punovuori K, Wickström SA (2020): How cancer invasion takes shape. *Nature* 585, 355–356
- Rho J, Takami M, Choi Y (2004): Osteoimmunology: Interactions of the Immune and Skeletal Systems. *Mol Cells* 17, 1–9
- Roberts AB, Sporn MB (1993): Mini-Review Physiological Actions and Clinical Applications of Transforming Growth Factor Beta (TGF-Beta). *Growth Factors* 8, 1–9
- Roodman GD, Dougall WC (2008): RANK ligand as a therapeutic target for bone metastases and multiple myeloma. *Cancer Treat Rev* 34, 92–101
- Salamanna F, Contartese D, Maglio M, Fini M (2016): A systematic review on in vitro 3d bone metastases models. A new horizon to recapitulate the native clinical scenario? *Oncotarget* 7, 44803–44820
- Salamanna F, Borsari V, Brogini S, Torricelli P, Cepollaro S, Cadossi M, Fini M (2017): A Human 3D In Vitro Model to Assess the Relationship Between Osteoporosis and Dissemination to Bone of Breast Cancer Tumor Cells. *J Cell Physiol* 232, 1826–1834
- Sarker MD, Naghieh S, Sharma NK, Chen X (2018): 3D biofabrication of vascular networks for tissue regeneration: A report on recent advances. *J Pharm Anal* 8, 277–296
- Schilling D, Todenhfer T, Hennenlotter J, Schwentner C, Fehm T, Stenzl A (2012): Isolated, disseminated and circulating tumour cells in prostate cancer. *Nat Rev Urol* 9, 448–463
- Schuster J, Zhang J, Longo M (2006): A novel human osteoblast-derived severe combined immunodeficiency mouse model of bone metastasis. *J Neurosurg Spine* 4, 388–391
- Shi Y, Massagué J (2003): Mechanisms of TGF- β signaling from cell membrane to the nucleus. *Cell* 113, 685–700
- Silverstein MJ, Gierson ED, Colburn WMJ, Cope LM, Furmanski M, Senofsky GM, Gamagami P, Waisman JR (1994): Can intraductal breast carcinoma be excised completely by local excision? Clinical and pathologic predictors. *Cancer* 73, 2985–2989
- Starkey JR, Liggitt HD, Hosick HL, Stanford DR (1984): Interaction of Metastatic Tumor Cells with Bovine Lens Capsule Basement Membrane. *Cancer Res* 44, 1585–1594
- Suva LJ, Washam C, Nicholas RW, Griffin RJ (2011): Bone metastasis: Mechanisms and therapeutic opportunities. *Nat Rev Endocrinol* 7, 208–218
- Tanaka Y, Nakayamada S, Okada Y (2005): Osteoblasts and osteoclasts in bone remodeling and inflammation. *Curr Drug Targets Inflamm Allergy* 4, 325–328
- Thibaudeau L, Taubenberger A V., Holzapfel BM, Quent VM, Fuehrmann T, Hesami P, Brown TD, Dalton PD, Power CA, Hollier BG, Hutmacher DW (2014a): A tissue-engineered humanized xenograft model of human breast cancer metastasis to bone. *Dis Model Mech* 7, 299–309

- Thibaudeau L, Quent VM, Holzapfel BM, Taubenberger A V., Straub M, Hutmacher DW (2014b): Mimicking breast cancer-induced bone metastasis in vivo: Current transplantation models and advanced humanized strategies. *Cancer Metastasis Rev* 33, 721–735
- Trost ME, Inkelmann MA, Galiza GJN, Silva TM, Kommers GD (2014): Occurrence of tumours metastatic to bones and multicentric tumours with skeletal involvement in dogs. *J Comp Pathol* 150, 8–17
- Vukicevic S, Kleinman HK, Luyten FP, Roberts AB, Roche NS, Reddi AH (1992): Identification of multiple active growth factors in basement membrane matrigel suggests caution in interpretation of cellular activity related to extracellular matrix components. *Exp Cell Res* 202, 1–8
- Walsh MC, Kim N, Kadono Y, Rho J, Lee SY, Lorenzo J, Choi Y (2006): OSTEOIMMUNOLOGY: Interplay Between the Immune System and Bone Metabolism. *Annu Rev Immunol* 24, 33–63
- Wang XY, Pei Y, Xie M, Jin ZH, Xiao YS, Wang Y, Zhang LN, Li Y, Huang WH (2015): An artificial blood vessel implanted three-dimensional microsystem for modeling transvascular migration of tumor cells. *Lab Chip* 15, 1178–1187
- Wong AD, Searson PC (2014): Live-cell imaging of invasion and intravasation in an artificial microvessel platform. *Cancer Res* 74, 4937–4945
- Wright LE, Ottewell PD, Rucci N, Peyruchaud O, Pagnotti GM, Chiechi A, Buijs JT, Sterling JA (2016): Murine models of breast cancer bone metastasis. *Bonekey Rep* 5, 804
- Wu M, Chen G, Li YP (2016): TGF- β and BMP signaling in osteoblast, skeletal development, and bone formation, homeostasis and disease. *Bone Res* 4, 16009
- Wu TT, Sikes RA, Cui Q, Thalmann GN, Kao C, Murphy CF, Yang H, Zhou HE, Balian G, Chung LWK (1998): Establishing human prostate cancer cell xenografts in bone: Induction of osteoblastic reaction by prostate-specific antigen-producing tumors in athymic and SCID/bg mice using LNCaP and lineage-derived metastatic sublines. *Int J Cancer* 77, 887–894
- Wu X, Gong S, Roy-Burman P, Lee P, Culig Z (2013): Current mouse and cell models in prostate cancer research. *Endocr Relat Cancer* 20, R155-70
- Xia TS, Wang GZ, Ding Q, Liu XA, Zhou W Bin, Zhang YF, Zha XM, Du Q, Ni XJ, Wang J, et al. (2012): Bone metastasis in a novel breast cancer mouse model containing human breast and human bone. *Breast Cancer Res Treat* 132, 471–486
- Yabushita H, Ohnishi M, Komiyama M, Mori T, Noguchi Mari, Kishida T, Noguchi Y, Sawaguchi K, Noguchi Masayoshi (2004): Usefulness of collagen gel droplet embedded culture drug sensitivity testing in ovarian cancer. *Oncol Rep* 12, 307–311
- Yang W, Lam P, Kitching R, Kahn HJ, Yee A, Aubin JE, Seth A (2007): Breast cancer metastasis in a human bone NOD/SCID mouse model. *Cancer Biol Ther* 6, 1295–1300
- Yi B, Williams PJ, Niewolna M, Wang Y, Yoneda T (2002): Tumor-derived platelet-derived growth factor-BB plays a critical role in osteosclerotic bone metastasis in an animal model of human breast cancer. *Cancer Res* 62, 917–923
- Yurchenco PD (2011): Basement membranes: Cell scaffoldings and signaling platforms. *Cold Spring Harb Perspect Biol* 3, a004911
- Zheng Y, Zhou H, Fong-Yee C, Modzelewski JRK, Seibel MJ, Dunstan CR (2008): Bone resorption increases tumour growth in a mouse model of osteosclerotic breast cancer metastasis. *Clin Exp Metastasis* 25, 559–567

ACKNOWLEDGEMENTS

First of all, I would like to express my deepest gratitude to my supervisor Prof. Arndt F. Schilling for providing this amazing opportunity to work here. Thank you for your patient guidance, support and new ideas during my scientific research and life in Göttingen. I also appreciate your encouragement and advices which help me overcome difficulties in my research work.

I would like to express my sincere gratitude to my second supervisor Prof. Fred Wouters, for his continuous support and help in my designing work. When there were difficulties, he always gave amazing suggestions and guided.

I would like to thank Dr. Kai Böker for his patient guidance, support and helpful discussions. Whenever I need his help, he was always there.

I would like to thank Dr. Juan Liu for her great help, encouragement, guidance during my application and study in UMG. Without her help, I would not be here.

I would like to thank Dr. Marina Komrakova and her husband for their kind and warm help in my daily life.

Special thank goes to Ramona Castro Machguth, Kathrin Hannke, Shahed Taheri, Samuel Siegk, Xiaobin Shang, Joachim Wagner, Eyck Rodenwaldt. Many thanks to all the teammates who helped me with my MD work.

Furthermore, I want to say thanks to Dr. Zhihong Xiao, Yaxuan Yao, Yan Chen, Lin Xie, Ruokun Huang, Dr. Kun Li, who shared lots of experimental tips and provided technical supports in my work.

Last, I would like to thank my family members for their support, understanding and encouraging when I'm busying working in the lab.

Thanks for everything!

CURRICULUM VITAE

My name is Zhiming Zhao, male, born on 29th September 1985 in Xiantao of Hubei province in China. I studied in Tongji Medical College of Huazhong University of Science and Technology from September 2002 to July 2009 and got my master degree of human medicine. During 7 years of medical education in China, I spend 2 years for clinical practice in Union hospital in Wuhan. On September 2009, I was employed by Wuhan Orthopedic hospital and started my career as an orthopedic surgeon. I passed the national exam for Chinese medical board in 2010. I was a visiting scholar in Beijing Jishuitan hospital for September 2017 to March 2018. In October 2018, I started medical doctorate study in department of trauma orthopedic and plastic surgery at Georg August University Medical Center Göttingen with the support of the scholarship from China Scholarship Council.